Characterization of whole-organism and cultured epithelial cell stress responses to nickel toxicity in a marine tunicate.

Celeste Valdivia

A thesis

submitted in partial fulfilment of the

requirements for the degree of

Master of Science

University of Washington

2026

Committee:

Alison M. Gardell

Steven B. Roberts

Jacqueline L. Padilla-Gamiño

Program Authorized to Offer Degree:

School of Aquatic and Fishery Sciences

Abstract

Characterization of whole-organism and cultured epithelial cell stress responses to nickel toxicity in a marine tunicate.

Celeste Valdivia

Chair of the Supervisory Committee:

Alison M. Gardell

School of Aquatic and Fishery Sciences

Botryllus schlosseri is a globally invasive colonial marine tunicate that relative to other chordates, possesses a remarkably high regenerative capacity through the maintenance of lifelong multipotent adult stem cells. *B. schlosseri* are comprised of several individual zooids that each contribute to the expansion of the colony through a form of weekly asexual budding termed blastogenesis, by which new clonal zooids arise as primary buds from the epithelial layers of the body walls of the prior zooid generation. As such, somatic cells of *B. schlosseri*, including those in the epithelia, have a significant potential to serve as powerful *in vitro* tools for revealing the cellular programs that drive regeneration and aging in one of our most closely related invertebrate species. Despite more than 40 years of research efforts, a continuous immortal cell line has not been established for *B. schlosseri*. For epithelial cells, the constrained cellular proliferation period for primary epithelial cells in culture presents a significant limitation in immortalization, with all documented cases entering a state of arrested cellular division after 24- to 72-hours. As such, characterizing the molecular networks regulating cell growth and arrest in this species is a critical step in developing strategies to overcome limited proliferation and

facilitate the development of an immortalized epithelial cell line. To address this, this thesis evaluated organismal and *in vitro* cellular responses of *B. schlosseri* to elevated concentrations of nickel, an oxidative stressor and clastogenic compound with the potential to serve as an immortalizing agent. In chapter 1, an *in vivo* study evaluated the phenotypic and molecular nickel-induced stress responses of whole *B. schlosseri* colonies. This study was the first to establish estimates of median lethal nickel concentrations (LC_{50}) for *B. schlosseri* at both 24- and 96-hours of exposure in full strength artificial seawater. *B. schlosseri* exhibited remarkably high nickel tolerance (24- hour LC_{50} = 177 mg L^{-1} and 96-hour LC_{50} =159 mg L^{-1}, nickel) where mortality was only observed at the highest dose administered (1000 mg L^{-1} nominal nickel (II) chloride [$NiCl_2$]). Although *B. schlosseri* persisted in the second-to-highest dose evaluated (100 mg L^{-1} nominal $NiCl_2$), colonies exhibited blastogenic arrest whereby primary buds suspended further growth and senescent zooids did not fully resorb. Differences in superoxide dismutase 1 (SOD1) activity for colonies in control, 1, or 100 mg L^{-1} nominal $NiCl_2$ were evaluated at both 24- and 96-hours post-exposure. *B. schlosseri* exhibited a moderate non-monotonic SOD1 activity response in which elevated activity was observed only in colonies exposed to the intermediate 1 mg L^{-1} nominal $NiCl_2$ dose. We then evaluated the transcriptomes of whole colonies exposed to control artificial seawater or 100 mg L^{-1} nominal $NiCl_2$. *B. schlosseri* colonies exhibited a tight transcriptional response with only 54 differentially expressed genes out of 13,970 reliably expressed gene transcripts. Significantly differentially expressed pathways included gene transcripts associated with redox balance, extracellular matrix maintenance, vasculature remodeling, cellular differentiation, and apoptosis. In chapter 2, a series of *in vitro* experiments updated the methodology for culturing *B. schlosseri* epithelial cells, assessed primary epithelial cell phenotypic responses to $NiCl_2$ exposure, and uncovered limitations for

total RNA isolation from primary epithelial cells with proposed approaches for improved RNA extraction outcomes. Primary epithelial cells were cultured under an explant tissue method that partially desiccated intact zooids and buds for improved attachment to the plastic culture-ware substrate. The media formulation was simplified from prior reported attempts, with a final media composition of a 1:1 mixture of supplemented media and sterile artificial seawater (~750 mOsmo/kg; pH 8.1). Under these culturing conditions, both zooids and buds in late blastogenesis produced a comparable number of epithelial cells and proliferated for up to 24-hours in culture. Cells displayed typical epithelial morphological characteristics as reported previously for this species, including the generation of tunic-like secretions in culture. In an acute nickel toxicity assessment, cells displayed no changes in phenotype or cell number, suggesting an overall tolerance to the chemical. Assessment of transcriptional responses to elevated nickel exposure for primary epithelial cells was attempted, however RNA quality and yield remained below the threshold required for bulk-RNA sequencing. In a systematic evaluation to improve RNA isolation, these cells were not conducive to typical methods of animal cell lysing including, needle shearing, chemical detergents, and bead beating. Proposed improvements for molecular phenotyping of epithelial cells will involve the evaluation of the protective role of tunic-like secretions as well as alternative enzymatic digestion for improved RNA isolation. Together, these findings provide valuable insights into the molecular networks that regulate nickel-induced cellular stress responses and identified key methodological barriers that remain to be addressed for working towards immortalization of primary epithelial cell cultures of *B. schlosseri*.

Table of Contents

Background 1
Chapter 1 5
1.1 Introduction 5
1.2 Methods 10
1.3 Results 18
1.4 Discussion 31
1.5 Conclusion 44
Chapter 2 46
2.1 Introduction 46
2.2 Methods 50
2.3 Results 60
2.4 Discussion 72
2.5 Future Perspectives 81
References 86

List of Figures

Supplemental Figure 1. Schematic illustration of the weekly blastogenic cycle of *Botryllus schlosseri* 3

Supplemental Figure 2. Schematic illustration of colony organization, individual zooid anatomy, and life history of *Botryllus schlosseri* 4

Figure 1.1. Exemplary healthy field-sourced *B. schlosseri* colonies acclimated to laboratory conditions and adhered to glass laboratory slides 12

Figure 1.2. Schematic representation of bioinformatics workflow for DEG analysis. 17

Figure 1.4. Mean health scores of colonies exposed to increasing concentrations of $NiCl_2$ over time 21

Figure 1.5. Best fit survivorship curve for *Botryllus schlosseri* at 24- and 96-hours post-exposure (hpe) 23

Figure 1.6. SOD1 activity (U mg^{-1} protein) in *B. schlosseri* colonies exposed to control (0), 1, or 100 mg L^{-1} nominal nickel (II) chloride for 24 or 96 hours post exposure (hpe) 25

Figure 1.7. Visualization of similarity of gene expression profiles across control and nickel treated samples 27

Figure 1.8. Clustering and heatmap of RNAseq data 28

Figure 1.9. Functional distribution of annotated differentially expressed genes (DEGs) 29

Figure 2.1. Exemplary field sourced *B. schlosseri* colony that may be used in cell culturing. 52

Figure 2.2. Graphical schematic of primary epithelial cell culture initiation from *B. schlosseri* colony 54

Figure 2.3. Zooid and primary bud tissue explants in culture 61

Figure 2.4. Peripheral expansion of primary epithelial monolayer sheets from explanted primary buds 62

Figure 2.5. Typical cell morphology for primary epithelial cells of *B. schlosseri* at 400x magnification under phase contrast microscopy. 63

Figure 2.6. Tunic-like secretion emerging from explanted tissue. 64

Figure 2.7. Formation of epithelial spheres derived from explanted stage D primary buds 65

Figure 2.8. Mean cell count after 24 hours in culture for primary epithelial cell cultures of stage D *B. schlosseri,* separated by explanted tissue type (primary buds and zooids). 67

Figure 2.9. Cell count outcomes of explanted tissue from *B. schlosseri* colonies pre-treated with nickel (II) chloride 68

Figure 2.10. Epithelial monolayer sheets before and after exposure to increasing concentrations of nickel (II) chloride 69

Figure 2.11. Paired changes in epithelial cell number following 24 hours post exposure to nickel (II) chloride in vitro across three *B. schlosseri* genets 70

List of Tables

Table 1.1. ICP-MS quality assurance results of measured nickel-60 (Ni-60) concentration for range-finding study exposure water samples 22

Table 1.2. ICP-MS quality assurance results of measured nickel-60 (Ni-60) concentration for RNA-seq study exposure water samples 22

Table 1.3. Nickel LC50 values reported for select marine invertebrates under seawater exposure conditions 24

Table 2.1. RNA concentration and purity metrics for primary epithelial cells of *B. schlosseri* ... 71

Acknowledgments

I would like to acknowledge my funding sources for this project. This research was funded by an NSF-BSF collaborative grant (BSF 2021650; NSF-MCB 2127516 and 2127517) awarded in part to my co-advisor Dr. Alison Gardell. I would like to acknowledge and thank my department for granting me a SAFS Finishing Fellowship, allowing me to complete the writing and synthesis of my thesis research. I would like to thank Dr. José Guzman for his support throughout my graduate experience and for being a pleasure to TA for.

To my co-advisor Dr. Alison Gardell, I express my deepest gratitude for your mentorship, guidance, and patience throughout this research project. It was a pleasure to be your first graduate student – thank you for taking a chance on me. Learning about the unexpected biological intricacies of this complex and unique species alongside you has been an intellectual joy. I would like to thank my co-advisor, Dr. Steven Roberts for introducing me to the bioinformatic workflows that allowed me to support the computational analyses of this thesis. I would like to thank Dr. Jacqueline Padilla-Gamiño for serving as a member of my thesis committee, where her invaluable guidance and perspective encouraged me to think critically and broadly about my research. To Zach, Megan, Chris, Grace, and the rest of my lab-mates, thank you for the support, kindness, and friendship that kept me motivated during both the exciting and challenging times of this project.

I would like to thank our collaborators Dr. Buki Rinkevich, Dr. Dietmar Kültz, and the everyone in the Kültz lab group for their expertise and support across this project. I would like to thank Dr. Theo Bammler, Sengkeo Srinouanprachanh, and James MacDonald at the University of Washington Genomics, Bioinformatics & Biostatistics, Microphysiological Systems Facility Core, for their support and contributions to the bioinformatic analyses of this thesis.

Dedication

This thesis is dedicated to my Mom, Dad, Analuz, Alejandro, Daisy, Nick, Grace, and Simon.

I could not have done this without your unwavering love and support.

I love you all so very dearly.

Background

The golden star tunicate, *Botryllus schlosseri* is a near-globally distributed marine invertebrate that has emerged as a highly relevant model for exploring mechanisms in regeneration (Qarri et al., 2020; Ricci et al., 2022), innate immunology (Cima et al., 2010; Goldstein et al., 2021), stress resilience (Franchi et al., 2017; Qarri et al., 2020; Zerebecki and Sorte, 2011), and phenotypic plasticity (Gao et al., 2022; Kültz et al., 2025; Tobias et al., 2024). Tunicates are sessile marine urochordates defined by a gelatinous, cellulose-like outer tunic, hermaphroditic reproductive anatomy, paired siphons and branchial basket for filter feeding and respiration, an endostyle homologous to the vertebrate thyroid, and a larval planktonic life stage (Supplemental Figure 2A-C.) As the closest extant relatives to vertebrates, tunicates bridge a key phylogenetic gap, providing a critical window into the evolution of key chordate traits (Holland, 2016). Of the three tunicate classes, ascidians are exceptional for their regenerative capacity, with species of the botryllid family (Botryllidae), *Botryllus* and *Botrylloides*, asexually regenerating entire zooid bodies as part of their regular life histories (Supplemental Figure 1). In addition, botryllid maintain regenerative abilities entirely lost in vertebrates where whole body regeneration can occur following traumatic injury or excision of all tissues except vascular remnants (Kassmer et al., 2019; Manni et al., 2019; Qarri et al., 2020). Altogether, *B. schlosseri* is an excellent system for exploring the molecular regulatory mechanisms defining cellular differentiation and regenerative processes, especially under the context of extreme stress.

Like other botryllid, *B. schlosseri* reproduces through two distinct modes that both generate the same adult body plan. The lifecycle of *B. schlosseri* begins as a sexually produced free-swimming larva that within hours of hatching, settles onto a substrate and metamorphoses into a single sedentary oozooid (the founding zooid of a colony) (Supplemental Figure 2C).

Within the first week of settlement, one to two clonal primary buds develop into blastozooids off the lateral body wall of the oozooid, initiating blastogenesis, a form of stem-cell mediated asexual reproduction. Blastogenesis proceeds cyclically (weekly at 18-20 °C) over the colony's life span, with the colony expanding to several hundred zooids that aggregate into star-shaped systems of 5 to 15 zooids, all embedded in a common tunic and connected by an extracorporeal vasculature system (Manni et al., 2014). The blastogenic cycle, first detailed by Sabbadin (1955) in a seven-stage system, characterizes the state of degeneration and development of the three constitutively co-occurring generations – the adult zooid, developing primary bud, and emerging secondary bud – each emerging from the preceding stage. In order to simplify the complexity of the staging system, the four main stages of blastogenesis were assigned A, B, C, or D (or takeover) (Mukai and Watanabe, 1976) (Supplemental Figure 1). Blastogenic takeover (TO) marks the transition between generations, during which the adult zooids close their siphons and undergo extensive apoptosis and autophagy (Cima et al., 2010) (Supplemental Figures 1 and 2). During this process, senescent TO zooids are resorbed and their cellular components are recycled within the colony to support the final maturation of developing primary buds into the next generation of zooids. (Franchi et al., 2016; Lauzon et al., 2007).

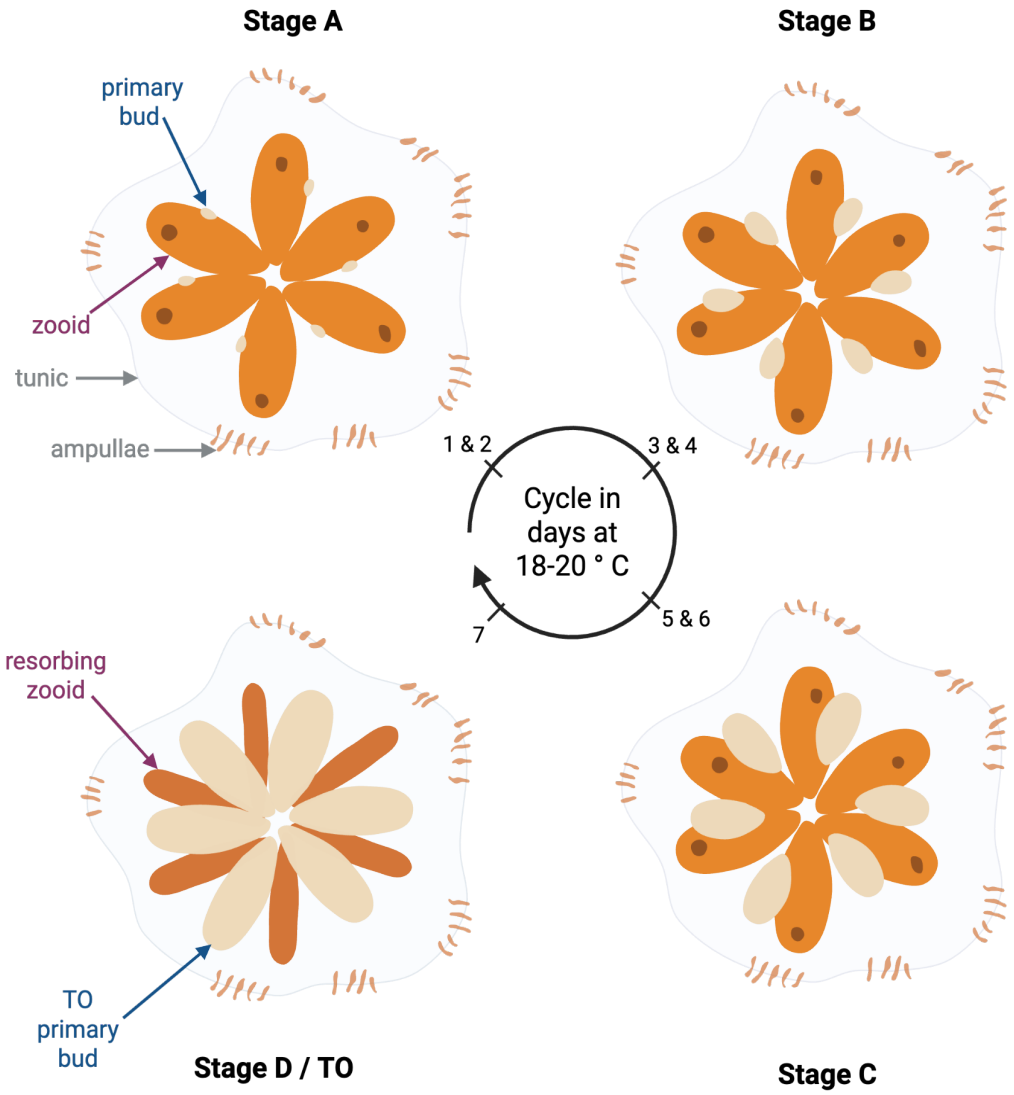

Supplemental Figure 1. Schematic illustration of the weekly blastogenic cycle of *Botryllus schlosseri*. Blastogenesis occurs weekly throughout a colony's lifespan at 18 to 20 °C. Key characteristics of the illustrated colony (made up of six zooids, clustered into a single star system) are highlighted in the initial and final blastogenic stages, stage A and D, respectively. Zooids in stages A through C maintain open incurrent siphons and sustain primary buds as they undergo growth and organogenesis (not detailed). At stage D during takeover (TO) zooids close incurrent siphons and are resorbed by the primary buds. When primary buds open their siphons and begin feeding, TO concludes and the cycle begins again as primary buds assume the role of the former generation of zooids. Created in BioRender. Valdivia, C. (2026) https://BioRender.com/lfqrgvs, licensed under CC BY 4.0.

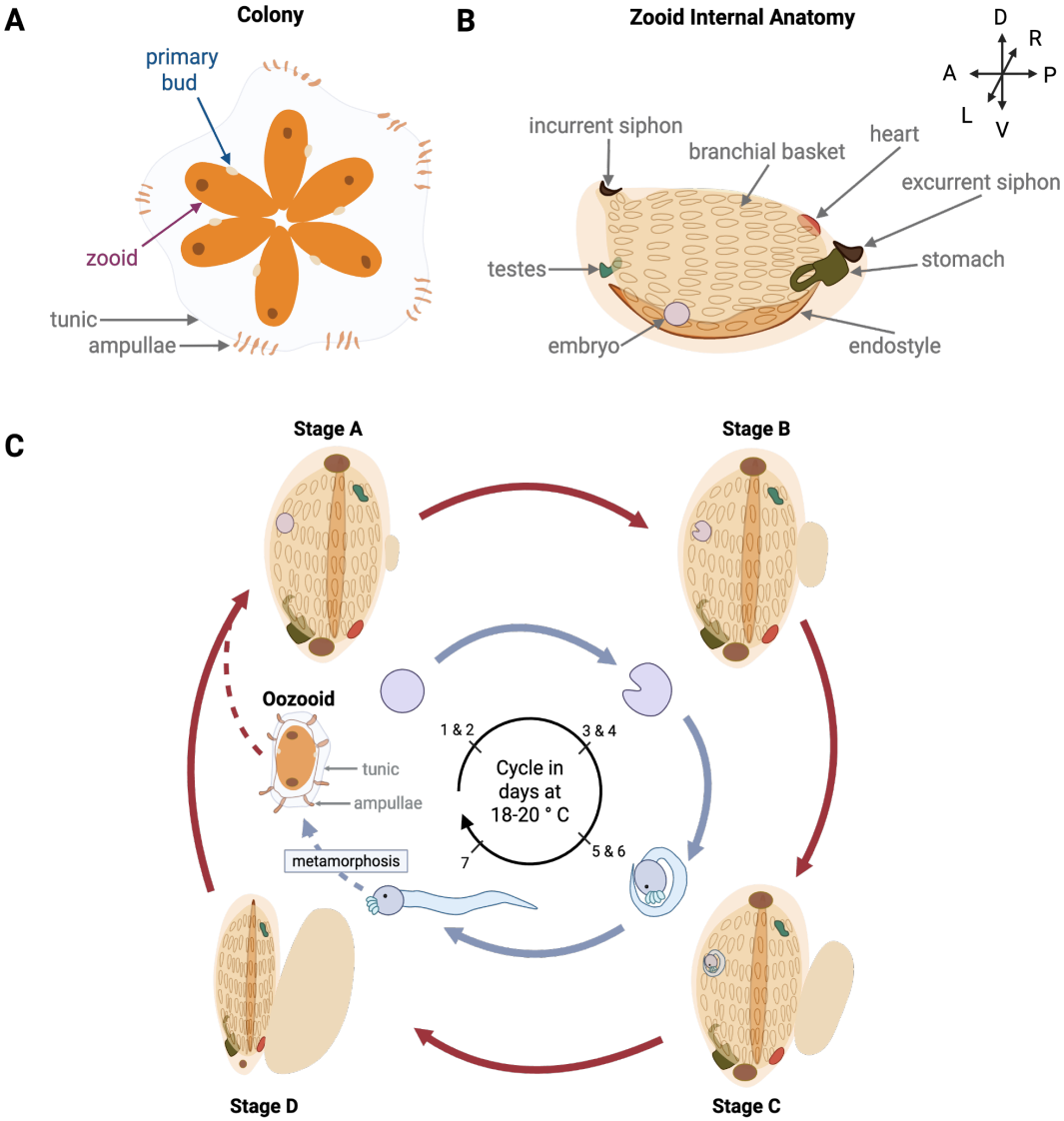

Supplemental Figure 2. Schematic illustration of colony organization, individual zooid anatomy, and life history of *Botryllus schlosseri*. (A) Representative colony organization of a single-star system or ramet made of six individual zooids that share a cloacal excurrent siphon. Zooids are embedded within a shared tunic and interconnected by an extracorporeal vascular system terminating in ampullae that fringe the colony. A single primary buds arise laterally from each adult zooid. (Not depicted here: younger colonies typically host a pair of primary buds on either side of the adult zooid, allowing for exponential doubling of the colony each week.) (B) Generalized internal anatomy of an individual zooid illustrating key tunicate features, including an incurrent and excurrent siphon, branchial basket, endostyle, heart, stomach, and reproductive structures. Ventral (V), dorsal (D), anterior (A), posterior (P), left (L), and right (R) axes illustrated to top right. (C) Sexual and asexual life history of B. schlosseri. The internal cycle with blue arrows illustrates progression of embryo to larval development. The outer cycle with red arrows illustrates asexual developmental progression of a zooid and its primary bud. Internally fertilized embryos develop within brooding zooids and are released during takeover as a free-swimming larva that rapidly settles and metamorphoses into a single founding oozooid. The oozooid enters the blastogenic cycle, initiating colony expansion and the asexual reproductive mode. Created in BioRender. Valdivia, C. (2026) https://BioRender.com/avhjt8x, licensed under CC BY 4.0.

Chapter 1

1.1 Introduction

Marine invertebrates regularly face a broad suite of environmental stressors, owing to the dynamic nature of their environments. Among the key environmental factors contributing to stress in marine invertebrates are pollutants like trace metals (Naranjo et al., 1996; Nydam et al., 2017), which have become ubiquitous in coastal habitats as a result of metal-based antifouling paints, mining operations, and industrial runoff (Kenworthy et al., 2018; Ya'la et al., 2025). While many trace metals function as essential micronutrients in marine invertebrates (Guillén Matus et al., 2024; Orihuela-García et al., 2023), concentrations exceeding physiological needs may result in bioaccumulation and downstream toxic effects (Blewett and Leonard, 2017; Orihuela-García et al., 2023). Nickel (Ni) is a trace metal that is rarely utilized in physiological or metabolic processes in marine invertebrates (Bible et al., 1988; Kor et al., 2022; Lebar et al., 2011), and is instead more widely recognized for its toxic effects (Blewett et al., 2016; Guillén Matus et al., 2024). In marine invertebrates, nickel uptake occurs primarily through dietary ingestion at the gut epithelia (Blewett and Leonard, 2017; Millward et al., 2012). Upon uptake at environmentally relevant concentrations (0.1-250 μg L^{-1}) nickel bioaccumulates in marine invertebrate tissues (Blewett and Leonard, 2017) and drives toxicity through respiratory inhibition, disrupted ionoregulation, and induction of oxidative stress (Blewett and Leonard, 2017). Through these main effects, nickel secondarily can impair embryonic development and promote DNA damage (Akpiri et al., 2017; Blewett et al., 2016; Dallas et al., 2013; Gissi et al., 2018).

Nickel-induced oxidative stress occurs through various mechanisms including mitochondrial dysfunction, redox homeostasis disruption, and antioxidant system suppression, which collectively promote reactive oxygen species (ROS) production and subsequent macromolecular damage (Blewett and Leonard, 2017; Brix et al., 2016; Stohs and Bagchi, 1994). At elevated nickel concentrations (125–3000 μg L^{-1}), antioxidant defenses can become impaired through post-translational enzyme modification and transcriptional suppression, as observed in green shore crabs where nickel-mediated histidine interactions reduce catalase (CAT) activity (Blewett and Wood, 2015) and in the copepod *Tigriopus japonicus*, where nickel resulted in reduced activity of superoxide dismutase (SOD), glutathione peroxidase (GPx), and glutathione-S-transferase (GST) (Wang and Wang, 2009). As nickel is consistently present in global open-ocean surface waters at background concentrations of approximately 2-8 nM (0.1-0.5 μg L^{-1}) (John et al., 2022), and is projected to increase in coastal areas in proportion to continued anthropogenic inputs (Gauthier et al., 2021; Orihuela-García et al., 2023), its bioaccumulation and potential toxicity in sessile marine invertebrates should also be expected to increase.

The globally invasive colonial marine tunicate, *Botryllus schlosseri*, preferentially colonizes and inhabits marinas and harbors, environments that function as sinks to anthropogenic pollutants such as trace metals (Hiscock, 2008; Kenworthy et al., 2018). While *B. schlosseri* is considered generally tolerant of environmental pollution (Gregorin et al., 2021; Naranjo et al., 1996), this species sequesters and incorporates trace metals at concentrations thousandfolds higher than the surrounding seawater (Guillén Matus et al., 2024). Interestingly, nickel is among the least accumulated in *B. schlosseri* – even relative to metals present at lower environmental concentrations (up to 9 mg L^{-1} in tissue versus 0.1 mg L^{-1} of nickel in surrounding seawater) (Guillén Matus et al., 2024). This selective pattern of metal accumulation suggests that *B.*

schlosseri possesses physiological mechanisms to regulate metal uptake, incorporation, and detoxification in a metal-specific manner. However, whether low nickel bioaccumulation in this species is a result of active sequestration and detoxification mechanisms or efficient excretion through ionoregulatory processes remains unresolved. Moreover, although cadmium (Cd) and copper (Cu) have been shown to induce transcriptional and enzymatic antioxidant responses in *B. schlosseri* (Franchi et al., 2017; Leprêtre and Kültz, 2025), and nickel clearly elicits oxidative stress responses in other marine invertebrates (Blewett et al., 2016; Dallas et al., 2013; Wang and Wang, 2009), it remains unclear how nickel may disrupt specific antioxidant defenses or reshapes the broader redox equilibrium in *B. schlosseri*.

In addition to *B. schlosseri* exhibiting a high tolerance to the persistent exogenous oxidative stress of their environments (Cima et al., 2015; Tasselli et al., 2017), this species also tolerates recurrent endogenous oxidative stress derived from its asexual reproductive mode (Supplemental Figure 1, Background). As a colonial tunicate, *B. schlosseri*, forms colonies of genetically identical zooids through weekly and cyclical blastogenesis, a type of asexual budding that enables continuous regeneration and rapid colony expansion (Manni et al., 2019). However, within the final blastogenic stage where buds takeover (TO) and assume the role of the next generation of zooids (Supplemental Figure 1 and 2, Background), senescent zooid apoptosis and degeneration drives intracellular accumulation of ROS (Cima et al., 2010; Franchi et al., 2017). Consistent with this, both laboratory-reared and field-sourced *B. schlosseri* consistently exhibit molecular markers of endogenous oxidative burden, with unusually high levels of 4-hydroxy-2-nonenal (HNE) adducted proteins across their proteomes (Kültz et al., 2025). HNE is a highly reactive electrophilic aldehyde generated through lipid peroxidation under oxidative stress that readily forms covalent post-translational adducts with nucleophilic amino acid residues on

proteins (Schneider et al., 2008). In vertebrates, HNE protein modification is associated with impaired function, disrupted cellular homeostasis, and disease pathophysiology (Liu et al., 2026; Shoeb et al., 2013). However, in *B. schlosseri*, HNE-adducted proteins have been proposed to serve a protective role as macromolecular sinks for lipid peroxidation products, an evolutionary adaptive arising from recurrent blastogenic oxidative stress (Kültz et al., 2025).

While *B. schlosseri* tolerates and proliferates under recurrent oxidative stress from the environment and life history style, it remains unknown how its redox physiology may respond to an acute and severe oxidative perturbation. As nickel toxicity in other marine invertebrates is largely driven by oxidative stress (Blewett and Leonard, 2017), evaluating the physiological and molecular responses of *B. schlosseri* under concentrated nickel exposure provides an opportunity to examine the mechanisms underlying oxidative stress tolerance. Assessing responses of extreme nickel exposure during late blastogenesis, when intrinsic oxidative burden is expected to be at its highest, offers an especially relevant context for examining the mechanistic regulation of redox homeostasis. Despite this potential, our understanding of *B. schlosseri* stress responses at the molecular level remains limited, even with extensive genomic and transcriptomic resources (Campagna et al., 2016; De Thier et al., 2024; Voskoboynik et al., 2013). Most existing transcriptomic studies have largely focused on transcriptionally profiling immune- and developmental-related genes in this species (Campagna et al., 2016; Oren et al., 2007; Ricci et al., 2016), leaving stress-responsive transcriptional networks completely understudied. Clarifying the transcriptional profile underlying stress responses in late blastogenic stage *B. schlosseri* represents a critical step toward understanding how this species tolerates and adapts to environmental stress such as that associated with a high nickel exposure.

To address this, the present study combines molecular and organismal phenotyping to comprehensively assess nickel-induced stress responses in colonies of *B. schlosseri*. Firstly, we evaluated the tolerance of colonies to increasing concentrations of nickel over an extended period of exposure (96-hours). Here we compared nickel-induced changes in morphology, superoxide dismutase (SOD) antioxidant activity, and approximated a crude median lethal concentration (crude-LC_{50}) at 24 and 96 hours of exposure. Using the 24-hour crude-LC_{50}, we selected a concentrated, yet sublethal, nickel dose to challenge colonies in late blastogenesis and evaluate transcriptomic changes associated with nickel stress response after 24-hours of exposure. Although previous studies suggest that *B. schlosseri* exhibits low nickel accumulation and generalized tolerance to metal exposure, it remains uncertain whether nickel challenge generates sufficient oxidative stress to transcriptionally activate classical antioxidant and metal detoxification pathways. We therefore evaluated whether transcripts encoding canonical antioxidant and redox regulatory pathways (e.g. *sod*, *gst*, *gclm*, and *mts*) were inducible, or whether nickel exposure elicited alternative strategies for maintaining redox balance and cellular integrity. By joining morphological phenotypes, antioxidant activity, and global transcriptional responses, this study provides a multi-level framework that clarifies how redox homeostasis is regulated in a stress-tolerant marine invertebrate, advancing our broader mechanistic understanding of how marine organisms maintain physiological equilibrium under increasing environmental stress.

1.2 Methods

1.2.1 *Animal Field Collection and Husbandry*

Colonies of *Botryllus schlosseri*, consisting of at least 100 zooids, were collected from floating docks at the City of Des Moines Marina (47°23'51.18"N, 122°19'46.01"W), Des Moines, Washington, USA, where high abundance of colonies are observed year-round. Field collections were conducted between April and May 2024 for the range-finding experiment and between September and November 2024 for the RNA-seq experiment. *B. schlosseri* colonies growing on Pacific blue mussels (*Mytilus sp.*) were preferentially selected for collection, as mussels typically supported larger colonies and could be removed from the substrate without damaging the colony. Pacific blue mussels with adhered colonies were gently removed by hand from the sides of the floating docks up to 36 cm deep into the water column and transferred into 400 mL containers filled with marina seawater. Containers were placed in an empty cooler to reduce temperature fluctuations throughout the sampling period (~1-2-hours).

B. schlosseri were transported back to the University of Washington, Tacoma (30.7 km transportation distance) and immediately processed. Colonies were peeled from Pacific blue mussel shells using a clean stainless steel razor blade and transferred to a 15 cm glass petri dish filled with marina seawater for health evaluation under a stereomicroscope (Nikon, SMZ-745T). Only healthy colonies were kept for lab acclimation – visually determined using the following criteria: a flat and firm tunic, normal zooid star-system formations, and at least one area or point of ampullae extension (Figure 1.1). Colonies were then tied to 76.2 x 50.8 x 1.2 mm glass slides with a cotton thread. Tied colonies were drip acclimated for one hour to the artificial seawater (Red Sea Salt; Red Sea, USA) in the University of Washington, Tacoma's recirculating artificial

seawater system (RAS) (18 °C; pH 8.0; 30 ppt). Slides were then transferred into glass staining racks to maintain colonies vertically. Colonies were held at a stocking density of 12 genets per 5-liter plastic container in the RAS and fed every other day with a mixture of Liquid RotiRich (Florida Aqua Farms) and Reef Phytoplankton (Seachem). Colonies were cleaned with a soft brush to remove any food debris and algal growth surrounding the ampullae and surface of the tunic and re-tied to their glass slides as needed to encourage gliding and adherence to glass slides.

Colonies used in the range-finding study were acclimated to the RAS for 11 days prior to experimentation. At the 9-day acclimation mark, colonies with at least 2 star-systems adhered to the glass slide and in good observable health (Figure 1.1A) (flat, firm, and clear tunic; extended ampullae; normal pigmentation) were subdivided using a clean razor blade into single star-system colonial fragments (ramets) (Figure 1.1B). Ramets for all range-finding experiments had an average of 11 zooids (± 4).

Colonies used in the RNA-seq experiment were maintained in the RAS for 10 ± 3 days prior to exposure. During this period, blastogenic cycles were monitored to identify colonies entering stage B for ramet division (Figure 1.1B). Colonies were starved at early stage C and exposures were initiated at late stage C to allow maturation toward stage D over the 24-hour exposure period.

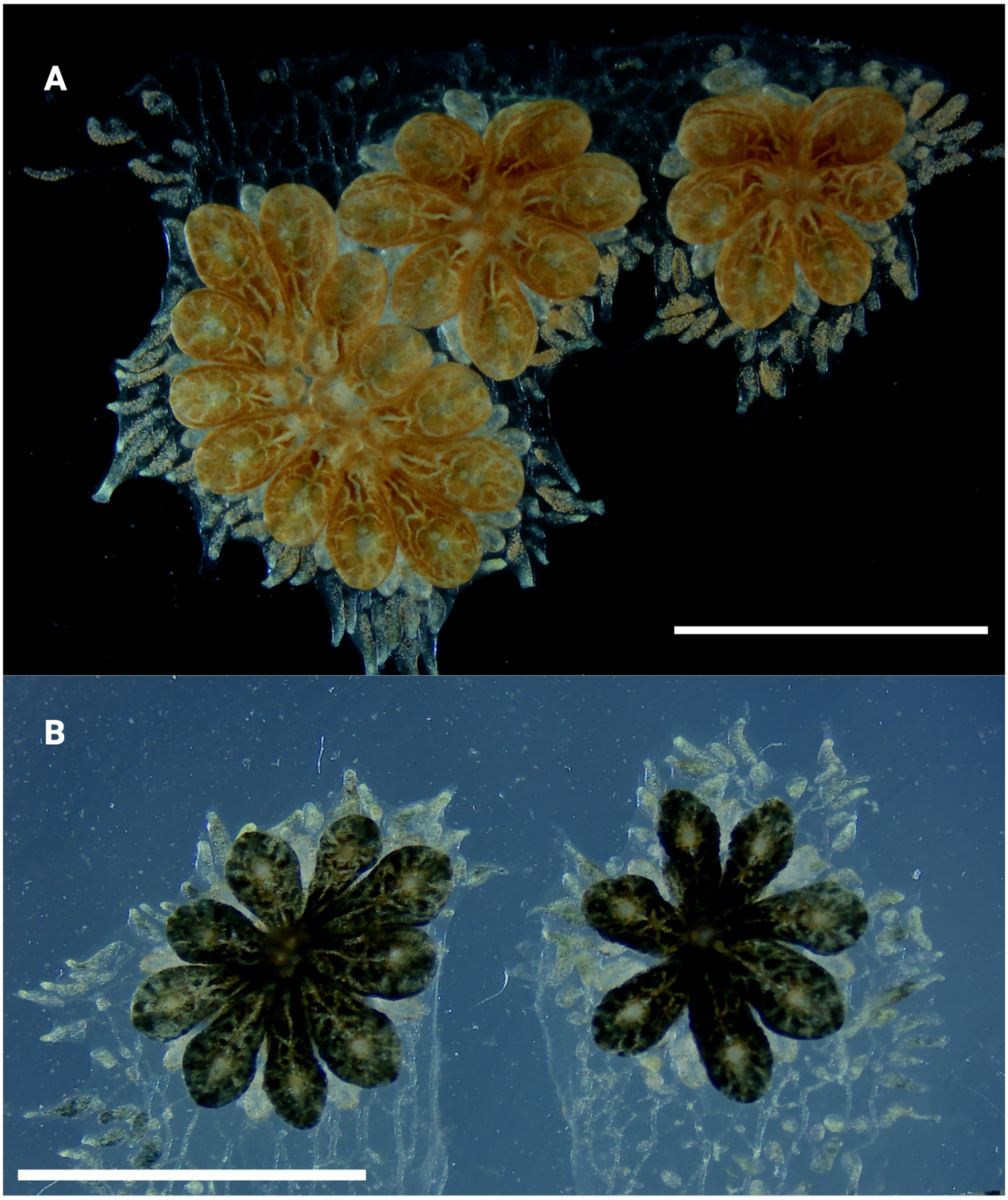

Figure 1.1. Exemplary healthy field-sourced *B. schlosseri* colonies acclimated to laboratory conditions and adhered to glass laboratory slides. (A) Orange color-morph colony of B. schlosseri composed of three star-systems. Ampullae extend beyond the borders of the clear and transparent tunic. Pigment intensity is low throughout the zooid bodies and ampullae indicating good health. (B) Black color-morph subdivided ramets of a B. schlosseri colony. Each star-system previously shared the same extracorporeal vascular system and tunic but were subdivided into separate ramets for experimental preparation. Ramets were divided with a clean stainless steel razor blade with any tunic or ampullae tissue between ramets excised to prevent re-fusion. White bars = 5 mm.

1.2.2 Range-finding Exposure Study

To establish a sublethal dose for subsequent RNA-seq experiments, a range-finding exposure study was conducted. For all range-finding exposures, a stock solution of 1 g L^{-1} nickel (II) chloride anhydrous ($NiCl_2$; Sigma-Aldrich, Cat. No. 339350) was prepared in Milli-Q water (18.2 MΩ·cm resistivity). Experimental range-finding concentrations of nickel (II) chloride were selected on a logarithmic scale from 0.1 to 1000 mg L^{-1} as a result of relevant literature (Trott et al., 1995) and previous pilot studies with *B. schlosseri* illustrating tolerance at lower concentrations (data not shown.) The stock solution was diluted to nominal nickel (II) chloride concentrations of 0.1, 1, 10, 100, and 1000 mg L^{-1} in freshly prepared, aerated artificial seawater (33 ppt, pH 8.2, 18 ˚C). After spiking with the appropriate volume of stock nickel (II) chloride, solutions were thoroughly mixed and left to equilibrate for 30 minutes. Aliquots of 250 mL were then distributed into exposure vessels (473 mL wide-mouth mason jars) and sampled for analytical chemistry and Ni concentration verification using inductively coupled plasma mass spectrometry (ICP-MS), using instrumentation available at the University of Washington, Tacoma.

B. schlosseri colonies adhered to glass slides, each containing two healthy ramets from the same genet, were transferred to exposure vessels and maintained in an environmental chamber (18 °C; 12:12 light:dark photoperiod). Colony health and survival were monitored over the 96-hour exposure period and were imaged under a stereomicroscope (Nikon, SMZ-745T) with a camera attachment (Excelis 4K Microscope Camera) at 24, 48, 72, and 96-hour timepoints. Mortality was defined by the absence of zooid body wall muscle responsiveness and cessation of hemolymph circulation. Ramets were removed at 24 and 96 hours using a sterile

steel razor blade and snap-frozen for downstream analysis of superoxide dismutase (SOD) activity.

1.2.3 Total Protein Concentrations

Whole frozen *B. schlosseri* ramets were weighed out and then homogenized in liquid nitrogen using a pre-chilled, autoclaved pestle. The pulverized samples were then resuspended in cold 1X PBS (0.5 mL per 100 mg of tissue) and centrifuged at 1,500 × g for 10 min at 4 °C. The resulting supernatant was collected for cytosolic protein analysis.

Total cytosolic protein concentrations were quantified using the Pierce BCA Protein Assay Kit (Thermo Fisher Scientific; Cat. Nos. 23225, 23227) with bovine serum albumin standards (BSA), at 562 nm on a microplate reader. Standard curves were generated for each assay plate using BSA standards ranging from 0 to 2 mg L^{-1}. For each plate, the mean absorbance of blank wells was calculated and subtracted from all standards and samples prior to model fitting. Plate-specific linear models were then fit to blank-corrected absorbance values as a function of known protein in mg L^{-1}. As mean blank subtraction normalized 0 mg L^{-1} standard technical replicates to ~0 absorbance, standard curves were fit through the origin (0,0) using a no-intercept linear model. This approach constrained the model to reflect expected relationship between protein concentration and absorbance after blank correction ($R^2 > 0.989$ per each plate). Protein concentrations of unknown samples were then calculated from the plate-specific slope and adjusted for dilution factor prior to downstream normalization of enzyme activity.

1.2.4 Superoxide Dismutase 1 Activity Assay

Superoxide dismutase 1 (SOD1) was isolated and quantified from cytosolic protein extracts using the colorimetric Invitrogen SOD Colorimetric Activity Kit (Cat. No. EIASODC),

following the manufacturer's instructions. One unit (U) of SOD is defined as the amount of enzyme required to exhibit 50% dismutation of superoxide radicals under the assay conditions. Absorbance was recorded at 450 nm using a microplate reader. SOD1 activity was measured in duplicate technical replicates per homogenate with absorbance recorded at 450 nm both prior to and following xanthine oxidase incubation using a microplate reader. For each well, the change in absorbance was calculated (ΔA450). Plate specific blank wells were included in each plate and mean blank ΔA450 values were calculated per plate and subtracted from all wells to generate blank-corrected absorbance values. A standard curve was generated for each plate using known SOD standards ranging from 0 to 2 U mL^{-1}. Because assay response is logarithmic, blank-corrected absorbance values were modeled as a function of the natural logarithm of known SOD activity. Plate-specific linear regressions were then used to calculate SOD activity (U mL^{-1}) for each unknown sample. Calculated SOD activity values were subsequently adjusted for dilution factor. Finally, SOD1 activity per mg of protein (U mg^{-1} protein) was calculated using the quantified values of protein concentration per homogenate from the BCA assay.

1.2.5 RNA-seq Experiment

Prior to the start of exposure, colonies of *B. schlosseri* were staged under a stereomicroscope and those with at least two ramets adhered to the glass slide, in stage C2, and in good health were selected to proceed in the study. Using a 1 g L^{-1} nickel (II) chloride stock solution, exposure vessels (473 mL wide-mouth mason jars) containing 250 mL of freshly prepared, aerated artificial seawater (33 ppt, pH 8.2) were spiked to a nominal concentration of 100 mg L^{-1} $NiCl_2$. Control artificial seawater (ASW, 33 ppt, pH 8.2) exposure vessels were prepared concurrently. The $NiCl_2$ solution was thoroughly mixed and allowed to equilibrate for 10 min, after which a 10-mL sample was collected from each vessel for quality assurance

analyses. After exposure water preparation, colonies were transferred into exposure vessels containing either control ASW or $NiCl_2$-spiked ASW. Colonies were then placed in an environmental chamber (18 °C; 12:12 h light:dark photoperiod; 90% humidity) and left for 24-hours. At the end of the 24-h exposure period, colonies were removed from their exposure vessel and rinsed in triplicate with fresh artificial seawater to remove any remaining nickel. Colonies post-exposure were imaged using a stereomicroscope and camera attachment. Colony ramets were preserved in RNAprotect Tissue Reagent (Qiagen; Cat. No. 76104) and stored at -80 °C until RNA extraction.

For RNA extraction, RNAprotect was removed from tubes before preserved ramets were pulverized in liquid nitrogen using a pre-chilled, autoclaved pestle. Total RNA was isolated with the RNeasy Mini Kit (Qiagen; Cat. No. 74104) following the manufacturer's protocol. RNA quality and integrity were assessed using an Agilent Bioanalyzer. From twelve biological replicates per treatment, the six samples per treatment with the most comparable RNA quality and yield were selected for sequencing.

1.2.6 RNA-seq Differential Gene Expression Analysis

Raw RNA-seq reads were processed using a standard transcriptomic workflow (Figure 1.2). Briefly, reads were aligned to a *B. schlosseri* transcriptome (file in preparation for publication) using Salmon (Patro et al., 2017). Transcript counts were summarized to the gene level with the tximport package in Bioconductor (Soneson et al., 2015). Gene annotation was performed using eggNOG. Gene-level counts were filtered to remove lowly expressed genes and normalized for library size using the trimmed mean of M-values (TMM) method implemented in the edgeR package (Robinson and Oshlack, 2010). Normalized counts were then analyzed with the limma-voom pipeline (Law et al., 2014), which models the mean-variance relationship of

log-transformed transcript counts and fits a weighted linear model to each gene. To account for within-group dissimilarity, sample-specific weights were estimated from regression residuals that measured how much each sample's expression deviated from its group mean across all genes; samples with larger deviations were down-weighted in the model. Differential expression between nickel-treated and control colonies was tested using empirical Bayes-moderated *t*-statistics, with significance determined at a false discovery rate (FDR) < 0.1.

Unannotated DEGs were further processed using BLASTx against the UniProt Swiss-Prot database (release 2025_03). A custom BLAST database was constructed locally, and DEGs were queried with an E-value cutoff of $1E^{-20}$, retaining the top hit per sequence. BLAST output was parsed and merged with UniProt annotation tables to append gene symbols, protein descriptions, and organism information to previously unannotated sequences.

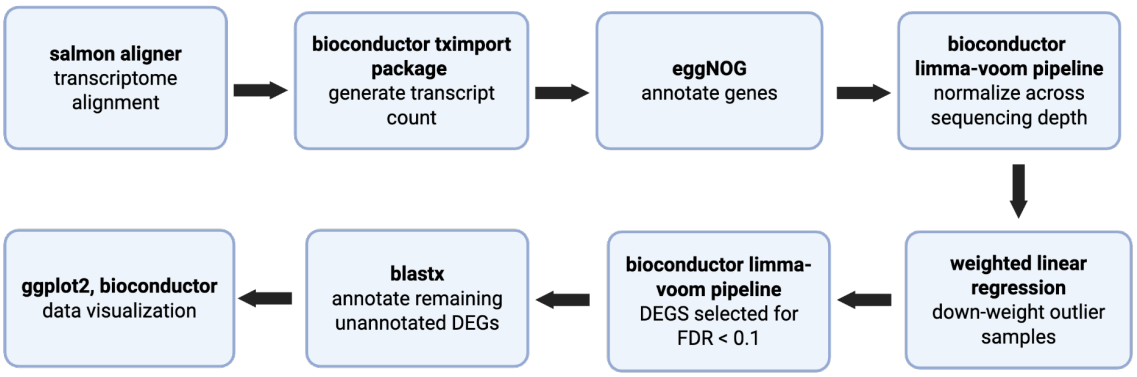

Figure 1.2. Schematic representation of bioinformatics workflow for DEG analysis. Created in BioRender. Valdivia, C. (2026) https://BioRender.com/816i1cq, licensed under CC BY 4.0.

1.2.7 Statistical analyses

SOD1 activity normalized to total protein concentration (U mg^{-1} protein) was analyzed to evaluate differences across control and two nickel exposure concentrations from the range-finding experiment at 24 and 96 hours post exposure. Statistical analyses were conducted in R

(version 4.5.2). A two-way analysis of variance (ANOVA) was performed on biological replicates with nominal nickel (II) chloride concentration and exposure duration (24 and 96 hpe) as fixed factors. Model assumptions of normality and homogeneity of variance were evaluated using Shapiro-Wilk and Levene's tests, respectively. When ANOVA indicated significant effects, Tukey-Kramer post hoc comparisons were conducted to evaluate pairwise differences among treatment groups within each time point. Statistical significance was assessed at a $\alpha = 0.05$.

All analysis scripts used for data processing and figure generation were version-controlled and are publicly available and maintained on GitHub (release v1.0-thesis).

1.3 Results

1.3.1 Phenotypic and Health Declines with Increasing Nickel (II) Chloride – Morphological Observations

In nominal concentrations below 100 mg L^{-1}, changes in observable health markers were minimal (Figures 1.3B2- B5 and 1.4). Colonies in the 0.1 mg L^{-1} nominal $NiCl_2$ treatment maintained typical morphology including, active hemolymph circulation, normal clustering of zooid systems, flat and clear tunics, and zooid contractions to physical stimulation. The colonies in the 1 and 10 mg L^{-1} nominal $NiCl_2$ treatments exhibited similar, but moderate, declines in health over time, maintaining active hemolymph circulation and zooid response, but, accumulating morphological indications of stress by 96 hpe, including hyperpigmentation, tunic puffing, and ampullar retraction, and ampullar dilation (Figure 1.3C2-B3).

All biological replicates in the 100 mg L^{-1} dose exhibited blastogenic arrest by 24 hpe, characterized by the halted development of primary buds, regardless of the blastogenic stage at

which exposure began (Figure 1.3C2- C5). Colonies at this dose remained alive over the duration of the 96-hour exposure but displayed increasingly slowed hemolymph flow rate in the vasculature. Furthermore, in the 100 mg L^{-1} dose, colonies exhibited hyperpigmentation, puffed tunic, retraction and swelling of ampullae, and dissociation of typical star-system architecture. Mortality was observed only at the highest concentration tested (1000 mg L^{-1}) over the 96-hour exposure period. Exposure to 1000 mg $L^{-1}$of nominal nickel (II) chloride resulted in 100% mortality by 48 hpe (Figure 1.4).

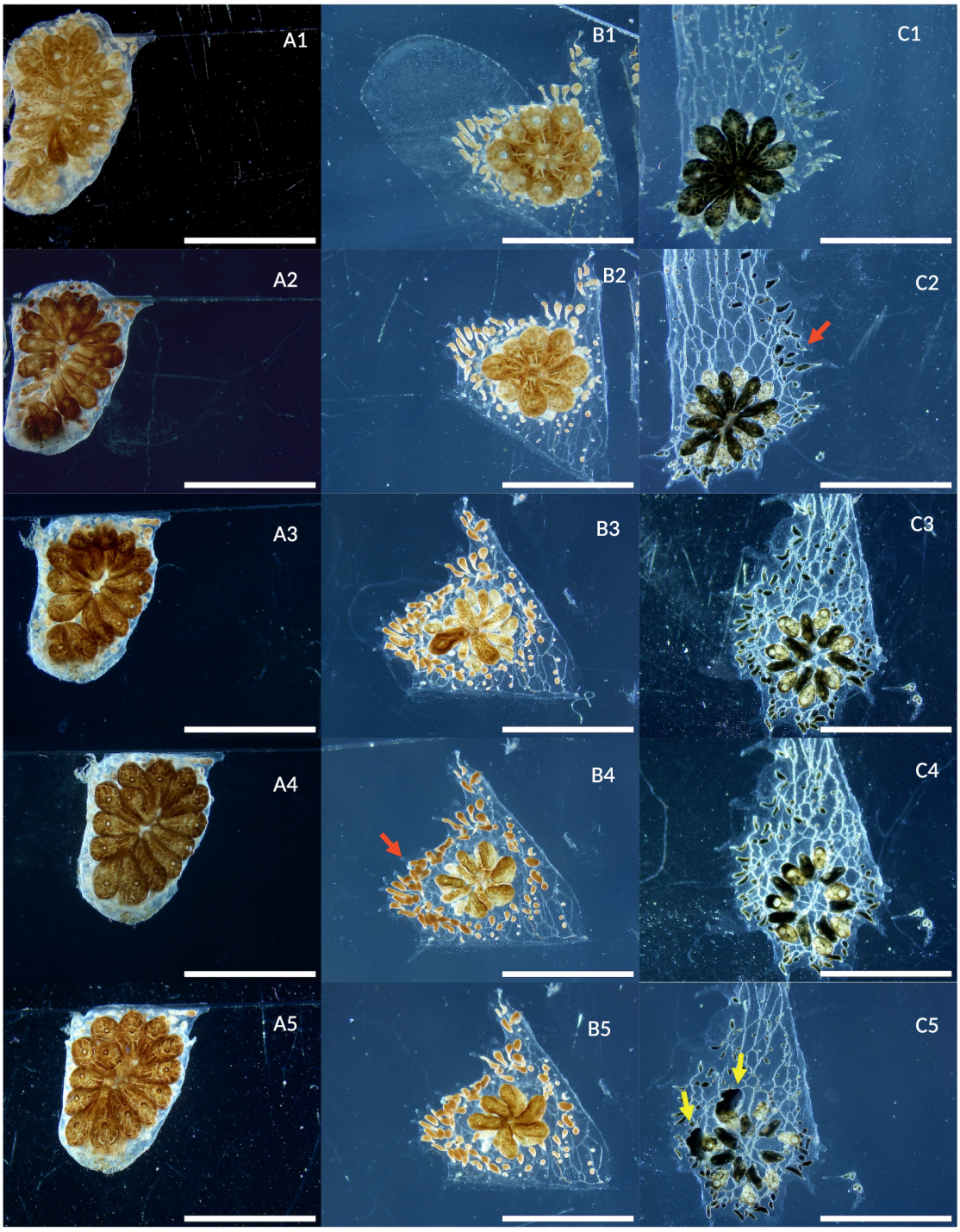

Figure 1.3. Changes in observable health over the course of nickel exposure in three colonies of *B. schlosseri*. From top to bottom, in order of pre-exposure, 24, 48, 72, and 96-hours post exposure (hpe). **(A1-A5)** Control (0 mg L^{-1} nickel (II) chloride). **(B1-B5)** Colony exposed to nominal 0.1 mg L^{-1} nickel (II) chloride. **(C1-C5)** Colony exposed to nominal 100 mg L^{-1} nickel (II) chloride. Onset of ampullae retraction (red arrows) and development of hemolymph abscesses in primary buds (yellow arrows). White bars, 5 mm.

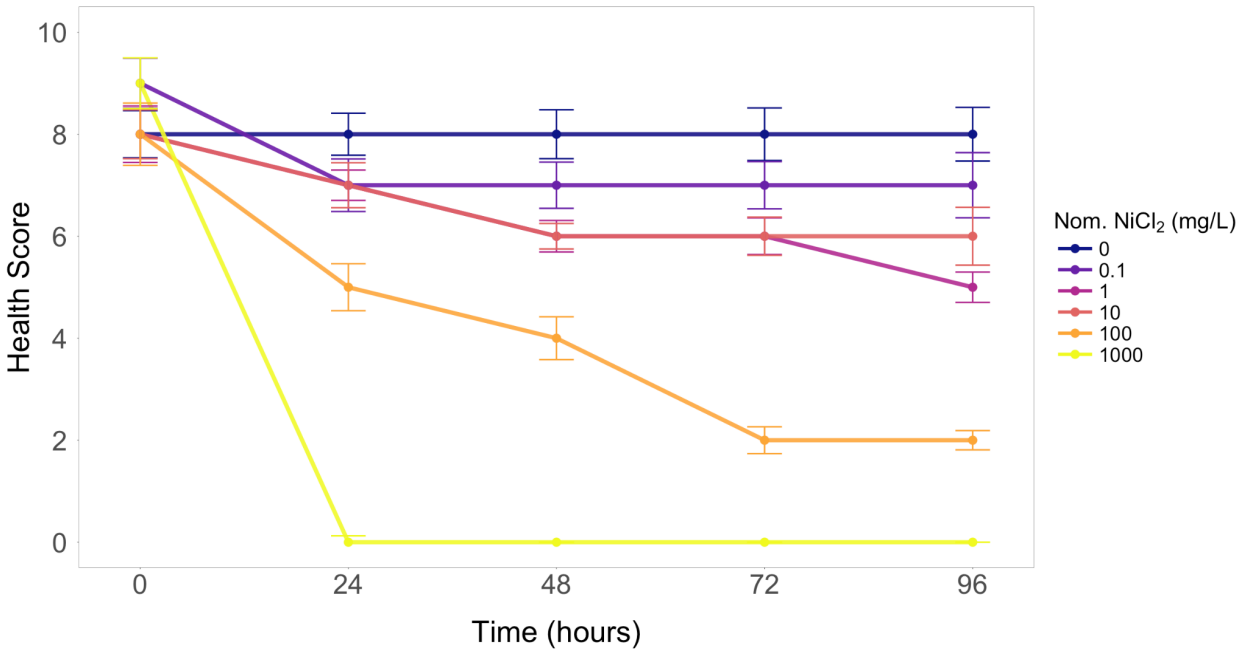

Figure 1.4. Mean health scores of colonies exposed to increasing concentrations of $NiCl_2$ over time. Health score defined as the following: 0 = dead, no blood flow; 2 = very bad with heartbeat, 4 = poor with retracted ampullae, high pigmentation, and puffy tunic; 6 = fair, part poor; 8 = good with most ampullae extended, normal tunic, and normal pigmentation, 10 = great with all ampullae extended, tunic flat, clear, and normal pigmentation. (n = 30).

1.3.2 Chemical Analysis

Nickel concentrations in control and treatment artificial seawater samples were verified by ICP-MS following nitric acid digestion. Measured dissolved nickel concentrations increased proportionally with nominal nickel (II) chloride additions across all treatments (Tables 1.1 and 1.2). ICP-MS analyses of field-sourced seawater collected in May 2025 from the City of Des Moines Marina (site of tunicate collection) detected dissolved nickel at a mean concentration of 1.3 ± 1.9 µg L^{-1} (Ni-60, n = 6).

Table 1.1. ICP-MS quality assurance results of measured nickel-60 (Ni-60) concentration for range-finding study exposure water samples. Stock solutions were prepared for each of the four iterations of range-finding study and spiked water distributed for each technical replicate. Ni concentrations were below the expected nominal Ni concentrations but fell within a proportionally increasing pattern with increasing target nominal $NiCl_2$ concentrations.

Analytical Chemistry ICP-MS Results for Range-finding Study						
Nominal NiCl2 mg/L	**Nominal Ni mg/L**	**Mean Ni-60 mg/L**	**SD Ni-60 mg/L**	**Min. Ni-60 mg/L**	**Max Ni-60 mg/L**	**Sample Size**
0	0	0.01	0.01	0	0.01	4
0.1	0.05	0.04	0.01	0.03	0.04	4
1	0.45	0.29	0.01	0.28	0.3	4
10	4.53	3.03	0.49	2.5	3.58	4
100	45.29	27.64	10.14	16.7	38.69	4
1000	452.88	289.66	30.11	261.16	319.56	4

Table 1.2. ICP-MS quality assurance results of measured nickel-60 (Ni-60) concentration for RNA-seq study exposure water samples. For each exposure vessel, exposure water was freshly prepared based on target nominal $NiCl_2$ concentrations. Measured Ni-60 concentrations were below expected nominal Ni concentrations, but consistent with measured Ni-60 concentrations of range-finding exposure water samples of the same target concentrations.

Analytical Chemistry ICP-MS Results for RNA-seq Study						
Nominal NiCl2 mg/L	**Nominal Ni mg/L**	**Mean Ni-60 mg/L**	**SD Ni-60 mg/L**	**Min. Ni-60 mg/L**	**Max Ni-60 mg/L**	**Sample Size**
0	0	0	0	0	0.01	10
100	45.29	38.07	9.13	29.06	54.44	9

1.3.3 Median Lethal Nickel Concentration Approximation

The median 24-hour lethal nickel concentration (LC_{50}) for *Botryllus schlosseri* was estimated from the nickel concentrations measured from stock solutions pre-exposure using ICP-MS and observed cumulative mortality after 24 and 96-hours of exposure. Because mortality was only observed at the highest concentration (ICP-MS measured mean 290 mg L^{-1}, SD = 30.1 mg L^{-1}), a full dose–response curve could not be modeled using traditional logistic or probit regression approaches. Instead, mortality proportions were plotted against the measured nickel

concentrations, and an approximate LC_{50} value was interpolated graphically by connecting the observed data points with a linear trend line. This approach provides an estimated threshold concentration for acute lethality under the conditions tested and serves primarily to inform subsequent sublethal exposure assays rather than to define a statistically modeled LC_{50} value. The 24-hour and 96-hour LC_{50} values were calculated to be 177 mg L^{-1} and 159 mg L^{-1} (about an 11% decrease) using a line of best fit (Figure 1.5).

LC_{50} values for other marine invertebrates span similar concentrations (Table 1.3). Most available nickel toxicity data for marine species is derived from mollusks, crustaceans, and echinoderms. Notably, nickel LC_{50} data for any tunicate species is absent from the literature.

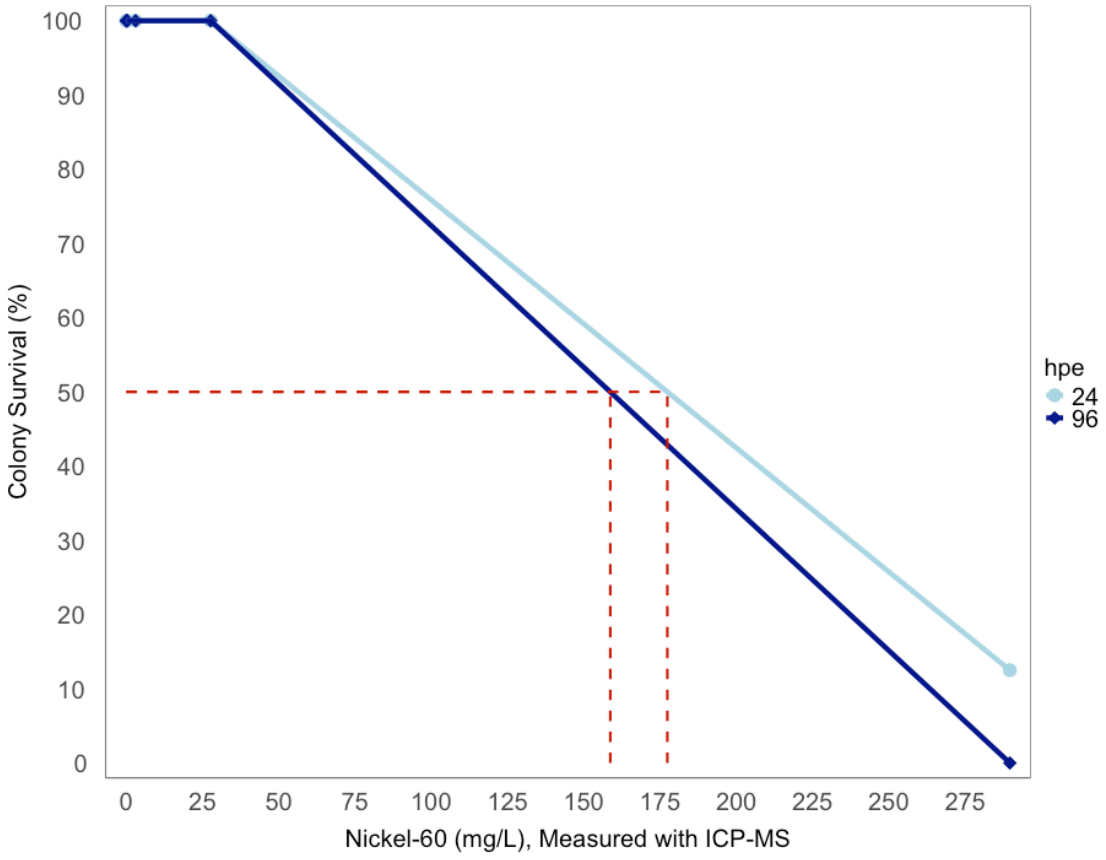

Figure 1.5. Best fit survivorship curve *for Botryllus schlosseri* at 24- and 96-hours post-exposure (hpe). 100% mortality observed only at the highest nickel dose. Mortality classified by cessation of blood flow throughout the colony. Red dashed intersecting lines mark crude 50% survival dose (crude-LC_{50}). Crude-LC_{50} Ni-60 values for 24-hpe and 96-hpe are calculated to be 177 and 159 mg L^{-1}, respectively.

Table 1.3. Nickel LC_{50} values reported for select marine invertebrates under seawater exposure conditions. Reported toxicity thresholds vary widely depending on species, life stage, exposure duration, and water chemistry parameters. Relevant water chemistry parameters include temperature, salinity, pH, and seawater composition (natural seawater [NSW] versus artificial seawater [ASW]). Values contextualize the nickel tolerance observed in *B. schlosseri* in the present study.

Species and Life Stage			Water Chemistry Parameters				Assay Parameters and Results			Source
Species	**Taxonomic group**	**Life stage**	**Temperature (°C)**	**Salinity (ppt)**	**Seawater Type**	**pH**	**Exposure (h)**	**Exposure Regime**	**LC50 (mg/L Ni)**	**DOI**
Botryllus schlosseri	**Tunicate (ascidian)**	**Adult**	**18**	**33**	**ASW**	**8.2**	**24**	**static**	**177**	**present study**
Botryllus schlosseri	**Tunicate (ascidian)**	**Adult**	**18**	**33**	**ASW**	**8.2**	**96**	**static**	**159**	**present study**
Allorchestes compressa	Crustacean (amphipod)	Juvenile	20	32	ASW	N/A	96	static	34	10.1016/0048-9697(94)90391-3
Babylonia areolata	Mollusk (gastropod)	Adult	24	37	ASW	7.8 to 8.2	96	static	34	10.1080/02772248.2013.864450
Crassostrea virginica	Mollusk (oyster)	Embryo	26	25	ASW	7.0 to 8.5	48	static	1	10.1007/BF00367984
Mya arenaria	Mollusk (clam)	Adult	20	20	NSW	7.8	96	static	320	10.1007/BF02097772
Asterias forbesi	Echinoderm (starfish)	Adult	20	20	NSW	7.8	96	static	150	10.1007/BF02097772
Macoma balthica	Mollusk (clam)	Adult	15	35	NSW	N/A	96	static	540	10.3354/MEPS024139

1.3.3 Superoxide Dismutase 1 Activity

Superoxide dismutase 1 (SOD1) activity differed significantly among colonies exposed to different nickel concentrations (two-way ANOVA, $F = 3.47$, $p = 0.041$), with a moderate effect size (partial $\eta^2 = 0.14$) that indicates ~14% of the variance in SOD1 activity was attributable to nickel exposure (Figure 1.6). Neither exposure duration nor the interaction between time and concentration significantly influenced SOD1 activity ($p > 0.05$). Tukey-Kramer adjusted pairwise comparisons did not detect significant differences among concentrations ($p > 0.05$), although Fisher's LSD comparisons indicated higher mean SOD1 activity at 1 mg L^{-1} nominal $NiCl_2$ relative to both the control and 100 mg L^{-1} treatments ($p < 0.05$). Together, these results suggest that nickel exposure elicits a modest, non-monotonic SOD1 enzyme activity response in

colonies of *B. schlosseri*, though variability among colonies limited the detection of pairwise differences following correction for multiple comparisons (Tukey-Kramer).

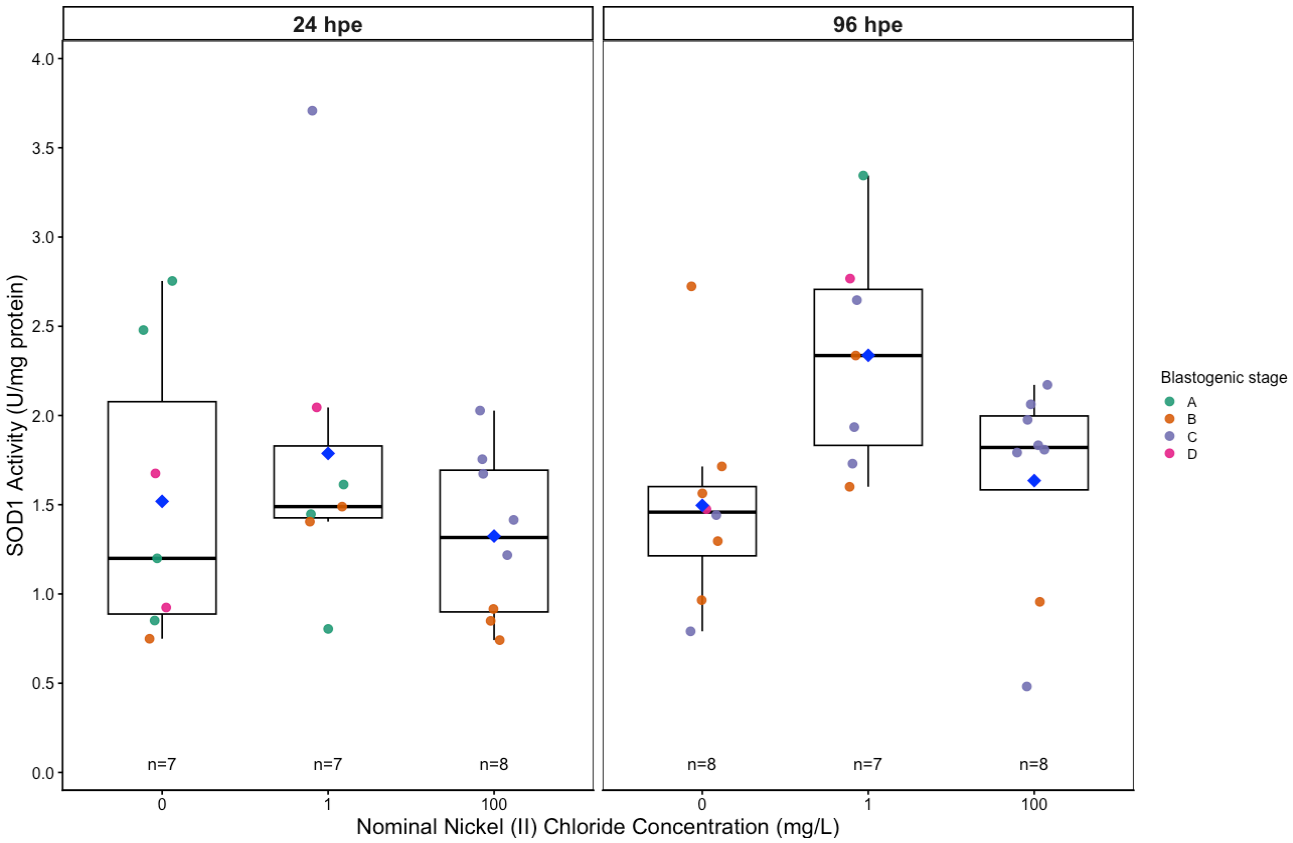

Figure 1.6. SOD1 activity (U mg^{-1} protein) in *B. schlosseri* colonies exposed to control (0), 1, or 100 mg L^{-1} nominal nickel (II) chloride for 24 or 96 hours post exposure (hpe). Points represent individual biological replicates colored by blastogenic stages. Boxplots display the median and interquartile range with whiskers extending to 1.5x the interquartile range. Mean SOD1 activity per treatment is indicated by blue diamonds. Two-way ANOVA detected a significant effect of nickel concentration on SOD1 activity ($p < 0.05$), but no effect of exposure duration or interaction ($p > 0.05$). Tukey-Kramer adjusted pairwise comparisons averaged across exposure duration were not significant ($p > 0.05$). Fisher's LSD comparisons indicated significantly elevated SOD1 enzymatic activity in colonies exposed to 1 mg L^{-1} relative to both colonies in the 0 mg L^{-1} ($p = 0.03$) and 100 mg L^{-1} ($p = 0.02$) nominal $NiCl_2$ treatments, irrespective of time post exposure. Sample size per group is indicated on the plot.

1.3.4 Sequencing and Quality Control

The samples were sequenced by NovoGene in paired-end mode (2 × 150 bp read length), yielding an average of 34.42 (± 6.25) million paired-end reads per sample. Quality control on the raw reads was performed using FastQC. Data quality was further ensured through assessment using a multidimensional scaling (MDS) plot (Figure 1.7). Nickel treated and control samples were somewhat separated along the first two dimensions of the MDS plot, although some overlap was observed with one nickel treated sample clustering near controls and vice versa (Figure 1.7). Meta-data confirmed that the two outlier samples were not mislabeled or swapped. Influence of outlier samples on the differential expression analysis was mitigated by the weighted linear regression implemented through the limma-voom pipeline (Law et al., 2014), which down-weighted samples with greater within-group dissimilarity based on robust regression residuals.

Dimension 1 (dim1) captured 18% of the total explained variance, indicating a moderate but consistent transcriptional shift in response to nickel exposure. Control colonies were more widely distributed across dim1 suggesting greater within-group variability under baseline conditions. Dimension 2 (dim2), which explained 11% of the total variance, captures subtler but distinct expression dissimilarity between nickel-treated and control colonies.

1.3.5 Differential Gene Expression in Nickel Exposed Colonies

Prior to conducting differential gene expression analysis, genes with no or very low expression were filtered and removed from the data set, leaving 13,970 genes from a total of 16,959. Among the identified genes, only 15 were downregulated and 39 upregulated in nickel treated colonies relative to control (FDR < 0.1) (Figure 1.8). The heatmap analysis depicts

distinct clustering of the nickel treated and non-treated samples. BlastX was performed against a non-restricted (nr) UniProt database to supplementally annotate gene terms (red text; Fig. 8) outside of what was available through eggNOG. Of the limited DEG list, 69% were successfully annotated using the above-described procedure (37 of 54). The most significantly over- and under-expressed genes in the nickel-treated group were *nas13* (logFC = 2.63; adjusted p-value < 0.05) and *colec11* (logFC = -3.39; adjusted p-value < 0.05), respectively.

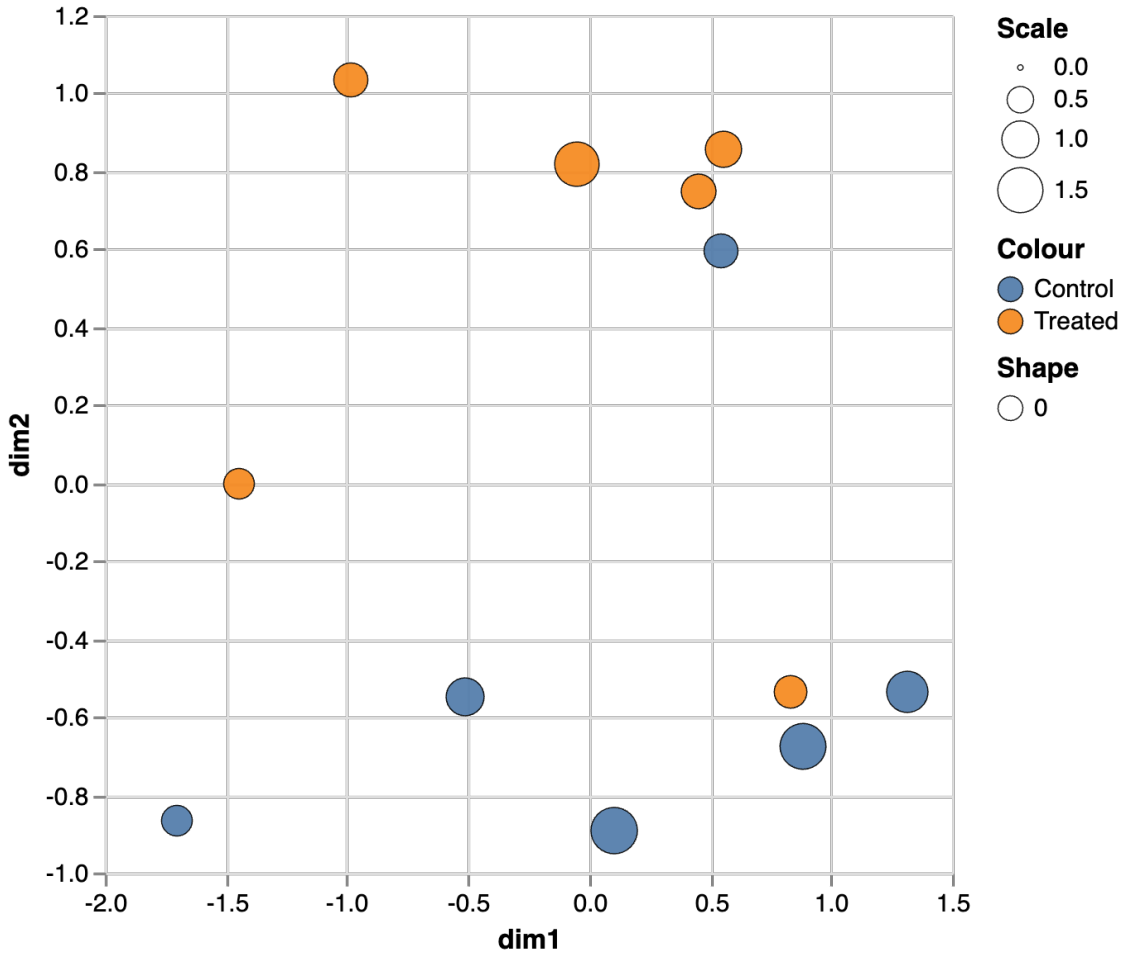

Figure 1.7. Visualization of similarity of gene expression profiles across control and nickel treated samples. Scale indicates relative weight of each sample to reflect within-group similarity.

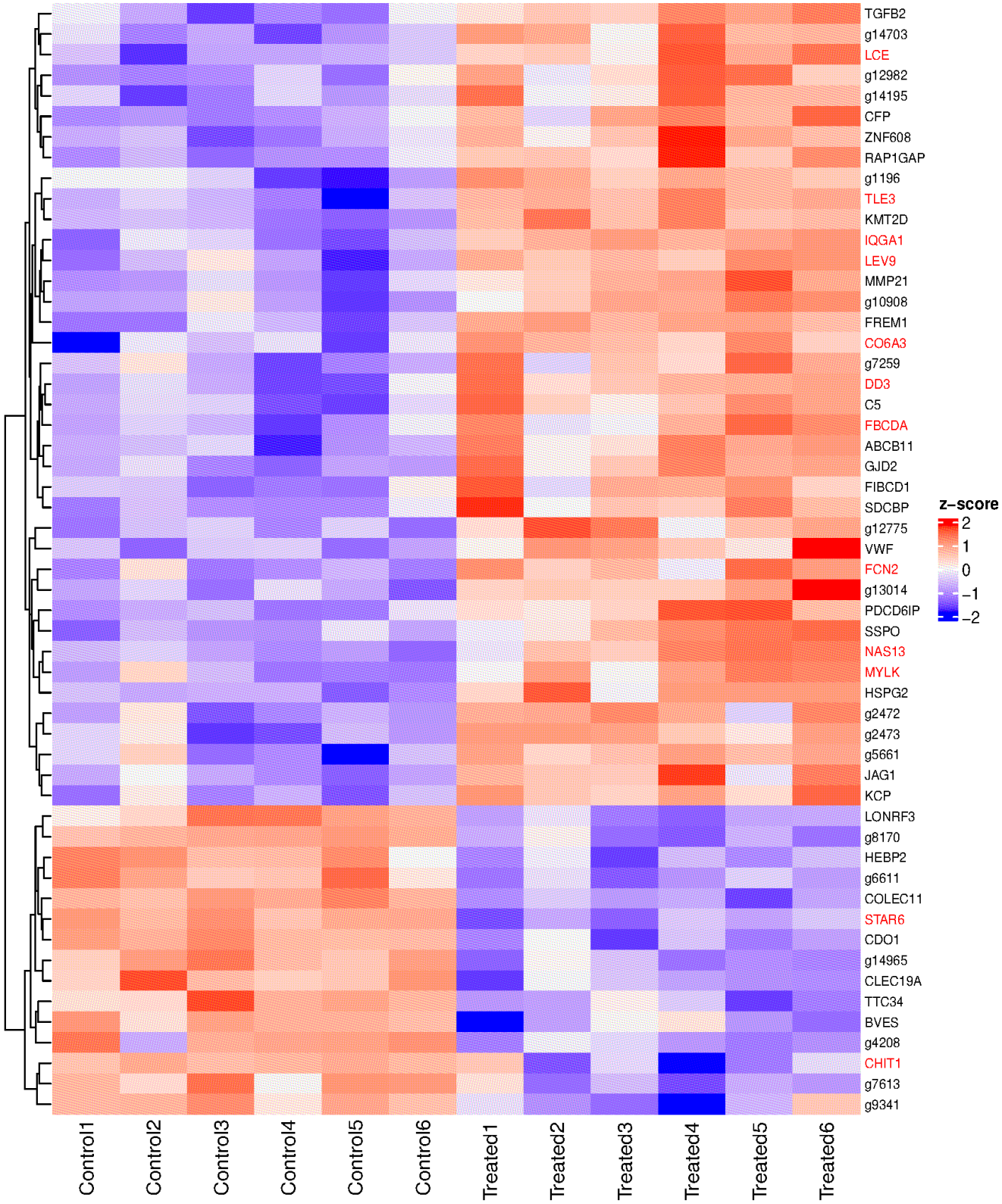

Figure 1.8. Clustering and heatmap of RNAseq data. Black gene symbols indicate annotation with *B. schlosseri* transcriptome. Red gene symbols indicate supplemental annotation using a non-restricted UniProt database.

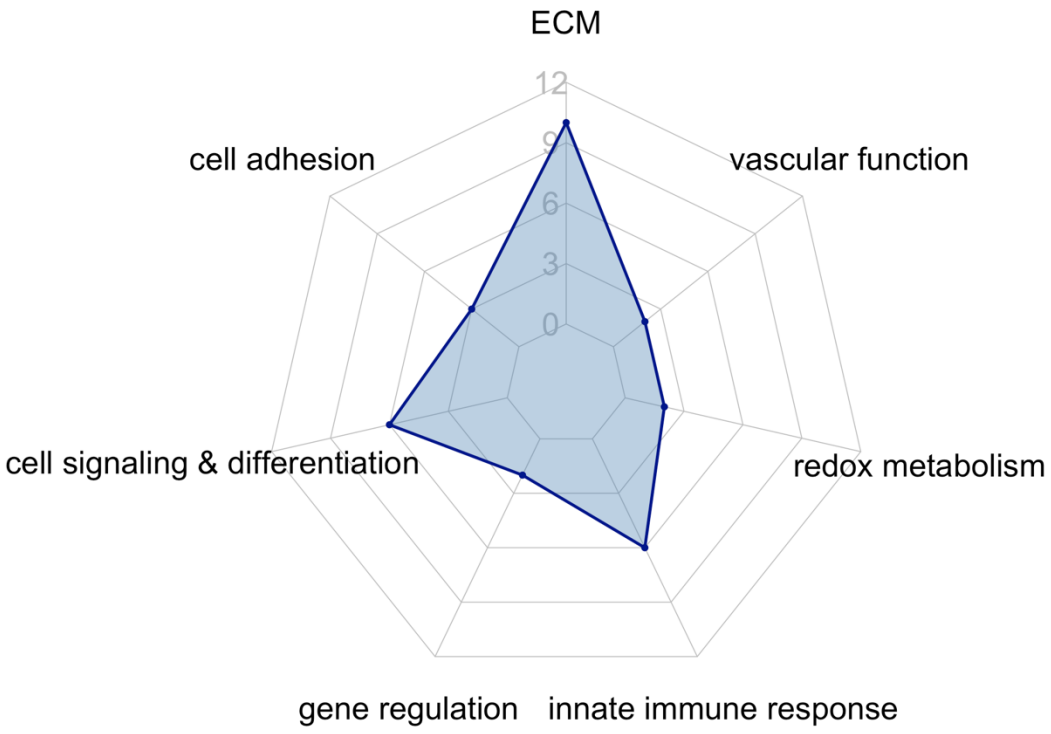

Figure 1.9. Functional distribution of annotated differentially expressed genes (DEGs). Spider plot illustrating the number of annotated DEGs following nickel exposure assigned to major functional categories. Of the 54 total DEGs identified, 37 were successfully annotated and are represented here. Categories include extracellular matrix (ECM), vascular function, redox metabolism, innate immune response, gene regulation, cell signaling and differentiation, and cell adhesion. Values indicate the number of DEGs associated with each functional category; genes with multiple functional annotations were assigned to their most relevant primary category.

1.3.6 ECM remodeling and basement membrane integrity

Extracellular matrix (ECM) organization emerged as the most prominent functional category comprising 30% of all the annotated DE genes (11 of 37, Figure 1.9). Nickel exposure increased the expression of several ECM components, including interstitial structural proteins such as collagen VI α3 (*col6a3*), SCO-spondin (*sspo*), fibrinogen C-domain–containing protein 1 (*fibcd1*), and LCE-family proteins. Nickel-exposed colonies also were found to have

upregulation of FRAS1-related extracellular matrix protein 1 (*frem1*) and heparan sulfate proteoglycan 2 (*hspg2*), transcripts involved in basement membrane assembly and integrity. Several enzymes involved in extracellular matrix reassembly were differentially expressed. Chitinase 1 (*chit1*) was downregulated while matrix metalloproteinase-21 (*mmp21*) and zinc metalloproteinase NAS-13 (*nas13*) were upregulated.

1.3.7 Detoxification and antioxidant transcriptional response

Heme-binding protein 2 (*hebp2*), associated with oxygen transport and oxidative stress signaling, and cysteine dioxygenase type 1 (*cdo1*), a regulator of intracellular cystine, were strongly downregulated in nickel exposed colonies. In contrast, a transcript annotated for the vertebrate ATP binding cassette subfamily B member 11 (*abcb11*), was upregulated.

1.3.8. Modulation of transcripts associated with cellular differentiation

Nickel exposure induced significant differential expression of several genes associated with regenerative signaling in *B. schlosseri*. Transcripts within and associated with the transforming growth factor beta (TGF-β) pathway were notably upregulated including *tgf-β2*, a key cytokine regulating cellular differentiation and migration. Moreover, additional regulatory components of the TGF-β/BMP axis were also upregulated including a Kielin/Chordin-like protein (*kcp*) homolog and a *tle*/*gro* family corepressor homolog. Beyond TGF-β associated pathways, *jag1*, a ligand of the Notch signaling cascade, was similarly upregulated in nickel exposed colonies. Collectively, these results represent an upregulation of multiple genes involved in developmental and differentiation signaling nickel exposure.

1.4 Discussion

1.4.1 B. schlosseri is highly tolerant to nickel exposure

Experimental nickel exposure of field-sourced *B. schlosseri* revealed a pattern of high survivorship, despite an eventual onset of morphological malformations including disrupted colonial architecture, vascular dilation, increased pigmentation, and weakened tunic integrity (Figure 1.3). Crude-LC_{50} nickel estimates of 177 mg L^{-1} at 24 hpe and 159 mg L^{-1} at 96 hpe (Figure 1.5), place *B. schlosseri* among the most nickel-tolerant marine invertebrates reported under full-strength artificial seawater conditions (Table 1.3) (Bryant et al., 1985; Calabrese et al., 1973; Eisler and Hennekey, 1977; Florence et al., 1994; Hajimad and Vedamanikam, 2013). ICP-MS analyses of field-sourced seawater from the City of Des Moines Marina detected low but measurable dissolved nickel concentrations (1.3 ± 1.9 µg L^{-1}, Ni-60, n = 6) at the time of specimen collection. These concentrations exceed observed trends (0.04-0.05 µg L^{-1}) of offshore Pacific Northwest surface water (Bates et al., 2021; Swam-Jaramillo et al., 2025), likely reflecting localized pollutant accumulation expected in enclosed marina conditions (Kenworthy et al., 2018). Nonetheless, field-site nickel concentrations remain several orders of magnitude lower than the concentrations required to induce mortality in this species (Figure 1.5). These findings provide a foundation for further refinement of nickel LC_{50} estimates for *B. schlosseri* within the upper thresholds of its observed tolerance range.

Although colonies survived under extremely high nickel concentrations, exposure to ≥100 mg L^{-1} nominal $NiCl_2$ induced distinct morphological changes beginning at 24-hpe including slowed hemolymph circulation, impeded primary bud development, failed zooid resorption, and overall blastogenic arrest (Figure 1.3A-3C). These phenotypes closely resemble

those observed following exposure to other oxidative stressors in *B. schlosseri*. For example, treatment with butylated hydroxytoluene (BHT), UV-B irradiation, and ionizing radiation all result in vascular dilation, halted zooid resorption, and arrest of blastogenesis (Qarri et al., 2020; Rinkevich and Weissman, 1990; Voskoboynik et al., 2002; Voskoboynik et al., 2004). In the cases of UV-B and BHT exposures, where colonies were also evaluated for their capacity to recover from stress, removal of the stressor was followed by coordinated apoptosis and phagocytosis of damaged tissues, with colonies resuming normal blastogenesis after one to two weeks (Qarri et al., 2020; Voskoboynik et al., 2002). Notably, mechanical disruption through zooidectomy or budectomy do not inherently halt blastogenesis (Rosner et al., 2019), indicating that blastogenic arrest is not triggered by structural disturbance alone, but instead reflects a stress-induced disruption to the physiological processes governing colonial blastogenesis.

Blastogenic progression in *B. schlosseri* is highly dependent on the coordinated apoptosis and phagocytic clearance of senescent zooids, which together enable the recycling of remnant macromolecular and nutrient resources to developing stage D primary buds (Franchi et al., 2016; Voskoboynik et al., 2004). Within the context of nickel-induced blastogenic arrest, suspension of complete zooid resorption and further primary bud growth, may reduce the metabolic demand and thus ROS generation occurring with blastogenic development (Cima et al., 2010; Franchi et al., 2017). As such, blastogenic arrest can be interpreted as part of a broader colonial maintenance strategy that reduces oxidative burden and potentially safeguards stem-cell niches from excessive oxidative damage to preserve future regenerative capacity (Qarri et al., 2020).

1.4.2 Modest non-monotonic response in SOD1 enzymatic activity with increasing nickel concentrations

Superoxide dismutase 1 (SOD1) is a primary cytosolic antioxidant enzyme that catalyzes the dismutation of superoxide radicals ($O_2^{\bullet -}$), a reactive oxygen species generated during normal cellular metabolism and elevated under oxidative stress (Sheng et al., 2014). Through conversion of superoxide into molecular oxygen (O_2) and hydrogen peroxide (H_2O_2), SOD1 functions as an upstream regulator of redox balance, with H_2O_2 subsequently detoxified by downstream antioxidant systems including catalase (CAT) and glutathione peroxidases (GPx) (Andrés et al., 2022). In *B. schlosseri* hemocytes, transcriptional modulation of these antioxidants has been reported to occur with blastogenesis-associated ROS accumulation and cadmium exposure (Franchi et al., 2017). However, to our knowledge, this study represents the first direct quantification of SOD enzymatic activity in *B. schlosseri* colonies under controlled experimental contaminant exposure.

SOD1 enzymatic activity in *B. schlosseri* exhibited a non-monotonic pattern across increasing nickel treatments, with modest elevation at 1 mg L^{-1} nominal $NiCl_2$ (0.29 mg L^{-1} Ni-60) and relatively reduced activity at 100 mg L^{-1} (27.64 mg L^{-1} Ni-60) comparable to control colonies after 96 hours of exposure (Figure 1.6). Only one other study has quantified SOD activity in this species, in which colonies were transplanted across coastal sites within the Lagoon of Venice (Tasselli et al., 2017). After 22 days of transplantation, colonies displayed varying levels of antioxidant activity, with elevated SOD activity for colonies transplanted to the more environmentally stressful location, characterized by higher temperature (17.7 °C), elevated pH (8.64), and a greater variety of competing benthic species (Tasselli et al., 2017). Together, these findings indicate that while SOD activity in *B. schlosseri* is responsive to environmental

stress and moderate contaminant levels, activity is constrained with exposure to elevated nickel concentration.

This non-monotonic pattern of SOD activity across increasing nickel concentration after an extended exposure period is similar to that of nickel-driven SOD activity in other marine invertebrates. In the copepod *Tigriopus japonicus*, SOD activity remained largely unchanged across nickel concentrations (0.125-3 mg L^{-1}) during the first four days of exposure. However, by day 12, SOD activity exhibited a non-monotonic pattern, with the highest activity observed at the intermediate nickel concentration (0.75 mg L^{-1}), while SOD activity at the highest concentration was comparable to that of lower-dose treatments (Wang and Wang, 2009). A similar trend was reported in Pacific abalone, where exposure to the highest tested concentration of $NiCl_2$ (nominal 0.4 mg L^{-1}) resulted in reduced SOD activity in hepatopancreas and gill tissues relative to lower concentrations (nominal 0.1 mg L^{-1}) after two weeks of exposure (Min et al., 2021). Although assessment of nickel-induced changes to SOD activity in the present study was limited to acute exposure (≤ 96-hours) rather than chronic, weeks-long treatments as in the studies above, the non-monotonic response observed here may represent a similar constraint in antioxidant functional capacity occurring over a shorter time frame at substantially higher nickel concentrations.

Notably, the absence of elevated SOD activity at the nominal 100 mg L^{-1} dose occurred concurrently with severe morphological disruption and health declines (Figure 1.3A-3C and 4), illustrating that SOD antioxidant activity is not further increased with increased physiological severity. In contrast, the elevated SOD activity observed at the lower nickel concentration indicates that nickel exposure elicits at least moderate levels of oxidative stress in this species. As such, antioxidant response against nickel-driven oxidative stress at the evaluated elevated

concentration may rely on a shift away from active enzymatic defense towards broader physiological constraints that reduce overall metabolic demand and endogenous ROS production, such as that which occurs through blastogenic developmental arrest.

1.4.3 Transcriptional landscape of nickel-exposed colonies

In contrast to the pronounced phenotypic changes observed with high nickel-dose exposure (Figure 1.3A-3C), the transcriptional response under these conditions revealed a more subtle but coordinated modulation of transcriptional programs (Figures 1.8 and 1.9). Notably, some of the most striking features of the transcriptomic landscape were defined not by what differed, but by what remained unchanged between control and nickel-treated *B. schlosseri*. Although SOD enzymatic activity was elevated at the lower nickel concentration, indicating that nickel exposure can elicit oxidative stress in *B. schlosseri*, SOD activity at 100 mg L^{-1} was comparable to control. Consistent with this, differential gene expression analysis between control and 100 mg L^{-1} nominal $NiCl_2$-treated colonies revealed no increased transcription of primary antioxidants at this elevated dose. Comparisons of SOD enzymatic activity with *sod* transcription of *B. schlosseri* colonies transplanted across different sites in the Lagoon of Venice demonstrated a decoupling of transcriptional gene expression and enzymatic activity where increased *sod* transcription did not occur at the most environmentally stressful site despite elevated SOD activity (Tasselli et al., 2017). In fact, *sod* transcription remained similar across both lagoon sites and was only upregulated in control laboratory reared colonies (Tasselli et al., 2017). In the context of experimental nickel exposure in other marine invertebrates, nickel elicits upregulation of antioxidant defense associated transcripts (e.g. *sod*, glutathione-S-transferase [*gst*], catalase [*cat*], and several metallothiones [*mt*]) at lower environmentally relevant concentrations within

the first 24-hours of exposure, with expression often declining over extended exposure durations (Banni et al., 2014; Dallas et al., 2013).

Yet these canonical antioxidant pathways were not differentially expressed in our study. Instead, across both control and nickel-exposed colonies, antioxidant defense associated mechanisms were equally elevated, including transcripts encoding for *sod* and glutathione peroxidase (*gpx*), primary enzymatic antioxidants. Moreover, no differential expression of glutathione synthetase (*gss*) and glutamate-cysteine ligase modifier subunit (*gclm*) was observed in nickel-treated colonies, both of which are catalysts required for glutathione synthesis, the primary endogenous non-enzymatic antioxidant (Dickinson and Forman, 2002). The lack of differential expression of antioxidant defenses in our data set could be a result of several competing, but non-mutually exclusive hypotheses. As both control and nickel-treated colonies were in late blastogenic stage D, a period of elevated oxidative stress, it may be that antioxidant networks operate at a constitutively elevated transcriptional baseline during late blastogenesis that are not further perturbed with exogenous oxidative challenge. Alternatively, the evaluated nickel concentration (100 mg L^{-1}) may represent a sufficiently high exposure level to elicit a rapid but transient transcriptional induction of antioxidant defenses that had already been attenuated by the 24-hour sampling time point. This interpretation is consistent with transcriptional trends observed in other nickel-exposed marine invertebrates where antioxidant transcripts initially increase but decline with prolonged exposure to lower environmentally relevant nickel concentrations.

Through its ROS-generating mechanisms, nickel can also act as an indirect genotoxin, producing varying degrees of DNA damage across an array of marine invertebrate species and their cell types (Akpiri et al., 2017; Dallas et al., 2013; Gallo et al., 2016). In nickel-exposed *B.*

schlosseri, however, many of the expected gene targets associated with genotoxic stress were not differentially expressed. Instead, transcripts involved in DNA-damage signaling and repair (e.g. ataxia-telangiectasia and rad3-related [*atr*] and ataxia-telangiectasia mutated [*atm*]) were similarly upregulated in both control blastogenic stage D and nickel-exposed colonies. These findings indicate that exogenous nickel exposure does not induce additional transcriptional activation of canonical DNA damage signaling and repair pathways beyond the elevated baseline observed during stage D.

Prior work directly measuring DNA fragmentation in *B. schlosseri* demonstrated that control blastogenic stage D ramets and BHT-induced clonal ramets under blastogenic arrest exhibited similar levels of DNA damage, suggesting that DNA fragmentation is intrinsically elevated during this developmental stage and is not increased during perturbation to redox homeostasis (Voskoboynik et al., 2004). In contrast, acute UV-B irradiation significantly increased DNA fragmentation in *B. schlosseri* hemocyte cultures, yet no detectable DNA repair occurred within a 24-hours of recovery (Svanfeldt et al., 2014). Notably when *B. schlosseri* is allowed to recover from BHT or UV-B irradiation, colonies eliminate all compromised zooids and most, if not all, primary buds (Qarri et al., 2020; Voskoboynik et al., 2002). As such the findings of the present study extend upon a previously proposed model in which *B. schlosseri* colonial genomic integrity is primarily maintained through apoptosis and phagocytic clearance of damaged somatic tissues, rather than through extensive DNA damage repair (Qarri et al., 2020; Svanfeldt et al., 2014). Within this framework, the absence of further transcriptional induction of canonical DNA repair genes in nickel-exposed colonies may reflect a colonial maintenance strategy in which transcriptional amplification of DNA repair pathways does not scale under

oxidative challenge and instead colonial genomic stability is preserved through selective removal of compromised tissue upon removal of the stressor.

1.4.4 Adjustments in redox metabolism and routes for nickel detoxification

Rather than broad differential expression of primary antioxidant enzymes or glutathione biosynthesis genes, nickel exposure resulted in selective modulation of redox-associated transcripts. Cysteine dioxygenase type 1 (*cdo1*) was significantly downregulated in nickel-exposed colonies. CDO1 catalyzes the oxidation of cysteine to cysteine sulfinic acid, the first step in taurine biosynthesis (Dominy et al., 2007). Taurine functions as an osmolyte, and in other marine invertebrates CDO1 is transcriptionally upregulated under both hypo- and hypertonic salinity stress (e.g., *Sinonovacula rivularis* and *Sinonovacula constricta*), reflecting CDO1's role in osmoregulation (Liang et al., 2025; Yihua et al., 2024). However, cysteine is one of the least abundant intracellular amino acids and is highly conserved within protein functional sites due to the unique nucleophilicity and metal-binding properties of its thiol group (-SH) (Poole, 2015). Given this constrained availability, downregulation of *cdo1* under nickel exposure may reflect a shift in cysteine allocation away from osmolyte synthesis and toward conservation for thiol-based redox buffering. This interpretation is consistent with mechanistic evidence from mammalian *in vitro* systems in which CDO overexpression in HepG2/C3A cells reduced intracellular cysteine and glutathione pools, ultimately resulting in increased cadmium toxicity (Dominy et al., 2007).

Although *B. schlosseri* is well known to bioaccumulate metals at concentrations exceeding that in the environment, nickel is among the least accumulated trace metals in this species (Guillén Matus et al., 2024). Consistent with this, canonical metal-sequestration pathways, including several metallothionein's, were not differentially upregulated under nickel

exposure. Metallothionein's are cysteine-rich proteins that bind trace metals through thiol groups and play an essential role in trace metal intracellular accumulation and detoxification in marine invertebrates (Fan et al., 2015). Together, the absence of transcriptional metallothionein induction and the comparatively low nickel bioaccumulation shown in prior studies suggest that *B. schlosseri* may reduce intracellular nickel through mechanisms alternative to thiol-based sequestration.

The transcript annotated as ATP-binding cassette transporter subfamily B member 11 (*abcb11*) was significantly upregulated in nickel exposed colonies. While a vertebrate ABCB11 ortholog is absent in marine invertebrates (Luckenbach and Epel, 2008; Shipp and Hamdoun, 2012), the annotation likely represents an ABCB-like transporter, similar to those described in the sea urchin, *Strongylocentrotus purpuratus* (Shipp and Hamdoun, 2012). ABCB-family transporters in marine invertebrates broadly mediate efflux of metals, ions, and xenobiotics, with loss-of-function studies demonstrating that their disruption greatly impairs metal efflux capabilities (Della Torre et al., 2014; Vyas et al., 2022). In the context of nickel exposure in *B. schlosseri*, the lack of metallothionein transcriptional induction and upregulation of an ABCB-like transcript suggests that nickel handling and detoxification may rely more predominantly on transporter-mediated efflux than on thiol-based chelation. However, further functional studies are needed to confirm the centrality of efflux in this species' nickel detoxification response.

1.4.4 Nickel induced colonial ECM and vascular remodeling

Nickel-exposed colonies showed upregulation of pathways associated with extracellular matrix (ECM) remodeling, basement membrane integrity, and vasculature dynamics. In *B. schlosseri* vascular vessels are formed from ectoderm-derived epithelium, where vessel lumens are lined with basal lamina and apical surfaces face the tunic (Rodriguez et al., 2017). The

vasculature in this species is thus closely integrated with the surrounding ECM and tunic, forming a ramified extracorporeal network linking a colony's zooids (Rodriguez et al., 2021). The morphological vascular shifts observed in nickel-exposed colonies, consisting of dilated but intact vessels, slowed but persistent hemolymph flow, and occasional localized hemolymph leakages suggests that nickel exposure compromises vascular wall stability without causing complete vascular regression.

Indeed, transcriptional signatures were consistent with these observations. *Vwf*, a marker of vascular injury in *B. schlosseri* (Oren et al., 2008), was upregulated. A *bves*-like adhesion transcript whose vertebrate homolog is required for cell-cell adhesion and barrier integrity (Brand, 2005; Osler et al., 2006), was downregulated, potentially reflecting reduced barrier cohesion in *B. schlosseri*. Furthermore, as basement membrane integrity is known to be essential for preventing complete vascular regression in colonial ascidians (Rodriguez et al., 2021; Rodriguez et al., 2021), increased expression of associated transcripts (e.g.HSP2 and FREM1) in nickel-exposed colonies suggests potential compensatory reinforcement of basement lamina domains across impacted tissues.

Matrix metalloproteases, MMP21 and NAS13, key mediators of ECM turnover, were also upregulated, suggesting active remodeling of interstitial matrix components. Upregulation of several cytoskeletal and adhesion-associated regulators (*rap1gap*, *mylk*, *iqgap1*, and *sdcbp*) further supports a model of altered epithelial tension and cell–matrix interactions (Du et al., 2020; Jaśkiewicz et al., 2018; Johnson et al., 2020; Shi et al., 2025; Yamaoka-Tojo et al., 2004), which aligns with the observed ampullar dilation and slowed hemolymph movement.

These findings indicate that nickel exposure elicits a coordinated ECM and epithelial remodeling response in *B. schlosseri*, affecting both interstitial matrix architecture and basement

membrane domains. This aligns with previous work demonstrating the central role of ECM dynamics in maintaining tissue integrity, hemocyte migration, and blastogenic transitions during whole-body regeneration and metal-induced stress (Leprêtre and Kültz, 2025; Ricci et al., 2022).

1.4.5 Disruption in cellular differentiation signaling under nickel exposure and reduced apoptosis

Several genes associated with cell fate specification, developmental signaling, apoptosis regulation, and wound healing were significantly upregulated in nickel-exposed colonies, including components of the TGF-β superfamily and Notch signaling pathways. Within the TGF-β regulatory axis, transforming growth factor beta 2 (*tgf-β2*) and several modulators of TGF-β signaling were significantly upregulated in nickel-treated colonies, including syndecan binding protein (*sdcbp*), kielin/chordin-like protein (*kcp*), and transducin-like enhancer of split (*tle*). TGF-β2 is a cytokine involved in various processes of development and regeneration across vertebrates and invertebrates, regulating cellular differentiation, migration, and apoptosis (Lévesque et al., 2007; Wu and Hill, 2009). In the tunicate species *Botrylloides leachii* and *Ciona robusta*, upregulation of TGF-β and associated signaling enhancers play a critical role during initial wound healing and regeneration (Spina et al., 2017; Zondag et al., 2016). In *B. schlosseri*, inhibition of gene regulators in the TGF-β pathway results in colonial malformations including disrupted zooid architecture (Rosner et al., 2014), similar to the nickel-induced morphological disruptions observed in the present study. Together, this evidence indicates that the TGF-β axis is a conserved pathway across tunicates that is critical in regulating cellular differentiation, tissue growth, regeneration, and colonial structure. While SDCBP is associated with TGF-β signal amplification (Zhang et al., 2025), KCP and TLE typically function as

suppressors of TGF-β signaling and instead are enhancers of bone morphogenetic proteins (BMPs) (Lin et al., 2005; Zhang and Dressler, 2013; Zondag et al., 2016).

In vertebrates, KCP is a secreted modulator of the TGF-β superfamily that antagonizes TGF-β signaling while enhancing BMP activity (Lin et al., 2005). TLE is also a well-recognized corepressor of TGF-β signaling in both mammalian systems (Zhang and Dressler, 2013), and invertebrate systems where TLE is homologous to groucho (GRO) (Zondag et al., 2016). Notably in the colonial tunicate *Botrylloides leachii*, *gro* downregulation (-3.1 fold) occurred concurrently with *tgfb2* upregulation (1.9 fold) during whole body regeneration (Zondag et al., 2016). This contrasting expression pattern between *B. leachii* undergoing active growth and *B. schlosseri* in a blastogenic arrested state suggests that transcriptional control of these cellular differentiation and tissue growth regulators can vary across developmental contexts but nevertheless converges on modulation of downstream developmental signaling pathways.

Modulation in cell fate signaling extended beyond the TGF-β pathway, where jagged1 *jag1*, a ligand in the Notch cascade (Grochowski et al., 2016), was significantly upregulated in nickel exposed colonies. Notch and TGF-β signaling are intimately connected but distinct pathways. In mammalian *in vitro* systems, TGF-β induces transcription of *jag1*, initiating downstream Notch signaling, which in turn confers a positive feedback loop by upregulating several TGF-β signaling components (Valdez et al., 2012; Zavadil and Cermak, 2004). The cross-talk between TGF-β and Notch signaling, has been proposed to be a key regulator of cellular quiescence (Niimi et al., 2007; Valdez et al., 2012), keeping cells from entering the cell cycle.

In addition to the transcriptional and phenotypic evidence of suspended cell growth for developing primary buds, *B. schlosseri* zooids also failed to be resorbed suggesting a disruption

to the typical apoptotic and phagocytic clearance that occurs with blastogenesis. Consistent with this observation, programmed cell death 6 interacting protein (*pdcd6ip*) was upregulated in colonies exposed to nickel. PDCD6IP overexpression is involved in the activation of apoptosis pathways in mammalian systems (Strappazzon et al., 2010). Moreover, in stage D resorbing zooids of *B. schlosseri*, *pdcd6ip* is downregulated relative to active filter-feeding zooids, suggesting a potential association between PDCD6IP expression and the suppression of apoptosis during earlier blastogenic stages (Anselmi et al., 2023). Within this context, *pdcd6ip* upregulation in late blastogenic stage nickel-exposed colonies contrasts with the downregulation observed in stage D control colonies, suggesting a transcriptional shift consistent with the suspension of blastogenesis-associated apoptosis under exogenous oxidative stress.

Collectively, these transcriptional patterns suggest that nickel exposure perturbs highly conserved developmental signaling networks that coordinate the cellular differentiation, proliferation, and apoptosis underlying blastogenic takeover in this species. The simultaneous modulation of these pathways indicate that nickel stress may shift colonies toward a state of reduced cellular turnover, characterized by suspended apoptosis and halted developmental progression, consistent with the observed phenotypic changes observed during blastogenic arrest (Figure 1.3). These findings further support the proposed model in which *B. schlosseri* circumvents extensive antioxidant and DNA damage repair responses in favor of mitigating oxidative stress through modulation of colony-wide developmental programs that limit associated metabolic and oxidative activity. Within this framework, the coordinated modulation of transcriptional cellular differentiation and apoptotic signaling may function to pause generational turnover, thereby reducing endogenous ROS generation and overall oxidative burden to preserve cellular integrity under elevated nickel exposure.

1.5 Conclusion

This study evaluated the heavy metal tolerance of *B. schlosseri* under acute nickel exposure. While colonies exhibited high survivorship even at elevated concentrations, this tolerance was accompanied by pronounced disruptions to physiological and developmental processes. Although colonies persisted in the second highest dose of nickel (II) chloride (100 mg L^{-1}), exposure resulted in halted primary bud growth progression, impaired hemolymph circulation, and failure of zooid resorption across all stages of the blastogenic cycle. Together, these phenotypic changes indicate that nickel exposure disrupts colony-level developmental processes associated with blastogenesis and generational turnover.

At the molecular scale, nickel elicited coordinated but limited transcriptional changes. Although antioxidant and genotoxic defenses associated with canonical metal response were not strongly induced by elevated nickel exposure, pathways associated with cysteine allocation and xenobiotic efflux were upregulated, signifying a limited detoxification response through metal sequestration. Instead, nickel exposure resulted in transcriptional changes to cellular differentiation and apoptotic signaling alongside restructuring of extracellular matrix and vasculature components. Collectively, these results suggest that colonies exposed to nickel during late blastogenesis rely less on transcriptional induction of classical antioxidant or DNA repair pathways and instead respond to nickel stress through modulation of developmental signaling and colony-wide remodeling. Such responses may stabilize cellular homeostasis under oxidative stress at the cost of colony structure and asexual reproduction. In *B. schlosseri* this model has been proposed to specifically preserve long-term colonial viability and stem-cell lineages for similar-stress induced disruption to somatic tissues of the colony (Qarri et al., 2020; Svanfeldt et al., 2014).

More broadly, these findings highlight an alternative strategy of oxidative stress tolerance in a colonial organism, where modulation of developmental timing and tissue turnover may mitigate oxidative burden without extensive activation of antioxidant pathways. This work provides a framework for exploring how cellular fate decisions are coordinated under environmental stress, offering insights into the gene networks that regulate transitions between cellular quiescence and growth. Moreover, characterizing the regulatory responses invoked under stress in a cosmopolitan colonial ascidian provides greater understanding of the mechanisms that may contribute to stress tolerance in other invasive marine organisms.

Chapter 2

2.1 Introduction

The colonial marine tunicate, *Botryllus schlosseri*, is a widely used experimental model employed for more than seventy years across the disciplines of developmental, immunological, and cellular biology (Burnet, 1971; Manni et al., 2019; Rinkevich and Rabinowitz, 1997; Sabbadin, 1955). Although much of our understanding of *B. schlosseri* biology is derived from *in vivo* research (Ben-Hamo and Rinkevich, 2021; Franchi et al., 2016; Kültz et al., 2025; Rodriguez et al., 2021), i*n vitro* studies using cultured *B. schlosseri* cells have expanded insights into the processes of cellular senescence (Rabinowitz and Rinkevich, 2004), stemness (Rabinowitz and Rinkevich, 2011), and ecotoxicological responses (Kamer and Rinkevich, 2002). As such, cell cultures provide an invaluable complementary system for investigating cellular processes such as growth and stress responses under controlled experimental conditions that are difficult to isolate in whole organisms. Together, these studies highlight the investigative potential of *in vitro* approaches for *B. schlosseri* and underscore the importance of continued methodological development. Thus far, cell cultures for this species have been initiated from several tissue types including embryonic (Rinkevich and Rabinowitz, 1994), hemolymph (Qarri et al., 2022; Qarri et al., 2023; Rinkevich and Rabinowitz, 1993), and epithelial tissues (Rabinowitz and Rinkevich, 2003; Rabinowitz and Rinkevich, 2004; Rabinowitz and Rinkevich, 2011; Rabinowitz et al., 2009; Rinkevich and Rabinowitz, 1997). Although cell culture studies of *B. schlosseri* remain scarce overall, most published efforts have focused on methodological

development for culturing epithelial cells, with many of these foundational studies conducted more than a decade ago and not reassessed since.

Nonetheless, this prior work set a critical foundation for primary epithelial cell culture in *B. schlosseri*, identifying key determinants of cell culture success and describing the cellular morphology and growth behavior *in vitro*. An important factor found to influence cell culture success was the state of colonial asexual development, also known as the blastogenic stage, at the time of tissue isolation (see Background, Supplemental Figure 1). In particular, primary buds isolated from colonies in stage D, the final blastogenic stage preceding generational takeover in which senescent zooids are resorbed and primary buds complete their maturation, produced adherent epithelial monolayers more frequently than buds isolated from earlier blastogenic stages (Rabinowitz and Rinkevich, 2003; Rabinowitz and Rinkevich, 2004). Cultured primary bud explants typically also formed hollow spherical structures composed of a single epithelial layer that either persisted in suspension or later settled to produce adherent epithelial sheets (Rabinowitz and Rinkevich, 2003; Rabinowitz et al., 2009). Once adhered to the culture substrate, epithelial monolayers expanded for approximately 24-72 hours before ultimately detaching and deteriorating, indicating that although short-term epithelial growth could be achieved *in vitro*, sustained cellular proliferation remained limited (Rabinowitz and Rinkevich, 2003; Rinkevich, 2011; Rinkevich and Pomponi, 2025).

As such, despite a clear potential for *in vitro* systems to advance our knowledge of *B. schlosseri* biology, progress remains constrained by the transient nature of primary cell cultures and the continued absence of an immortalized, continuous cell line (Rinkevich and Pomponi, 2025). Continuous cell lines for any marine invertebrate remain extremely scarce overall (Domart-Coulon and Blanchoud, 2022; Rinkevich and Pomponi, 2025). Only two continuous

marine invertebrate cell lines have been reported in the literature for one species in each of the following phyla: Cnidaria (Kawamura et al., 2021) and Porifera (Hesp et al., 2023). To date, it remains unclear why continuous cell lines for marine invertebrates are difficult to establish, despite the retention of lifelong pluripotent and totipotent adult stem cells and extensive regenerative capacity observed across various taxa (Rinkevich, 2005; Rinkevich, 2011; Rinkevich and Pomponi, 2025).

Several reviews for advancing continuous cell line development in marine invertebrates have proposed the integration of multi-*omics* tools to optimize cell culture parameters and improve characterization of cellular responses to *in vitro* conditions (Domart-Coulon and Blanchoud, 2022; Rinkevich, 2005; Rinkevich and Pomponi, 2025). The effectiveness of this approach has been demonstrated in primary lymphoid cells of Kuruma prawn (*Marsupenaeus japonicus*). In this system, transcriptional downregulation of VEGF3 and its receptor over culture progression guided targeted, time-dependent media supplementation that recovered VEGF signaling and extended cell culture longevity (Tsuchiya et al., 2023). Despite the potential utility of this approach, the application of -*omics* based assessments remains limited across marine invertebrate cell cultures efforts (Kawamura et al., 2021; Tsuchiya et al., 2023) and has not yet been integrated in cell culture attempts for any cell type of *B. schlosseri*. This absence represents a critical gap, particularly given the extensive genomic and transcriptomic resources available for *B. schlosseri* and highlights the need for renewed and integrative methodological development for cell culturing of this species.

In addition to the limited application of -*omic* tools for improved longevity of primary cell cultures, there has been limited methodological development for targeted immortalization strategies in marine invertebrates. For mammalian primary cell culture systems, cellular

immortalization has frequently been achieved through the application of chemical immortalizing agents (Desaulniers et al., 2023; Mo et al., 2021; Trott et al., 1995; Tveito et al., 1989). Immortalizing agents can induce genomic instability, generating novel proliferative genotypes that, under selective culturing, support sustained cell division. When such genome reorganization enhances cell survival under stress, this process, known widely as stress-induced evolution (SIE), can stabilize adaptive phenotypes within the cell population and facilitate establishment of an immortalized cell line (Mojica and Kültz, 2022; Wagner et al., 2019). Despite the prevalence of this cellular immortalization strategy in mammalian systems, the use of immortalizing agents remains under-evaluated in marine invertebrate continuous cell line development (Crane, 1999; Hetrick et al., 1981).

Nickel, in particular, has been demonstrated to promote immortalization in mammalian cell cultures that otherwise exhibit low spontaneous cellular immortalization transformation rates. In the presence of nickel, cultured mammalian cells incurred significant clastogenic damage and increased proliferative rates without extensive cell death (Trott et al., 1995), reflecting the weakly genotoxic nature of nickel, which primarily induces DNA damage at the chromosomal level through indirect mechanisms, including oxidative stress, disruption of DNA repair machinery, and epigenetic alterations such as DNA methylation and histone modifications (Costa, 2019; Guo et al., 2019; Huang et al., 1993; Martinez-Zamudio and Ha, 2011; Permenter et al., 2011; Trott et al., 1995).

In marine invertebrates, nickel toxicity has primarily been studied at environmentally relevant concentrations ranging between 0.1 to 250 $\mu g\ L^{-1}$, comparable to levels detected in coastal surface waters (Blewett and Leonard, 2017). At these concentrations, nickel impairs embryonic development, ionoregulation, respiration, and generates oxidative stress in marine

invertebrates (Attig et al., 2010; Blewett and Leonard, 2017; Blewett and Wood, 2015; Blewett et al., 2016; Gissi et al., 2018). In addition, similar, sublethal concentrations of nickel have been shown to generate DNA damage in marine invertebrates through many of the same mechanisms described in mammalian systems (Akpiri et al., 2017; Dallas et al., 2013; Millward et al., 2012). However, nickel's potential relevance as an SIE immortalizing agent in *B. schlosseri* primary epithelial cells has never been investigated.

In this context, the present study aimed to: (a) re-evaluate and optimize epithelial cell culturing methodologies for *B. schlosseri*, (b) characterize nickel-induced lethality and morphological responses in *B. schlosseri* primary epithelial cells, and (c) isolate RNA for bulk RNA-sequencing from cultured epithelial cells acutely exposed to a sublethal nickel concentration. Through this scaffolded and integrative approach, we sought to establish a highly robust and reproducible methodology for *B. schlosseri* epithelial cell culturing that could support transcriptomic characterization of cellular responses to nickel. Altogether, this study addresses a critical knowledge gap and provides a foundation for future investigations leveraging SIE as a tool for cellular immortalization in this species.

2.2 Methods

2.2.1 Animal Field Collection and Husbandry

Colonies of *Botryllus schlosseri*, were collected from floating docks at the City of Des Moines Marina (47°23'51.18"N, 122°19'46.01"W), Des Moines, Washington, USA over a period of approximately 5 months from April to September of 2025. *B. schlosser*i colonies growing on Pacific blue mussels (*Mytilus sp*.) were collected from floating docks (up to 36 cm depth), placed in 400 mL containers with marina seawater, transported to the University of Washington,

Tacoma (30.7 km transportation distance) in an empty cooler back to minimize temperature fluctuations in containers (~17-20 °C).

Upon intake, colonies were immediately processed for acclimation to the University of Washington (UW), Tacoma's recirculating artificial seawater system (RAS). Specifically, colonies were gently peeled from Pacific blue mussel shells with a sterile razor blade, transferred to glass Petri dishes with field-site seawater, and evaluated under a stereomicroscope (Nikon, SMZ-745T), with only healthy colonies retained based on tunic integrity, normal zooid organization, and visible ampullae extension (Figure 2.1). Selected colonies were tied to 76.2 × 50.8 × 1.2 mm glass slides with cotton thread and drip-acclimated for one hour to artificial seawater (ASW) prepared by dissolving Red Sea Salt (Red Sea, USA) in deionized water and maintained in the UW Tacoma recirculating artificial seawater system (RAS; 18 °C, 30 ppt, pH 8.0). Colonies were held at a stocking density of 12 genets per 5-liter plastic container in the RAS and fed every other day a mixture of Liquid RotiRich (Florida Aqua Farms) and Reef Phytoplankton (Seachem). Colonies were maintained in the RAS for approximately 10 days, during which blastogenic cycles were tracked to target tissue excision of colonies entering stage D.

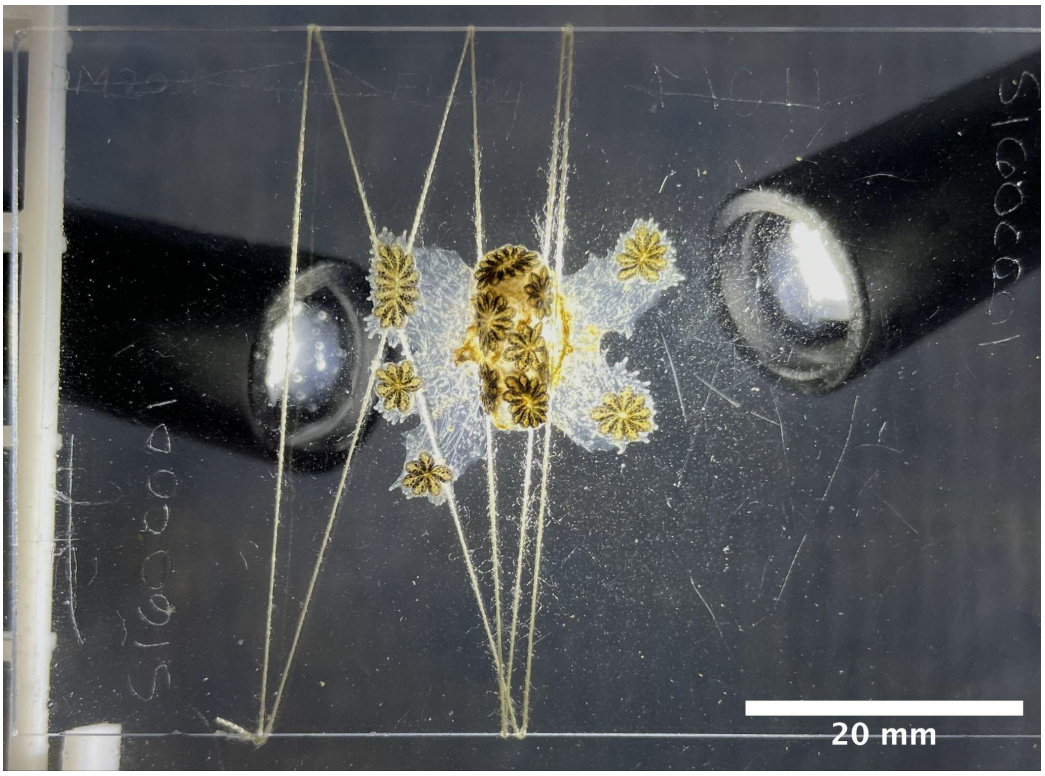

Figure 2.1. Exemplary field sourced *B. schlosseri* colony that may be used in cell culturing. Here some star-system zooid clusters glide from the center portion of the colony and adhere to the glass slide using their terminal ampullae. Markers of good health include flat and clear tunic as well as normal pigmentation across the zooids and ampullae.

2.2.2 Tissue Isolation and Primary Cell Culture Maintenance

Unless otherwise stated, all reagents were obtained from Thermo Fisher Scientific (Gibco, USA). Briefly, all solutions required for tissue isolation and cell culturing were prepared prior to the start of dissection. A 2.8X PBS solution, isosmotic with seawater (~750 mOsm kg^{-1}), was prepared from a 10X PBS stock in cell culture grade water. DMEM media was supplemented with 5% fetal bovine serum (One Shot™; Gibco; Thermo Fisher Scientific; Cat. No. A5670401), 1% penicillin-streptomycin, 1% amphotericin B, and 0.5% gentamicin, then subsequently filtered through a 0.2 µm bottle-top filtration system (Corning). Sterile moderately hyposaline artificial seawater (sterile-ASW) was prepared in Milli-Q water using Red Sea Salt (Red Sea, USA) to 25 ppt and

sterilized by vacuum filtration (0.2 µm bottle-top filter; Corning). Complete tunicate culture media (TCM) was prepared freshly for each culturing attempt from a 1:1 mixture of supplemented media and sterile-ASW for a final osmolality of ~710 mOsmo/kg and pH 8.1.

Large colonies of ≥100 zooids identified to be in late blastogenesis were starved 24-hours before progressing into blastogenic stage D. Upon entering mid to late stage D, where primary buds appeared to be equal or slightly larger than resorbing zooids, colonies were transferred to a 15 cm glass petri dish with fresh artificial seawater for dissection. Under a dissecting microscope, the tunic around the zooid bodies was carved using the needle tips of a pair of sterile, 28-G insulin needles. Exposed zooids and primary buds were excised with fine microdissection forceps and set into separate cell strainers immersed in 10 mL of ASW supplemented with 0.1% amphotericin B. Following tissue collection, zooids and buds were transferred separately into 1.5-mL microcentrifuge tubes pre-aliquoted with 1 mL of TCM.

In a biosafety cabinet, 1.5-mL tubes containing zooids and buds were removed of TCM then rinsed in triplicate with 2.8X PBS and transferred in suspension into bud or zooid - designated culture dishes. Zooids and buds were then evenly distributed using sterilized microforceps into uncoated, cell-culture–treated wells or dishes at a density of 17 tissue pieces per cm^2. Tissues were allowed to partially desiccate for approximately 10 min to ensure stable adhesion prior to media addition (Figure 2.2). Complete-TCM was then added dropwise in between tissue pieces to minimize tissue displacement (670 µL per cm^2). Plates were incubated in an environmental chamber set to 20 °C, 90% humidity, no photoperiod, and no CO_2 supplementation. After a minimum of 18 to 24-hours and up to 3 days post-seeding, tissue

fragments were removed, revealing adherent epithelial sheet monolayers. Cultures kept for longer periods were given 50% media changes every week.

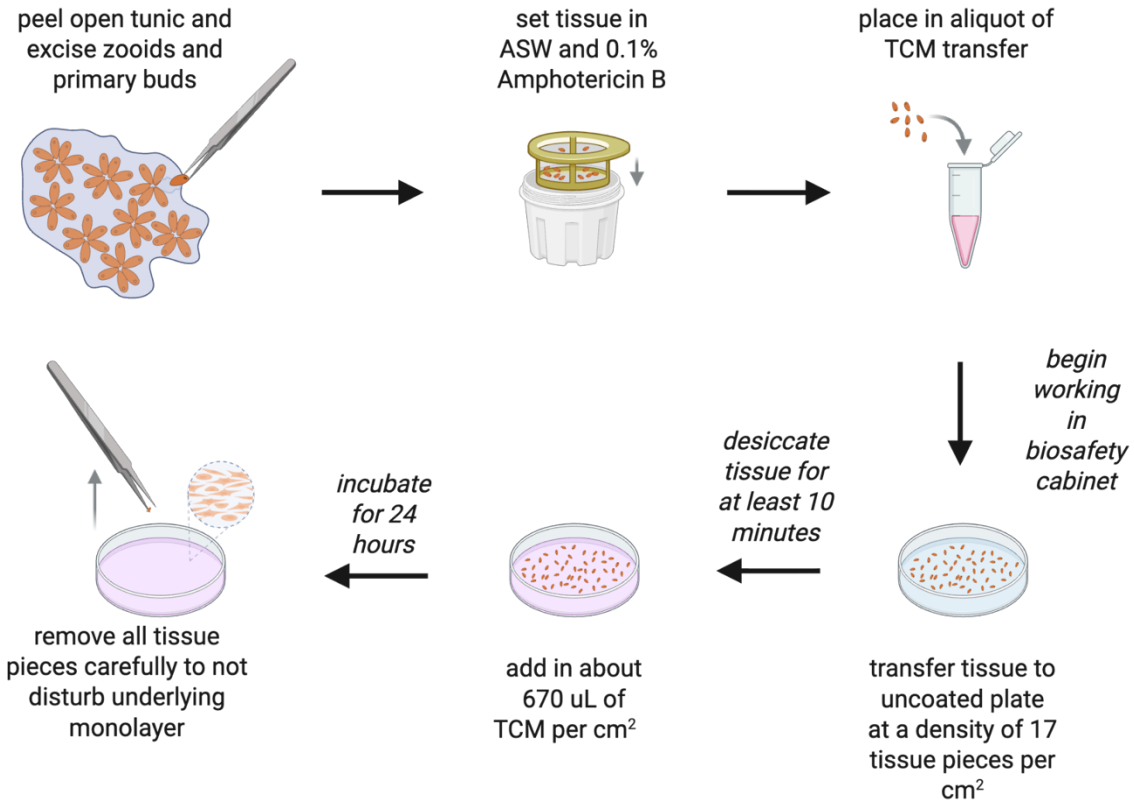

Figure 2.2. Graphical schematic of primary epithelial cell culture initiation from *B. schlosseri* colony. Created in BioRender. Valdivia, C. (2026) https://BioRender.com/uwoirc8, licensed under CC BY 4.0.

2.2.3 Pilot study evaluating pre-nickel treatment of B. schlosseri prior to primary epithelial cell isolation

From a stock solution of 1 g L^{-1} nickel (II) chloride ($NiCl_2$; Sigma-Aldrich, Cat. No. 339350) prepared in Milli-Q water (18.2 MΩ·cm resistivity), nominal concentrations of 5 and 45 mg L^{-1} nickel (II) chloride dilutions were freshly prepared in 1000 mL of aerated artificial seawater (ASW, 33 ppt, pH 8.2). After spiking with the appropriate volume of stock nickel (II)

chloride, solutions were thoroughly mixed and left to equilibrate for 30 minutes. Aliquots of 250 mL were then distributed into exposure vessels (473 mL wide-mouth mason jars).

Twelve *B. schlosseri* colonies of 5 to 9 zooids, various blastogenic stages, and acclimated to lab conditions for 7 days were randomly distributed across nickel-spiked or control ASW exposure vessels. Colonies were then placed in an environmental chamber set to a 12:12 photoperiod and maintained at 20°C over the 24-hour exposure. At the end of the exposure, colonies were rinsed with freshly prepared ASW and dissected for their zooids and buds. Colonies in stage D were dissected for only their primary buds, stage C for both primary buds and zooids, and stages A and B for only their zooids. This variability in the ratio of zooid versus bud isolation across stages resulted from the technical challenges of isolating primary buds of earlier stages due to their small size. Zooids and buds were isolated as described in section 2.2.2. Tissue explants from the same genet were seeded together in the same well on a 12-well plate. Tissue explants were monitored over a 72-hour period with tissue attachment and monolayer growth outcomes were recorded daily.

2.2.4 Nickel (II) chloride range-finding study for primary epithelial cell cultures

A stock solution of 5 g L^{-1} nickel (II) chloride ($NiCl_2$; Sigma-Aldrich, Cat. No. 339350) was prepared in cell culture grade water then subsequently filtered through a sterile luer-lok syringe filter (0.22 μm). Aliquots of complete TCM were spiked with calculated volumes of $NiCl_2$ stock solution to generate nominal concentrations of 0.2, 2, 20, 200, and 2000 mg L^{-1}. $NiCl_2$-spiked media was prepared fresh for each biological replicate to ensure consistency across exposure days and was stored at 4 °C for no longer than 4 days.

Following the above-described procedure for tissue isolation, 3 genets of *B. schlosseri* were utilized to conduct a range-finding study for epithelial cells exposed to nickel (II) chloride.

Tissue from a single genet was evenly distributed (17 tissue pieces per cm^2) across a tissue culture treated 6-well plate (Corning Costar), with each well assigned a different nickel treatment. Upon seeding, complete-TCM was added (670 µL per cm^2) and tissue was allowed to incubate for 24-hours prior to beginning the exposure procedure. After 24-hours of incubation, tissue was removed gently and 50% of complete-TCM was removed and replaced with 50% $NiCl_2$-spiked-media or a control. Treatments in wells were thus either 0, 0.1, 1, 10, 100, and 1000 mg L^{-1} nominal $NiCl_2$. Epithelial sheet adhesion and cell morphology were monitored and imaged daily using an inverted microscope under phase-contrast illumination.

2.2.5 RNA-seq experiment for nickel versus untreated primary epithelial cells in vitro

Using the 5 g L^{-1} nickel (II) chloride ($NiCl_2$; Sigma-Aldrich, Cat. No. 339350) stock solution, $NiCl_2$ spiked media (200 mg L^{-1}) was prepared in complete TCM. Eight genets of *B. schlosseri* at stage D were dissected to obtain 100 zooids and 100 primary buds as described in the above protocol. For each genet, half of each tissue type was distributed across two 6 cm tissue culture treated petri dishes (Corning Costar). Upon seeding tissue, complete TCM was added (670 uL per cm^2) and the tissue was incubated for 24 hours prior to the exposure procedure. After 24-hours of initial incubation, tissue pieces were removed gently and cells were evaluated using an inverted microscope under phase-contrast illumination (EVOS XL Core). Fifty percent of the complete TCM was removed and replaced with $NiCl_2$ spiked TCM or with control complete TCM.

Cells were left to incubate in treatment for 18 hours, after which all media was removed. Cells were immediately washed in triplicate with 2.8X PBS. Upon ensuring removal of all residual liquid, RLT lysis buffer (Qiagen) supplemented with 1% beta-mercaptoethanol (β-ME)

was pipetted directly onto cells according to manufacturer's instructions and subsequently further homogenized using a cell scraper. Lysed cells and lysis buffer were transferred to a 1.5 nuclease-free tube and immediately frozen in the -80 °C freezer.

2.2.6 Metabolic Activity Assay for Primary Epithelial Cell Cultures Across Time

Three stage D *Botryllus schlosseri* colonies were isolated for their zooids and primary buds as described in the above protocol. For each genet, tissue was allocated to three wells per plate (technical replicates) across three 12-well tissue-culture-treated plates (Corning; Costar), with a plating density of ~1 tissue piece per cm^2. Tunicate culture media for MTT assay was prepared with non-phenolic DMEM based media (Gibco; Thermo Fisher Scientific; Cat No. A1443001). All remaining wells were filled with cell culture grade sterile water to maintain plate humidity and placed in a 20 °C humidified incubator.

At 2, 4, and 24-hour timepoints post seeding, tissue was removed from wells gently and remaining epithelial monolayer sheets were washed in triplicate with 2.8× PBS to remove cellular debris. To each well containing cells, 500 µL of fresh non-phenolic TCM was added in addition to 50 µL of a 12-mM MTT stock solution. Three empty wells per plate were also incubated with non-phenolic TCM and MTT, serving as negative controls. MTT spiked plates were incubated for 4 hours at 20 °C in a humidified incubator. After incubation with MTT, 500 µL of SDS-HCl solution (10 mL 0.01 M HCl, to 1 mg SDS) was added, thoroughly mixed, and left to incubate for 18-hours at 37 °C in a humidified chamber. At the end of the incubation period, wells were re-homogenized, and the plate was placed without lid into a microplate reader to measure absorbance values read at 570 nm. Wells were normalized according to the average of blank wells absorbance for each plate.

2.2.7 Image analysis workflow for cell count and morphology

All images were taken using phase contrast microscopy with an EVOS XL Core phase contrast microscope, producing .tiff images with a standard 2048 x 1536 pixel ratio (Invitrogen). All image analyses were performed in Fiji (ImageJ2) version 2.16.0/1.54p, build 26d66057dd. For measurements of cell and tissue size, all images were set to scale using a standard stage micrometer for which the known distance in pixels for a 2048 x 1536 pixel image was globally applied for each objective.

For cell count comparisons between zooid and bud tissue, 10 random images at 100x magnification were selected and defined as technical replicates per tissue type for each genet evaluated. Images were first converted into an 8-bit grayscale format. The image was then adjusted for brightness/contrasts so that cell outlines appeared nearly black and contrasted with a fully white background. The image threshold was adjusted to isolate the black outlines using a threshold value of 255 on the 8-bit grayscale pixel intensity scale. Cell counts were then estimated using the *Analyze Particles* function, with circularity set to 0.00–1.00 and a size filter of 30-100 pixels, corresponding to the expected size range of individual cells at 100x magnification in 2048 x 1536 pixel images. Automated counts were visually confirmed by inspecting the particle detection overlay, where ellipses marking detected particles were superimposed on the original image to verify that cellular debris or large tissue remnants and fragments were excluded. Technical replicates for each tissue type per genet were averaged prior to estimating biological replicate means and generating graphical visualization.

For cell count comparisons before and after 24 hours of exposure to nickel (II) chloride *in vitro*, 2-3 paired images of the same epithelial monolayer sheet were evaluated at each time point for each genet and treatment combination. Images were acquired at 200x magnification. Prior to analysis, images were converted to 8-bit grayscale, and the *Subtract Background* command was

applied using a rolling ball radius of 20 pixels to reduce variation caused by uneven illumination. Images were then converted to binary format, enabling application of the *Watershed* command to distinguish individual cell boundaries within epithelial monolayer sheets. Thresholds were subsequently adjusted to highlight all cells. A cell count estimate was then produced using the *Analyze Particles* function, set to a circularity of 0.00-1.00 and a pixel range of 100-500, corresponding to the approximate size of epithelial cells at 200x magnification in a standard 2048 x 1536 pixel image. Automated segmentation outputs were visually inspected by comparing overlaid detected particles to the original images to confirm accurate cell identification. In cases where image quality was severely compromised by media precipitation or debris, cells were counted manually using the *Marker* tool in Fiji. Changes in cell number for each per paired set of epithelial monolayer images were quantified as a $\log_2$ fold change between the 0 and 24 hpe timepoints. Log_2 fold changes were averaged across technical replicates within each genet-treatment combination prior to graphical visualization.

2.2.7 Statistical analyses and visualization

All data processing, summary statistics, and visualization were performed in R (version 4.5.2). Raw experimental data were recorded in Google Sheets and imported into R for downstream analysis. Image-derived measurements quantified using Fiji were likewise compiled and analyzed in R. Data manipulation was performed using dplyr and tidyr packages. All figures were generated using the ggplot2 package in R.

Cell counts were quantified from phase contrast micrographs at 200x magnification using Fiji, with each image corresponding to a single bud- or zooid-derived tissue explant. Individual tissue explants per genet were treated as technical replicates. For each genet, cell counts were averaged across tissue explants within each tissue type to generate a single mean cell count per

genet-tissue combination. These genet-level means were treated as biological replicates for statistical analysis. Differences in cell counts between bud- and zooid-derived epithelial cells were assessed using a paired t-test, pairing tissue types within genets.

For explant attachment and monolayer formation analyses of the pilot nickel-pretreatment study, each well corresponded to a unique genet and was therefore treated as a biological replicate. Tissue explant outcomes were grouped by blastogenic stage and nickel chloride pre-treatment. Because the number of tissue pieces seeded per well varied among genets, tissue explant outcomes were summarized and visualized as counts per well rather than proportions. In cases where multiple genets were represented within the same stage and pre-nickel treatment combination, values were summarized descriptively as the mean count per well. Numbers of contributing genets were indicated for each group. No formal statistical analyses were performed on data generated from the pilot nickel-pretreatment study. Results are presented descriptively to characterize patterns of attachment and outgrowth across developmental stages and nickel pre-treatments.

All analysis scripts used for data processing and figure generation were version-controlled and are publicly available and maintained on GitHub (release v1.0-thesis).

2.3 Results

2.3.1 Cell morphology and yield according to tissue type seeded

Seeded tissue pieces from both primary buds and zooids ranged from 574 to 1072 μm in length from incurrent to excurrent siphon (mean = 818 μm, ± 147 μm) (Figure 2.2). All tissue pieces adhered to the plastic substrate using the partial desiccation method described above. Small portions of the epithelial monolayers were occasionally observed expanding from under

the tissue explant (Figure 2.3). Upon removal of the tissue at 24-hour post seeding, epithelial monolayers comprising an average of approximately 200 cells (Figure 2.5) were revealed.

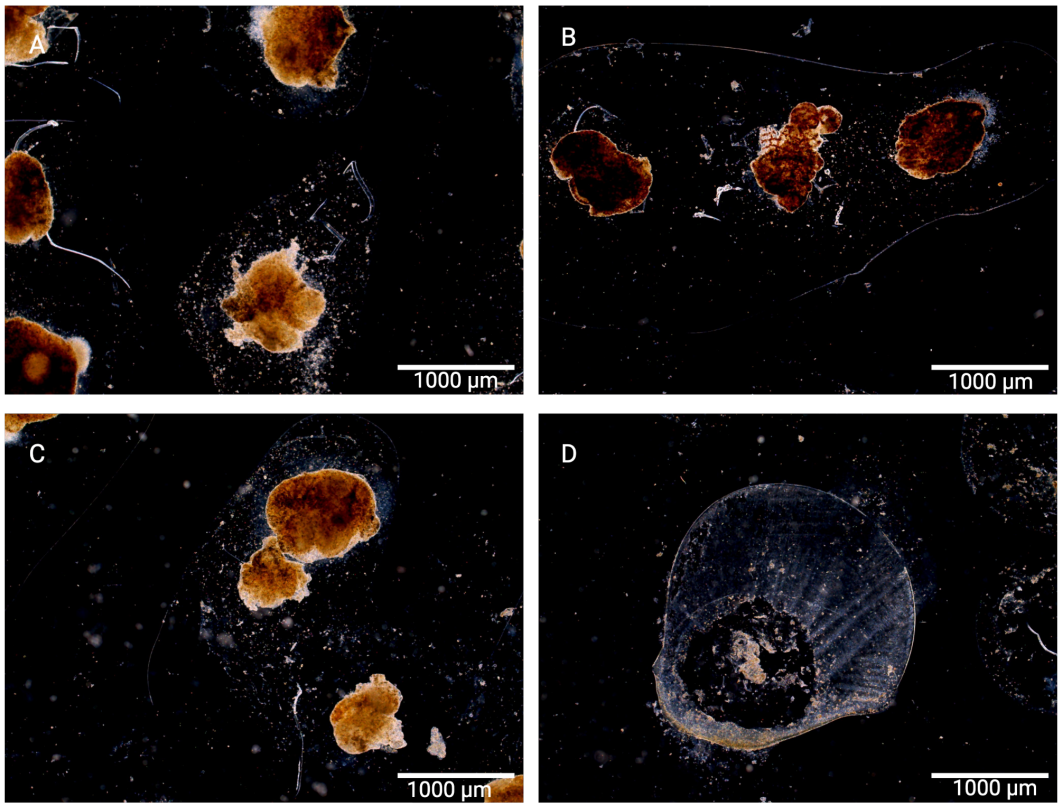

Figure 2.3. Zooid and primary bud tissue explants in culture. 40x magnification under phase contrast microscopy within the first hour post seeding (A-C) and after tissue removal 24 hours post seeding (D). A tunic-like excretion formed along the area where the tissue had previously adhered (D).

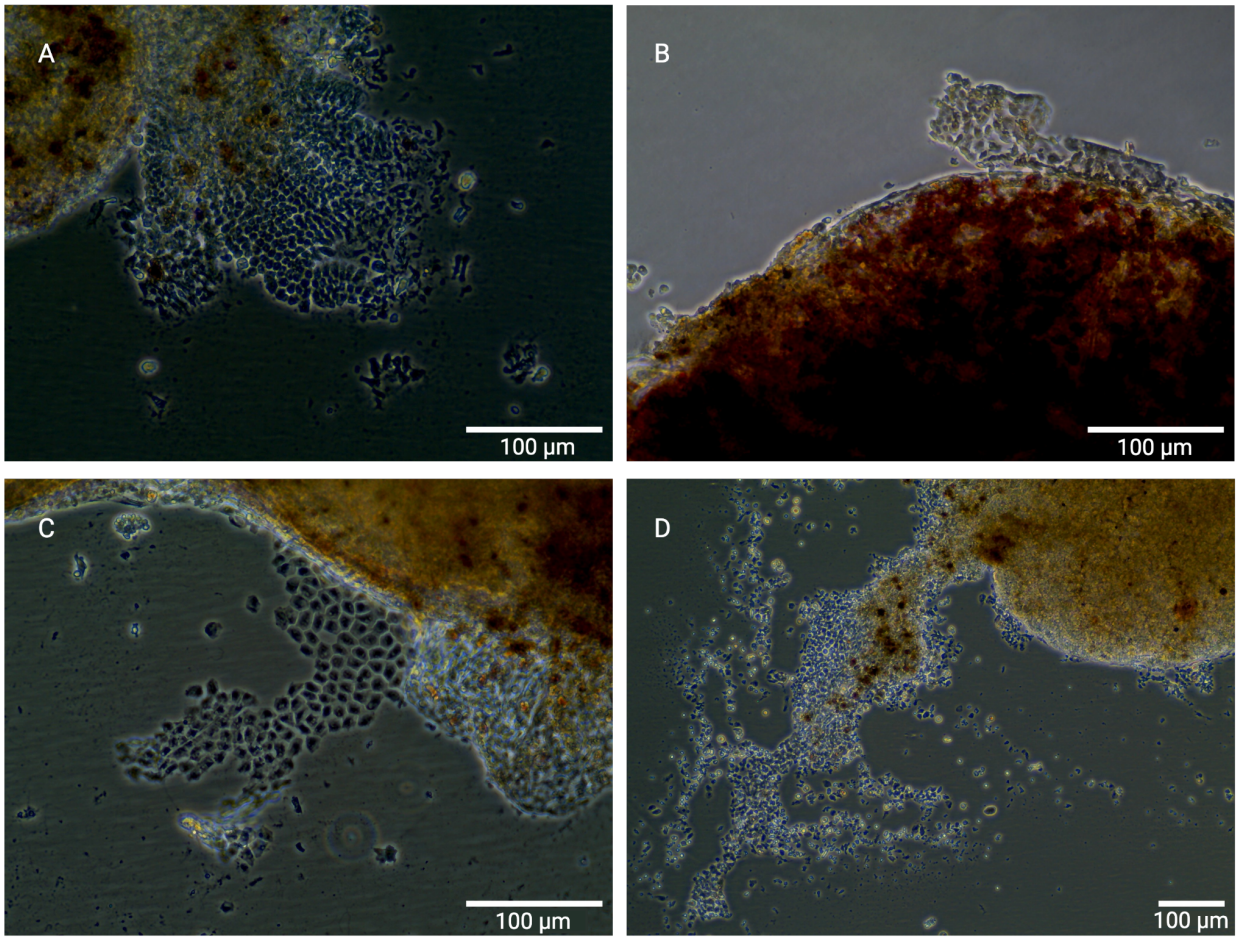

Figure 2.4. Peripheral expansion of primary epithelial monolayer sheets from explanted primary buds. Epithelial sheets began to emerge from the tissue within 2 to 3 days post seeding but showed no further increase in cell number after this period. Epithelial monolayers were kept up to 30 days in culture with no dissociation or significant morphological changes to tissue or epithelial sheets.

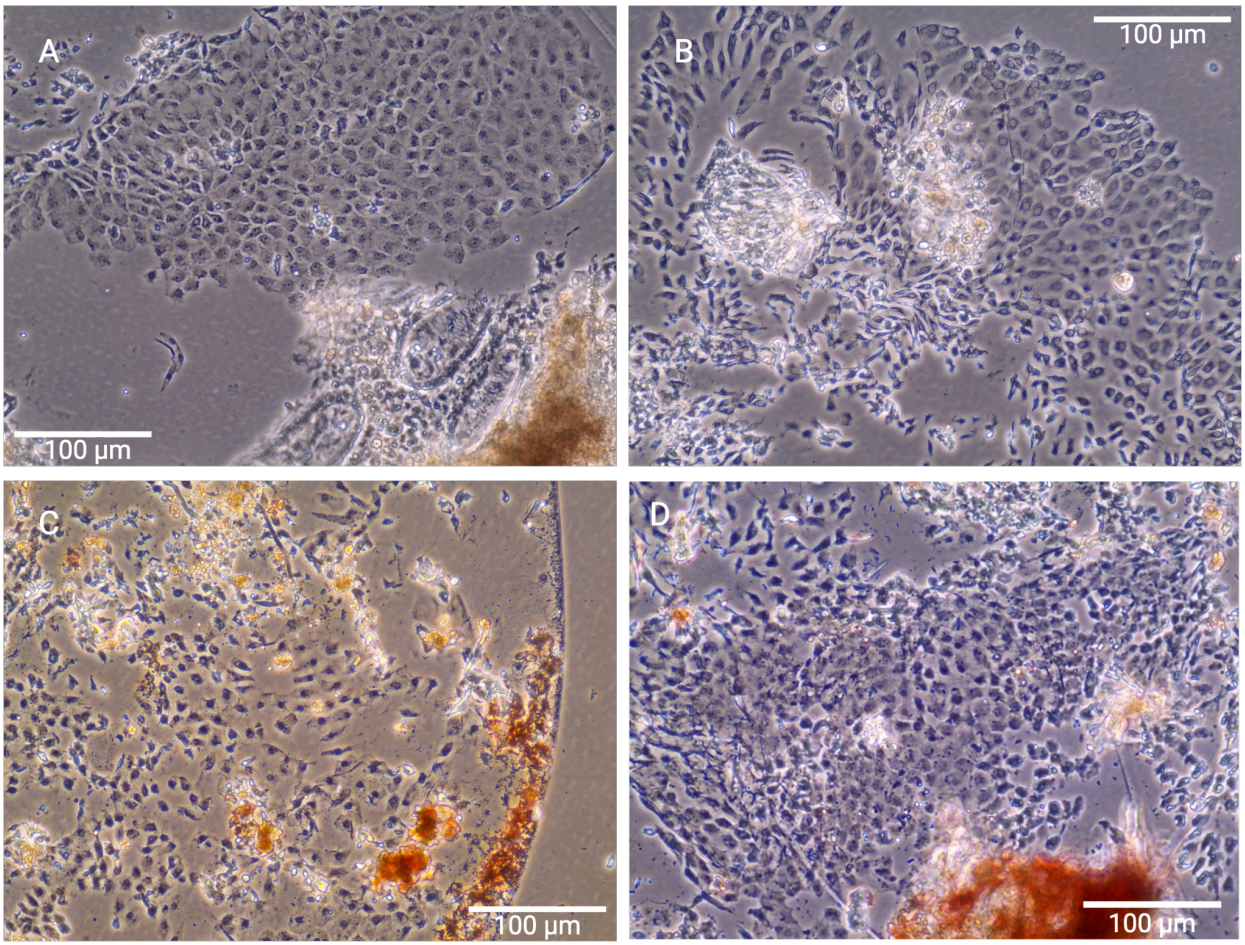

Figure 2.5. Typical cell morphology for primary epithelial cells of *B. schlosseri* at 400x magnification under phase contrast microscopy. A and B are representative images of cells derived from primary buds while C and D are cells derived from zooids. Cells maintain a flat cuboidal shape with varying degrees of continuous intracellular junctions. Zooidal derived cells are often surrounded by greater levels of cellular debris originating from explanted tissue (C and D). In all cells, nuclei are highly visible under inverted phase contrast microscopy relative to the clear cytoplasm.

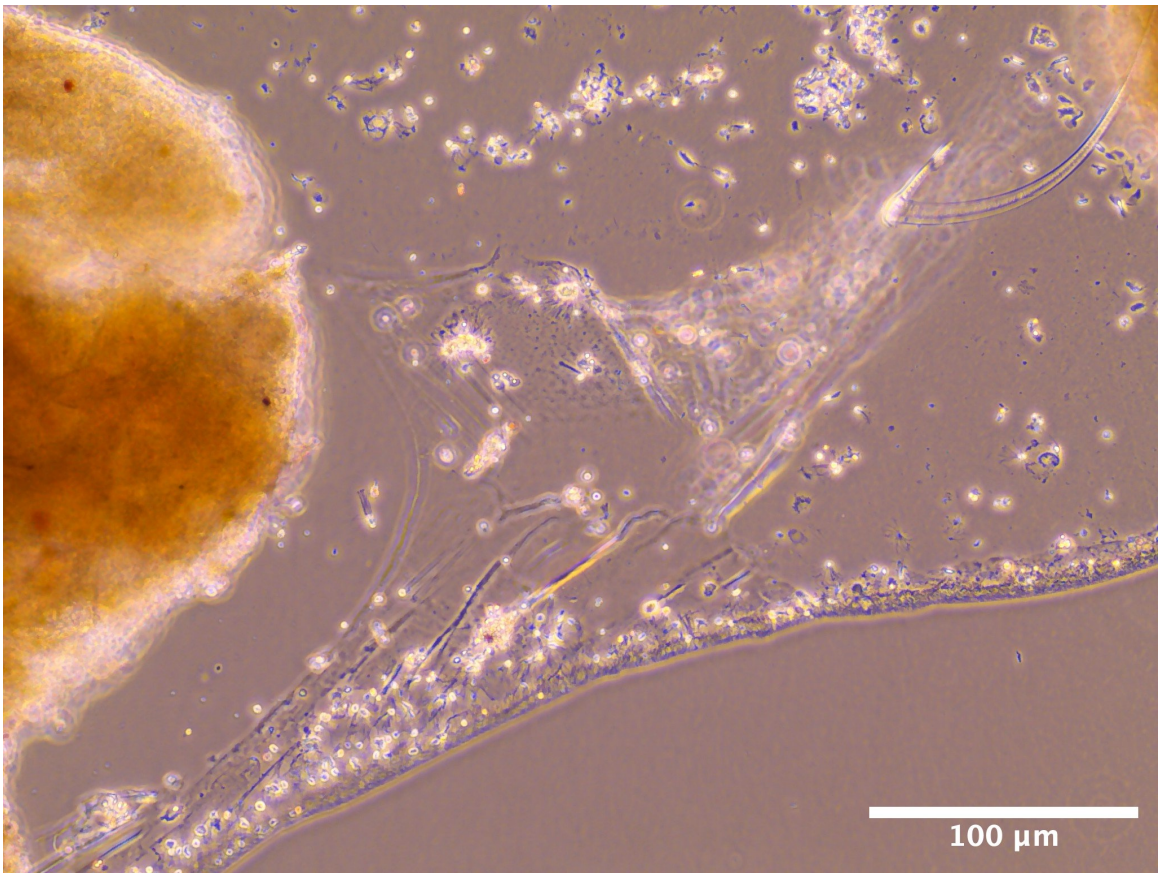

Figure 2.6. Tunic-like secretion emerging from explanted tissue. 400x magnification under phase contrast microscopy.

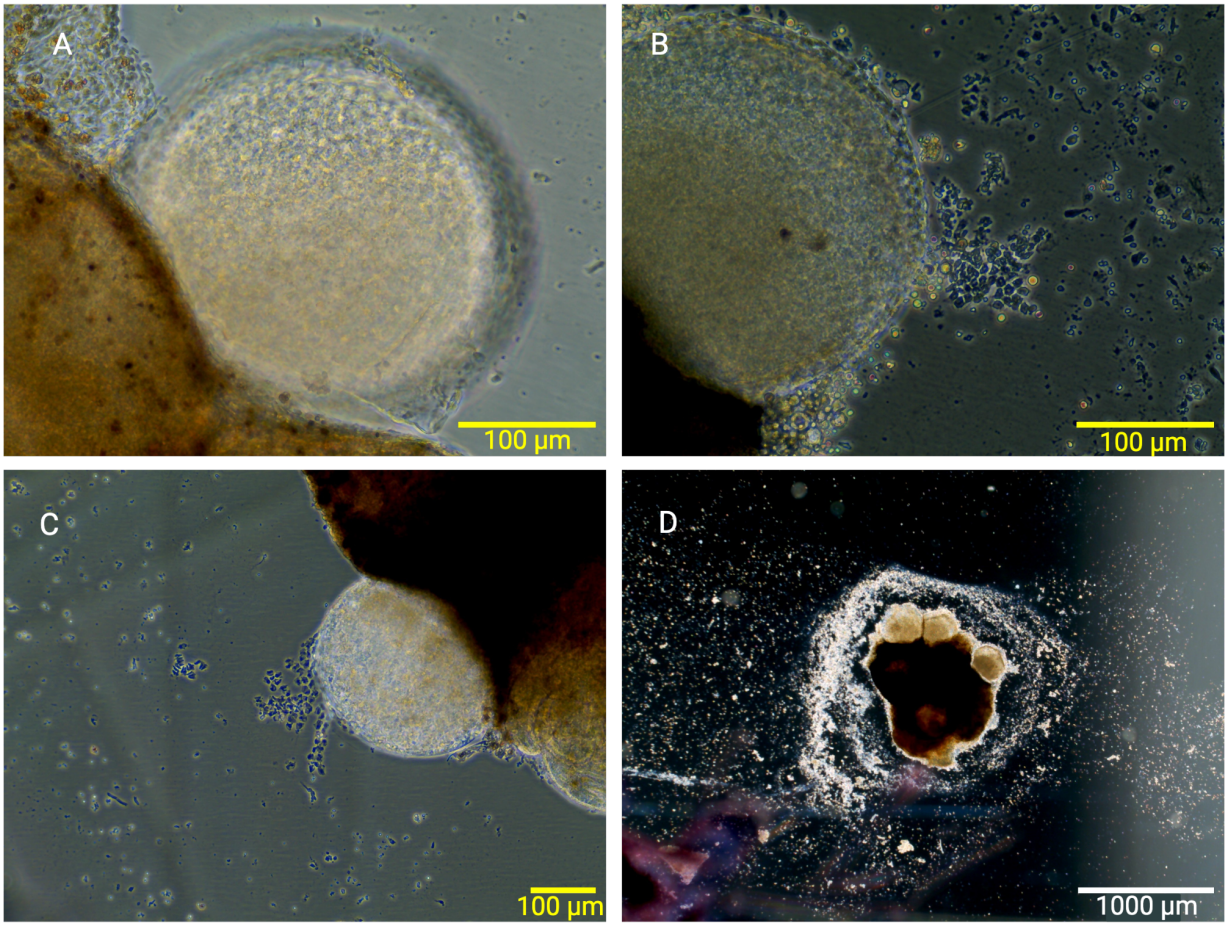

Figure 2.7. Formation of epithelial spheres derived from explanted stage D primary buds. Spheres become apparent less than 24 hours after seeding 400x magnification (A). Primary epithelial cells are observed emerging from spheres 2 to 3 days post seeding, in image B (400x magnification) and C (200x magnification), respectively. Spheres persist on tissue explant 5 days post seeding (D), 40x magnification.

Epithelial cells derived from both primary bud and zooid tissue explants exhibited similar morphological characteristics (Figure 2.5), presenting a typical cuboidal shape of similar size. Nuclei of epithelial cells were visually apparent under phase contrast microscopy. Epithelial monolayers ranged from tight continuous sheets to sparse, loosely interconnected cells. Tunic-like secretions were regularly observed emerging from explanted tissue pieces (Figures 2.3D and 2.6). Periodically, epithelial monolayer sheets were observed emerging from underneath the tissue; however, monolayer sheet expansion beyond the tissue was limited and occurred only

during the first 24-hours of culturing (Figure 2.5). No cell division occurred beyond the first 24-hours, whether the tissue was removed early (24-72-hours) or maintained in co-culture with primary cells. Epithelial spheres occasionally appeared on explanted primary buds, forming early during culturing (before 24-hours post seeding) and persisting on tissue for at least 5 days (Figure 2.7). Epithelial cells periodically emerged and adhered from epithelial spheres after 2 days in culture (Figure 2.4B-C).

Both seeded zooid and bud tissue explants yielded comparable primary epithelial cell count, with mean values of approximately 230 cells per seeded tissue explant (Figure 2.8). Variability in cell yield was greater among zooid-derived epithelial monolayer sheets than among primary buds, as indicated by a higher standard deviation in cell count (zooid: SD ±102; buds: SD ±18). No significant difference in mean cell count was detected between bud- and zooid-derived epithelial cells (paired *t*-test, $p > 0.05$), though statistical power was limited by the small number of genets.

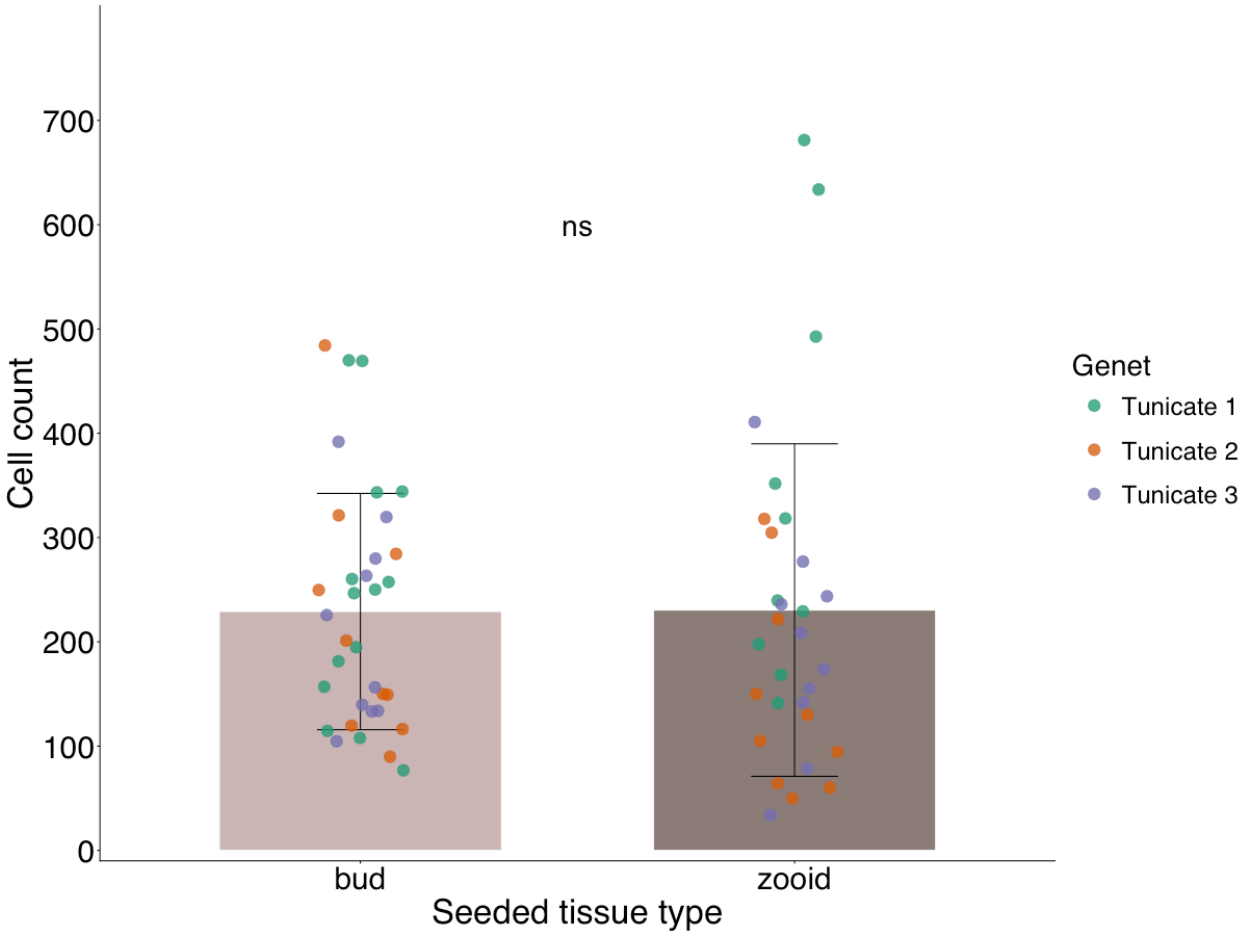

Figure 2.8. Mean cell count after 24 hours in culture for primary epithelial cell cultures of stage D *B. schlosseri*, separated by explanted tissue type (primary buds and zooids). Points represent genet-level means (n = 3). Individual tissue explants were treated as technical replicates (total n = 10) across three seeded wells and were averaged within each genet and tissue combination prior to analysis. A paired t-test detected no significant difference for cell counts derived from zooid or bud explants ($p > 0.05$).

2.3.2 Impact of nickel exposure on cell morphology or count

Across all tested nickel concentrations, the number of cultured epithelial cells did not significantly change following an acute 24-hour exposure (Figures 2.9-2.11). This remained true regardless of nickel exposure occurring before seeding (Figure 2.9) or concurrent during culturing (Figures 2.10 and 2.11). Nickel exposure had no visible impact on cell morphology, as

assessed by phase-contrast microscopy; cells retained their cuboidal shape and maintained intercellular junctions within epithelial sheets (Figure 2.10).

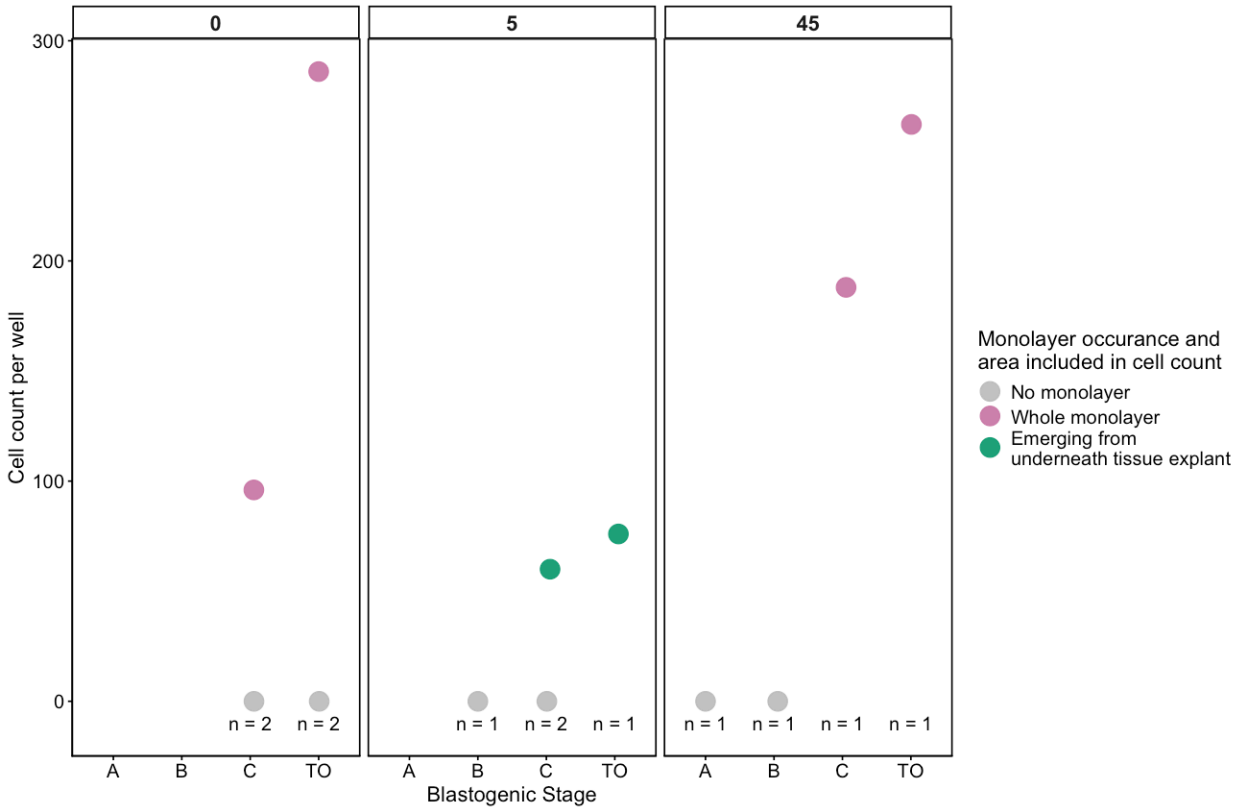

Figure 2.9. Cell count outcomes of explanted tissue from *B. schlosseri* colonies pre-treated with nickel (II) chloride. Colonies were exposed for 24-hours to either 0 (control), 5, or 45 mg L^{-1} of nominal $NiCl_2$, then dissected to obtain primary buds and zooids for explant cell cultures. After 18-hours in culture, epithelial monolayer outgrowth was assessed and total cells per monolayer were counted for each well. Across the 12 wells evaluated, a mean of 7 ± 2 (SD) tissue explants were seeded per well. Points represent total cell counts per well, with each well producing only one monolayer per explanted tissue. Colors indicate whether the monolayer was fully visible or partially obscured beneath adhered tissue at the time of imaging. Numbers below points denote the number of genets for each stage and pre-treatment group.

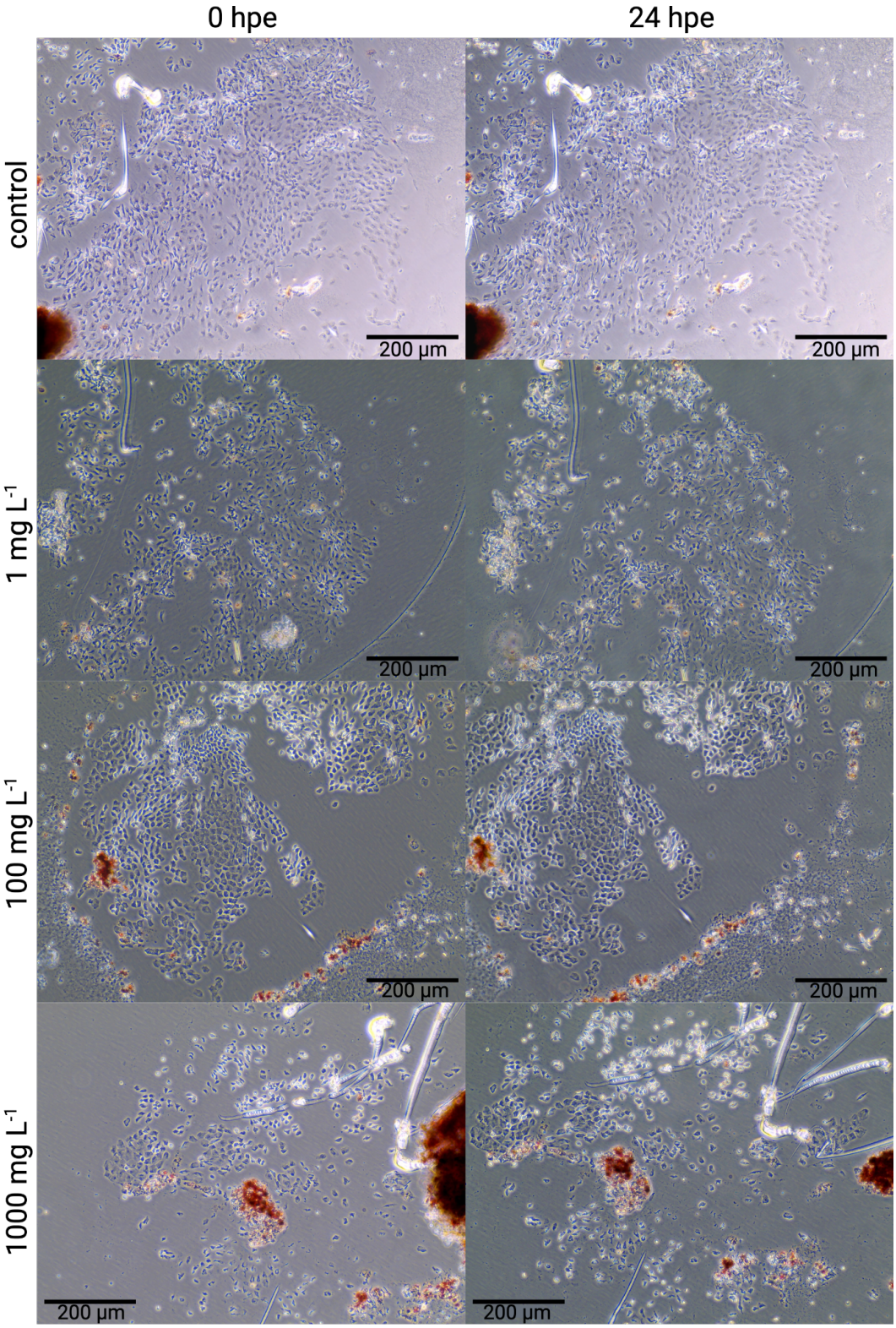

Figure 2.10. Epithelial monolayer sheets before and after exposure to increasing concentrations of nickel (II) chloride. 200x magnification under phase contrast microscopy.

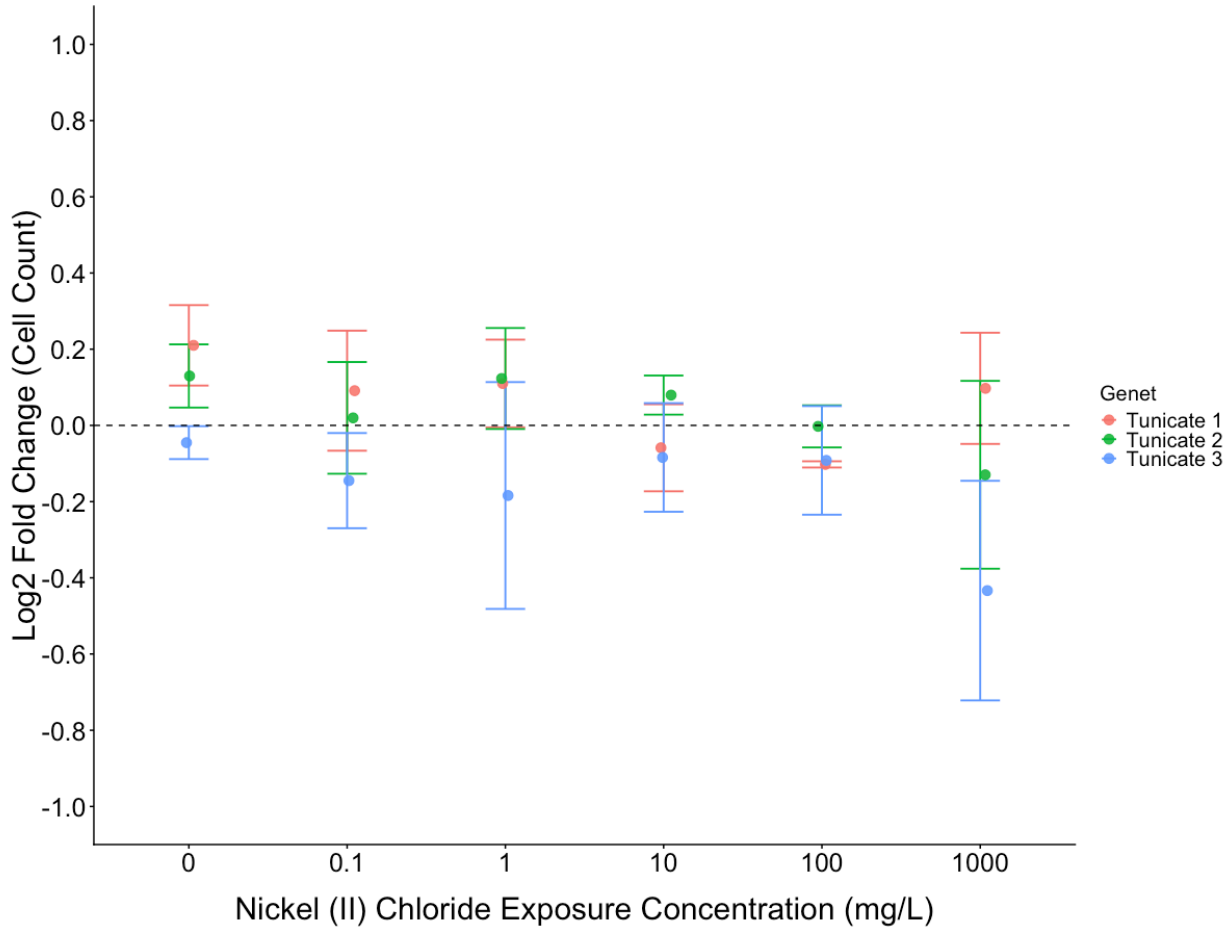

Figure 2.11. Paired changes in epithelial cell number following 24 hours post exposure to nickel (II) chloride *in vitro* across three *B. schlosseri* genets. For each genet and $NiCl_2$ concentration, 2-3 epithelial monolayers from explanted tissue were imaged before (0 hours post exposure) and 24 hours post-exposure (hpe). Cell counts were estimated from each image using a standardized automated cell count workflow in Fiji. Log_2 fold changes were calculated for each epithelial monolayer and averaged within each genet-treatment combination. Points represent the genet-level mean log_2 fold changes. Error bars represent standard deviation in cell count across technical replicates of paired epithelial monolayer images.

2.3.3 RNA yield and quality of extracted cells

RNA extracted from both nickel-exposed and control primary epithelial cells yielded consistently low quantities and variable quality (Table 2.1). RNA concentrations measured by NanoDrop ranged from 0.8 to 7.9 ng μL^{-1}, corresponding to total RNA yields of approximately 30-300 ng per sample. Across samples, A260 over A280 absorbance ratios ranged from 1.46 to

2.45, with 31% of samples failing the minimum purity threshold of 1.8 to 2.0 and all samples not meeting the standard minimum for total RNA (100 ng) required for bulk RNA-seq.

RNA yield and purity were not influenced by treatment type, as similarly low concentration and variable quality absorbance ratio were observed in both control and nickel-treated samples. Independent RNA integrity assessment performed by Novogene further indicated poor RNA integrity across samples with low RIN scores consistent with RNA degradation.

Table 2.1. RNA concentration and purity metrics for primary epithelial cells of *B. schlosseri*. RNA concentration and quality were initially estimated using NanoDrop spectrophotometry. Total RNA quantity, integrity, and fragment size distribution were assessed by NovoGene. All samples yielded total RNA quantities and DV200 values below the recommended input threshold for successful RNA-seq library preparation.

Sample ID	Treatment	Estimated RNA Conc. (ng/uL)	Volume (µL)	RNA Conc. (ng/µL)	Total RNA (ng)	A260/A280	RIN	DV200 (%)
P2.1	Control	0.8	31	0.5	14.2	1.95	1.3	63.5
P2.2	Nickel Exposed	1.3	31	0.7	20.6	1.75	1.5	72.4
P4.1	Control	1.1	31	0.5	14.4	1.75	1.4	58.9
P4.2	Nickel Exposed	1.2	31	0.5	16.7	2.18	1.3	61.7
P5.1	Control	3.9	31	2.3	71	1.98	1	63.3
P5.2	Nickel Exposed	4.7	31	2.3	71.6	1.94	1.4	57.8
P6.1	Control	2.2	31	1.3	40.6	1.71	1	62.9
P6.2	Nickel Exposed	2.1	31	0.7	20.9	2.03	1.1	61.2
P7.1	Control	1.3	31	0.6	17.5	2.02	1.4	64.6
P7.2	Nickel Exposed	1.8	31	1	31	2.45	1.1	65.3
P8.1	Control	2	31	0.8	24.6	1.68	1.1	64.4
P8.2	Nickel Exposed	1.4	31	0.4	12.5	2.06	1.7	56.9

2.3.4 Cell viability assessment using MTT assay

No formazan crystal product was recovered from epithelial cells incubated with SDS-HCl. Under phase contrast microscopy, cells appeared intact and adherent to the substrate after the 18-hour incubation with SDS-HCl. Absorbance values across all time points remained near or below baseline and comparable to negative controls. Furthermore, absorbance values for wells containing cells were similar to those of blanks resulting in some samples falling within the negative range when normalized against the blanks. Given the limited number of biological replicates and failure to solubilize formazan crystals, results for the viability of cultured epithelial cells of *B. schlosseri* remain inconclusive.

2.4 Discussion

2.4.1 Stage D zooids and primary bud tissue explants produce similar cell types and yields

With the exception of one study that observed epithelial monolayer development from explanted zooids (Rabinowitz and Rinkevich, 2004), prior efforts for initiating epithelial cell cultures from *B. schlosseri* have predominantly utilized primary buds (Rabinowitz and Rinkevich, 2003; Rabinowitz and Rinkevich, 2004; Rabinowitz and Rinkevich, 2011; Rabinowitz et al., 2009; Rinkevich and Rabinowitz, 1997). Although epithelial monolayer formation from mid-takeover (TO/stage D) zooids has been qualitatively reported (Rabinowitz and Rinkevich, 2004), the present study quantitatively compares cell yield from both stage D zooid and primary bud explants, demonstrating comparable cell numbers and epithelial morphology across tissue types for short-term culturing under this method (Figure 2.5 and 2.7). Nonetheless, replication of this approach across laboratories and expanded cell yield

quantification using additional genets will be necessary to confirm the robustness and reproducibility of this proposed method.

The culturing strategy used in the present study for *B. schlosseri* primary epithelial cells differs from previously reported approaches (Figure 2.2). Although earlier studies also employed a tissue explantation technique for both fragmented and intact zooids and primary buds, explants were allowed to settle passively onto the culturing dish, relying on low media volumes to promote tissue contact with the substrate (Rabinowitz and Rinkevich, 2011). Under that culturing strategy, primary bud explants across blastogenic stages reportedly exhibited multiple outcomes at varying frequencies including: failure to produce primary cells, formation of unadhered hollow epithelial spheres, formation of epithelial spheres that later adhered and developed into monolayers, or direct adhesion followed by epithelial monolayer formation (Rabinowitz and Rinkevich, 2003). Consequently, for that approach only a subset of primary bud explants across the various blastogenic stages successfully adhered to the substrate (29-60%), with adhesion occurring over a broad temporal window (2 to 9 days post-seeding) (Rabinowitz and Rinkevich, 2004; Rabinowitz et al., 2009). Under that prior method, stage D primary buds exhibited the highest consistency of epithelial monolayer formation with 20% developing monolayer sheets without passing through the intermediate epithelial sphere stage, while only 4% of stage D explants formed epithelial spheres (Rabinowitz and Rinkevich, 2003; Rabinowitz et al., 2009). These outcomes were largely consistent regardless of the media type, supplements, or substrate composition evaluated (Rabinowitz and Rinkevich, 2003; Rabinowitz et al., 2009).

In contrast, the culturing method described here bypasses the free-floating tissue phase by directly promoting tissue adhesion through a brief partial desiccation step. This results in complete adherence of all tissue to the culturing dish prior to media addition. Such an approach

is commonly implemented for explantation strategies of other adherent primary cell cultures (Gardell et al., 2014; Wang et al., 2016). Consistent with prior studies, we periodically observed the formation of epithelial spheres from explanted stage D primary buds (Figure 2.7), however, the frequency at which this structure formed was not recorded (Rabinowitz and Rinkevich, 2004).

Incorporation of a partial desiccation step improved monolayer formation reproducibility, with epithelial cell growth observed from both zooid and bud explants at a much higher consistency (~70-96%) than previously reported (Rabinowitz and Rinkevich, 2003; Rabinowitz et al., 2009). Brief partial desiccation likely enhances tissue explant adhesion by reducing the thin fluid barrier between the tissue and culture substrate, allowing closer positioning of the explant and minimizing tissue displacement during early incubation. However, despite increased occurrence of monolayer formations associated with improved explant adhesion, partial desiccation may come at the expense of limited peripheral expansion of epithelial monolayer sheets (Figure 2.5), a growth pattern that has otherwise been widely observed in previous studies (Rabinowitz and Rinkevich, 2003; Rabinowitz and Rinkevich, 2004; Rabinowitz et al., 2009; Rinkevich and Rabinowitz, 1997). Under the conditions used here, epithelial monolayers generally remained underneath or in close proximity to the explanted tissue (Figure 2.5).

In *B. schlosseri*, weekly blastogenic budding relies on the coordination and growth of two thin ectoderm-derived epithelial monolayers of the zooid, the epidermis and the peribranchial epithelium. These epithelia give rise to new buds in coordination with haemoblasts located in the mesenchymal space between the two epithelial layers (Ricci et al., 2016). Although zooid and bud explants maintain intact epithelial tissue structures and may retain some of the associated cell populations, the partial desiccation step may disrupt or damage peripheral

epithelial cells or associated haemoblast populations, especially given that both the epidermal and peribranchial epithelia consist of a single layer of epithelial cells (Ricci et al., 2016). Consequently, while partial desiccation improves explant adhesion, it may reduce the number of viable cells capable of migrating outward, resulting in monolayers that remain localized underneath the tissue explant where desiccation stress may be comparatively minimal. The transferability of the present studies explanation culturing technique across earlier blastogenic stages remains to be assessed. Nonetheless, the updated explantation strategy outlined in this study enables investigations in which maximizing cell yield per tissue explant from late blastogenic stage zooids and primary buds is a primary objective.

Tunic-like secretions were consistently observed to co-occur with epithelial cells derived from both tissue types (Figures 2.3D and 2.6). Similar tunic-like secretions have been reported in earlier studies employing passive settling of primary bud explants (Rabinowitz et al., 2009). The consistent presence of these secretions across culturing methodologies and tissue types suggests that extracellular matrix (ECM) production is an intrinsic feature of *B. schlosseri* epithelial cells *in vitro* rather than a methodological artifact. In explant culture systems, retention of ECM components surrounding the tissue fragment can promote cell migration and survival by providing structural scaffolding and localized biochemical signaling cues (Hendijani, 2017). Accordingly, the presence of tunic-like secretions in epithelial cell cultures of *B. schlosseri* may contribute to the establishment of a microenvironment that supports epithelial cell attachment and localized monolayer formation. Importantly, this phenotype reflects the retention of *in vivo* phenotypic behavior despite limited proliferation, as epithelial cells in whole colonies of *B. schlosseri* and other ascidians are the primary producers of the tunic matrix (Kimura and Itoh, 2007; Kuroiwa et al., 2025; Zaniolo, 1981).

2.4.2 Nickel tolerance of B. schlosseri primary epithelial cells relative to whole-colony stress responses

The apparent nickel tolerance of *B. schlosseri* primary epithelial cells is broadly consistent with or potentially exceeds the high tolerance and persistence observed in whole colonies exposed to comparable concentrations of nickel (II) chloride. Notably, *in vivo* nickel exposure prompted transcriptional upregulation of genes linked to epithelial basement membrane integrity (FREM1 and HSPG2), coincident with visibly compromised zooid and primary bud body walls and degraded surrounding tunic (see Chapter 1, Sections 1.3.1 and 1.3.6). These findings suggest that in whole *B. schlosseri* colonies, nickel exposure disrupts epithelial and extracellular matrix integrity and elicits a compensatory transcriptional response. However, visible indicators of cytotoxic stress or monolayer sheet disruption in cultured epithelial cells exposed to equivalent concentrations of nickel (II) chloride were not observed. Collectively, this data indicates that nickel induces stress that is more readily detected in whole colonies than in cultured primary epithelial cells of *B. schlosseri*. Importantly, while primary cell cultures may often closely replicate aspects of *in vivo* biology, the discrepancies between whole organismal and isolated cellular stress responses are a widely recognized feature of comparative assessments between *in vivo* and *in vitro* models (Bellot et al., 2012; Ranasinghe et al., 2025). Although primary epithelial cells were initially expected to be more sensitive to nickel exposure, exhibiting cytotoxic responses at lower concentrations than those inducing mortality in whole colonies, several explanations may account for the lack of detectable cellular responses to *in vitro* exposure.

The absence of additional cell division after the initial 24-hour culturing period, prior to the *in vitro* nickel challenges, may have influenced the magnitude of observable stress response in primary epithelial cells. Prior work similarly reported that primary epithelial cells of *B.*

schlosseri fail to divide after 24 to 72-hours of tissue explant attachment and interpreted this phenotype as cellular quiescence (Rabinowitz and Rinkevich, 2003; Rinkevich, 2011). However, quiescent cells are defined by their capacity to reenter the cell cycle (Marescal and Cheeseman, 2020; Terzi et al., 2016), a feature that has not yet been demonstrated for proliferatively arrested *B. schlosseri* primary epithelial cells. As such, this phenotype may alternatively reflect irreversible cellular senescence (Terzi et al., 2016). Additional studies are needed to distinguish whether arrested proliferation for *B. schlosseri* primary epithelial cells are a product of quiescence, senescence, or if the cell cycle arrest between these states is truly unresolvable.

Nonetheless, both quiescence and senescence are inducible survival strategies that can be triggered by cellular stress (Fridlyanskaya et al., 2015; Peddibhotla et al.). Primary cell isolation during the early culturing period is often a substantial cellular stress event and has been demonstrated to increase stress-protein synthesis (e.g. heat shock-like proteins) while reducing responsiveness to subsequent stressors during the initial 24 to 72-hours in culture (Wolffe and Tata, 1984). Although primary cells may recover from the initial stress of culture, return to a normal physiological state, and resume cellular division (Wolffe and Tata, 1984), the stress associated with the *in vitro* environment can also impose substantial stress. In some cases, this stress may trigger proliferative arrest programs such as senescence or quiescence (Alessio et al., 2021; Ben-Porath and Weinberg, 2004; Yao, 2024), potentially limiting the detectability of additional stress phenotypes that could be observed following nickel challenge (Payea et al., 2024; Valcourt et al., 2012). Importantly, the lack of overt morphological indicators of stress in non-proliferative cells does not imply a lack of biological activity, as transcriptomic, proteomic, and metabolic profiles have been widely characterized for both quiescent and senescent cells (Fernandez et al., 2025; Lee et al., 2017; Outskouni et al., 2025).

In addition to proliferative arrest potentially dampening detectable morphological indicators of stress, the morphological stability of nickel-challenged *B. schlosseri* primary epithelial cells could also potentially be attributed to a buffering effect of the tunic-like secretions produced in culture (Figure 2.3D and 2.6). While nickel is known to bioaccumulate in whole *B. schlosseri* exposed to environmentally relevant concentrations (Guillén Matus et al., 2024), the extent to which nickel bioaccumulates at extremely elevated concentrations remains unknown for both whole colonies and directly-exposed isolated cells. In tunicates, the tunic functions as a protective extracellular barrier that limits direct exposure of underlying tissues to environmental stressors (Hirose et al., 1991). The presence of tunic-like secretions surrounding cultured primary epithelial cells may then reduce the bioavailability of nickel at the cellular surface. Consequently, further research is needed to evaluate whether tunic-like secretions in culture inhibit nickel access to the cellular surface of primary epithelial cells.

2.4.3 Resistance to chemical lysis and low cell counts impede downstream endpoint assays for primary epithelial cells of B. schlosseri

To contextualize the morphological nickel tolerance of *B. schlosseri* primary epithelial cells and whether nickel could potentially elicit responses for stress induced evolutionary pathways, an RNA-seq experiment was conducted to evaluate the transcriptional response of isolated cells to acute nickel (II) chloride exposure. Ultimately, RNA extractions of these samples failed to produce the sufficient RNA yield and quality required for bulk RNA-seq (Table 2.1). Several subsequent trials were conducted to identify the underlying technical issue and produce RNA samples of higher yield and quality. During these attempts, cells were carefully inspected using phase contrast inverted microscopy during the initial cell lysing step to verify maximal transfer of lysate from the cell culturing dish to the subsequent RNA extraction tube.

For all samples, despite vigorous cell scraping in the presence of the Qiagen RLT lysis buffer, many cells were observed to remain intact and unresponsive to mechanical and chemical lysis. As such, subsequent RNA isolation attempts utilized enhanced methods for mechanical lysis in the presence of Qiagens RLT lysis buffer including syringe needle cell shearing or bead beating at ambient temperatures. These samples were then extracted using the Qiagen RNeasy Micro Kit, an RNA extraction method optimized for lower cell input. Nonetheless, the RNA quality and yield of such samples remained unviable for bulk RNA-seq.

Even while employing the Qiagen RNeasy Micro kit for low cell input, low RNA yield and variable quality may reflect a combination of limited cellular biomass, technical challenges for complete lysis of highly adherent cells, and potential downstream carry over of extracellular matrix components from remaining tissue debris and tunic-like secretions produced in culture (Figure 2.3D and 2.6). The absence of cellular proliferation after the initial 24-hour culturing period aligns with a quiescent or senescent cellular state (Yao, 2024). Quiescent and senescent cells commonly exhibit reduced transcriptional activity and elevated RNA decay mechanisms, complicating the isolation and recovery of sufficient quantities of high-quality RNA (Marescal and Cheeseman, 2020; Noren Hooten and Evans, 2017; Van Velthoven and Rando, 2019). Notably, RNA isolation has been successfully accomplished from quiescent and senescent mammalian cell cultures (Jeyapalan and Sedivy, 2013; Johnson et al., 2017); however, no such reports exist for marine invertebrate primary cell cultures in similarly arrested states (Rinkevich and Pomponi, 2025). Even still there remains a wider scarcity for transcriptional profiling of any marine invertebrate cell cultures, with no transcriptional data available for cultured adherent cell types of any tunicate species (Granger Joly De Boissel et al., 2017; Kawamura et al., 2021; Tsuchiya et al., 2023). These combined challenges impeded successful recovery of RNA from

primary epithelial cell cultures of *B. schlosseri* and will need further targeted methodological optimization to overcome these limitations.

Given the challenges encountered during RNA isolation, we next sought to ascertain the viability of cultured primary epithelial cells of *B. schlosseri* using the MTT (3-[4,5-dimethylthiazol-2-yl]-2,5 diphenyl tetrazolium bromide) assay. The MTT assay has been reported to be a viable approach for quantifying metabolic activity of *B. schlosseri* cells in suspension, but has not yet been employed for adherent cell cultures of this species (Kamer and Rinkevich, 2002; Rabinowitz and Rinkevich, 2003). Preliminary optimization trials revealed limitations to MTT assay sensitivity for sparse, yet highly adherent *B. schlosseri* primary epithelial cells. Adherent *B. schlosseri* primary epithelial cells are largely unresponsive to conventional approaches for cellular disaggregation such as trypsinization (data not shown). As such, cell numbers per technical replicate remained a confounding and uncontrollable variable during the MTT assay. Although the predicted minimum cell output per tissue piece was met, metabolic activity remained undetectable with the MTT assay as the expected formazan crystal product was not successfully solubilized despite replicating the appropriate solubilization step with SDS-HCl, as previously described for this species (Rabinowitz and Rinkevich, 2003). Inspection of the cells after incubation with SDS-HCl revealed intact and adherent cells despite the presence of the strong solubilization buffer. As such, the same challenges occurring with RNA extraction of primary epithelial cells appear to inhibit the applicability of the MTT assay as well.

2.5 Future Perspectives

2.5.1 Evaluating the extent of tunic-like secretion buffering chemical lysis and recommendations

Overall, the chemical tolerance observed for primary epithelial cells of *B. schlosseri* seems to persist across various types of chemical exposure. Not only were morphological markers of cytotoxicity not inducible by metal exposure, but common reagents for cell lysis, including SDS-HCl and Qiagens RLT Lysis Buffer, were ineffective for disrupting cellular membranes. Given the lack of studies evaluating endpoint assays that require complete cellular lysis of cultured primary epithelial cells for any tunicate species (Rinkevich and Pomponi, 2025), it is unclear whether this phenotype is a common feature of cultured tunicate epithelial cells that produce tunic-like secretions. We hypothesize that the chemical tolerance observed in primary epithelial cells of this species arises from a buffering effect provided by production of a tunic-like secretion in culture observed here and in previous studies (Rabinowitz et al., 2009).

The tunic of *B. schlosseri* is a cellulosic-based integumentary tissue that is a feature unique to tunicates and not present in any other chordate (Hirose, 2009). Although the tunic matrix contains protein, lipid, sulfated glycan, and mucopolysaccharide components (Zhao and Li, 2014), the cellulose-like polysaccharide, tunicin, dominates its composition (Hirose et al., 1991), with the tunic reported to yield 60% cellulose by dry weight (Berrill, 1947). The cellulose of the tunic is structurally similar to that of plant cellulose (Helbert et al., 1998; Kimura and Itoh, 2007). As such, in order to visualize the extent of tunic-like secretion and whether it directly encases epithelial cells or only surrounds the epithelial monolayer sheet, we suggest utilizing calcofluor white, a stain that binds to β-1,3 and β-1,4 polysaccharides, such as those found in cellulose (Harrington and Hageage, 2003). Calcofluor white has been previously used for staining the tunic of larval ascidian from the species, *Phallusia mammillata* (Lanoizelet et al.,

2023), so its applicability for *in vitro* staining of tunic-like secretions of *B. schlosseri* primary epithelial cells is highly viable. In addition, structural analyses of *B. schlosseri* primary epithelial cells using transmission electron microscopy could help identify the site of tunic-like secretions biogenesis and provide further insights into potential cellulosic structure and function. Such analyses have been performed before for other tunicate species but never replicated for *in vitro* cells of *B. schlosseri* (Kimura and Itoh, 2007).

Visualizing the extent and distribution of tunic-like secretions produced in culture will be critical for addressing the challenges associated with cellular lysis. In addition to the chemical buffering effects of the tunic, the tunic of *B. schlosseri* is known for its exceptional resistance to mechanical stress (Kwon et al., 2023), and it is therefore plausible that tunic-like secretions surrounding cultured primary epithelial cells confer mechanical-stress protection. In the absence of cryogenic flash freezing in liquid nitrogen prior to the addition of Qiagen RLT lysis buffer, the method for cell lysis employed in RNA isolation of whole colonies (see Chapter 1, Section 1.2.4), the tunic-like secretions may enhance cellular resistance to commonly used mechanical disruption methods, including cell scraping, syringe-needle shearing, and bead beating. If tunic-like secretions do enhance mechanical and chemical resistance to lysis in *B. schlosseri* primary epithelial cell cultures, this would underscore the need to incorporate targeted enzymatic digestion of the secreted extracellular matrix for effective RNA isolation. Namely, using an enzyme such as cellulase to digest the tunic-like secretions prior to RNA extraction may improve isolation efficiency (Shehadul Islam et al., 2017). Although it is likely that an unknown combination of enzymatic, chemical, and mechanical disruption will be required for successful isolation of nucleic acids and proteins of cultured primary epithelial cells of *B. schlosseri* (Danaeifar, 2022).

2.5.2 Improving metal genotoxicity assessment for marine invertebrate cell cultures

Existing studies for marine invertebrate cell cultures have primarily focused on endpoint assays to evaluate the feasibility of using *in vitro* marine invertebrate models for high-throughput ecotoxicological screening, including measures of viability, metabolic activity, and DNA damage (Akpiri et al., 2017; Downs et al., 2010; Kamer and Rinkevich, 2002; Radford et al., 2000; Zhang et al., 2017). Addressing metal stress in the context of cultured marine invertebrate cell morphology is critical for distinguishing tolerable stress from complete cellular failure (Gardell et al., 2014). For example, cells may remain metabolically active, conveying functional capacity, but exhibit morphological indicators of stress, such as weakened adhesion or arrested cellular division (Cooper, 2000; Slavov et al., 2011). A holistic approach to characterizing metal toxicological responses is especially important in non-model marine invertebrate cell cultures where baseline cell morphology and behavior are not well defined.

Nickel functions as an indirect or weakly genotoxic carcinogen in mammalian systems, with cellular immortalization occurring through a broad suite of mechanisms including oxidative stress, impaired DNA repair, chromosomal damage, DNA methylation, and histone modifications (Costa, 2019; Dallas et al., 2013; Martinez-Zamudio and Ha, 2011; Permenter et al., 2011; Trott et al., 1995). Although nickel genotoxicity has been repeatedly demonstrated in marine invertebrates, resulting in DNA damage through several of these same pathways, there is no evidence to date that nickel induces cellular immortalization in any marine invertebrate system (Akpiri et al., 2017; Dallas et al., 2013; Gallo et al., 2016; Millward et al., 2012). A As such, it remains unclear whether stress-induced evolution via nickel exposure, such as that observed in mammalian primary cell cultures (Mo et al., 2021; Trott et al., 1995), is a transferable strategy for cellular immortalization in marine invertebrate primary cell cultures.

The persistence of *B. schlosseri* primary epithelial cells exposed to high concentrations of nickel (II) chloride may suggest conditional feasibility of this immortalization approach, particularly if proliferatively arrested cells are in a reversible quiescent state capable of reentering the cell cycle with compromised DNA repair fidelity (Leung et al., 2024). However, quiescent cells subjected to stress can alternatively transition into stress-induced senescence without reentering the cell cycle (Yao, 2024). As such, the timing of nickel exposure for *B. schlosseri* primary epithelial cells may be a critical determinant for whether stress exposure promotes adaptive heritable phenotypes, irreversible proliferative arrest, or cell death (Wagner et al., 2019). Addressing these uncertainties will require overcoming current limitations in effective cellular lysis in *B. schlosseri* primary epithelial cells. Improving lysis efficiency will enable the detection of DNA damage, cell viability assessment, and molecular characterization necessary to evaluate stress-mediated genotoxic responses relevant for cellular immortalization efforts in *B. schlosseri*.

Overall, there is a relatively small community of researchers working on *B. schlosseri* cell cultures (Domart-Coulon and Blanchoud, 2022). Addressing the methodological challenges and remaining knowledge gaps outlined here will require coordinated efforts within this community, including increased open access to optimized workflows, reporting of negative results, and deliberate emphasis on reproducibility across research groups. A commonly cited obstacle to develop continuous cell lines in any marine invertebrate species is the lack of published unsuccessful approaches, which often leads to repeated attempts of similar failed culturing strategies (Grasela et al., 2012; Rinkevich and Pomponi, 2025). Given the sensitivity of primary cell culture outcomes to subtle differences in dissection, isolation, culturing, and lysis

practices, sharing both robust methods and failed culturing attempts will be essential for advancing the cellular characterization and immortalization of *B. schlosseri*.

References

Akpiri, Rachael U., Konya, Roseline S. and Hodges, Nikolas J. (2017). Development of cultures of the marine sponge *Hymeniacidon perleve* for genotoxicity assessment using the alkaline comet assay. *Environ. Toxicol. Chem.* 36, 3314–3323.

Alessio, Nicola, Aprile, Domenico, Cappabianca, Salvatore, Peluso, Gianfranco, Di Bernardo, Giovanni and Galderisi, Umberto (2021). Different Stages of Quiescence, Senescence, and Cell Stress Identified by Molecular Algorithm Based on the Expression of Ki67, RPS6, and Beta-Galactosidase Activity. *Int. J. Mol. Sci.* 22, 3102.

Andrés, Celia María Curieses, Pérez De La Lastra, J. M., Juan, C. A., Plou, F. J. and Pérez-Lebeña, E. (2022). Chemistry of Hydrogen Peroxide Formation and Elimination in Mammalian Cells, and Its Role in Various Pathologies. *Stresses* 2, 256–274.

Anselmi, C., Caicci, F., Bocci, T., Guidetti, M., Priori, A., Giusti, V., Levy, T., Raveh, T., Voskoboynik, A., Weissman, I. L., et al. (2023). Multiple Forms of Neural Cell Death in the Cyclical Brain Degeneration of A Colonial Chordate. *Cells* 12, 1041.

Attig, H., Dagnino, A., Negri, A., Jebali, J., Boussetta, H., Viarengo, A., Dondero, F. and Banni, M. (2010). Uptake and biochemical responses of mussels Mytilus galloprovincialis exposed to sublethal nickel concentrations. *Ecotoxicol. Environ. Saf.* 73, 1712–1719.

Banni, M., Hajer, A., Sforzini, S., Oliveri, C., Boussetta, H. and Viarengo, A. (2014). Transcriptional expression levels and biochemical markers of oxidative stress in Mytilus galloprovincialis exposed to nickel and heat stress. *Comp. Biochem. Physiol. Part C Toxicol. Pharmacol.* 160, 23–29.

Bates, E. H., Alma, L., Ugrai, T., Gagnon, A., Maher, M., McElhany, P. and Padilla-Gamiño, J. L. (2021). Evaluation of the Effect of Local Water Chemistry on Trace Metal Accumulation in Puget Sound Shellfish Shows That Concentration Varies With Species, Size, and Location. *Front. Mar. Sci.* 8, 636170.

Bellot, G. L., Tan, W. H., Tay, L. L., Koh, D. and Wang, X. (2012). Reliability of tumor primary cultures as a model for drug response prediction: expression profiles comparison of tissues versus primary cultures from colorectal cancer patients. *J. Cancer Res. Clin. Oncol.* 138, 463–482.

Ben-Hamo, O. and Rinkevich, B. (2021). Botryllus schlosseri—A Model Colonial Species in Basic and Applied Studies. In *Handbook of Marine Model Organisms in Experimental Biology*, pp. 385–402. Boca Raton: CRC Press.

Ben-Porath, I. and Weinberg, R. A. (2004). When cells get stressed: an integrative view of cellular senescence. *J. Clin. Invest.* 113, 8–13.

Berrill, N. J. (1947). The structure, development and budding of the ascidian, eudistoma. *J. Morphol.* 81, 269–281.

Blewett, T. A. and Leonard, E. M. (2017). Mechanisms of nickel toxicity to fish and invertebrates in marine and estuarine waters. *Environ. Pollut.* 223, 311–322.

Blewett, T. A. and Wood, C. M. (2015). Low salinity enhances NI-mediated oxidative stress and sub-lethal toxicity to the green shore crab (Carcinus maenas). *Ecotoxicol. Environ. Saf.* 122, 159–170.

Blewett, T. A., Smith, D. S., Wood, C. M. and Glover, C. N. (2016). Mechanisms of Nickel Toxicity in the Highly Sensitive Embryos of the Sea Urchin *Evechinus chloroticus* , and the Modifying Effects of Natural Organic Matter. *Environ. Sci. Technol.* 50, 1595–1603.

Brand, T. (2005). The *Popeye* Domain-Containing Gene Family. *Cell Biochem. Biophys.* 43, 095–104.

Brix, K. V., Schlekat, C. E. and Garman, E. R. (2016). The mechanisms of nickel toxicity in aquatic environments: An adverse outcome pathway analysis. *Environ. Toxicol. Chem.* 36, 1128–1137.

Bryant, V., Newbery, D. M., McLusky, D. S. and Campbell, R. (1985). (Corophiumv01Utator, Macoma balthica). *Mar Ecol Prog Ser*.

Burnet, F. M. (1971). "Self-recognition" in Colonial Marine Forms and Flowering Plants in relation to the Evolution of Immunity. *Nature* 232, 230–235.

Calabrese, A., Collier, R. S., Nelson, D. A. and MacInnes, J. R. (1973). The toxicity of heavy metals to embryos of the American oyster Crassostrea virginica. *Mar. Biol.* 18, 162–166.

Campagna, D., Gasparini, F., Franchi, N., Vitulo, N., Ballin, F., Manni, L., Valle, G. and Ballarin, L. (2016). Transcriptome dynamics in the asexual cycle of the chordate Botryllus schlosseri. *BMC Genomics* 17, 275.

Cima, F., Manni, L., Basso, G., Fortunato, E., Accordi, B., Schiavon, F. and Ballarin, L. (2010). Hovering between death and life: Natural apoptosis and phagocytes in the blastogenetic cycle of the colonial ascidian Botryllus schlosseri. *Dev. Comp. Immunol.* 34, 272–285.

Cima, F., Ballarin, L., Caicci, F., Franchi, N., Gasparini, F., Rigon, F., Schiavon, F. and Manni, L. (2015). Life history and ecological genetics of the colonial ascidian Botryllus schlosseri. *Zool. Anz. - J. Comp. Zool.* 257, 54–70.

Cooper, G. M. (2000). The Eukaryotic Cell Cycle. In *The Cell: A Molecular Approach. 2nd edition*, p. Sinauer Associates.

Costa, M. (2019). Mechanisms of Nickel Carcinogenicity and Genotoxicity. In *Toxicology of Metals, Volume I*, pp. 231–243. Boca Raton: CRC Press.

Crane, M. S. J. (1999). Mutagensis and cell transformation in cell culture. *Methods Cell Sci.* 245–252.

Dallas, L. J., Bean, T. P., Turner, A., Lyons, B. P. and Jha, A. N. (2013). Oxidative DNA damage may not mediate Ni-induced genotoxicity in marine mussels: Assessment of genotoxic biomarkers and transcriptional responses of key stress genes. *Mutat. Res. Toxicol. Environ. Mutagen.* 754, 22–31.

Danaeifar, M. (2022). New horizons in developing cell lysis methods: A review. *Biotechnol. Bioeng.* 119, 3007–3021.

De Thier, O., M.Tawfeeq, M., Faure, R., Lebel, M., Dru, P., Blanchoud, S., Alié, A., Brown, F. D., Flot, J.-F. and Tiozzo, S. (2024). First chromosome-level genome assembly of the colonial tunicate *Botryllus schlosseri*.

Della Torre, C., Bocci, E., Focardi, S. E. and Corsi, I. (2014). Differential ABCB and ABCC gene expression and efflux activities in gills and hemocytes of Mytilus galloprovincialis and their involvement in cadmium response. *Mar. Environ. Res.* 93, 56–63.

Desaulniers, D., Cummings-Lorbetskie, C., Leingartner, K., Meier, M. J., Pickles, J. C. and Yauk, C. L. (2023). DNA methylation changes from primary cultures through senescence-bypass in Syrian hamster fetal cells initially exposed to benzo[a]pyrene. *Toxicology* 487, 153451.

Dickinson, D. A. and Forman, H. J. (2002). Cellular glutathione and thiols metabolism. *Biochem. Pharmacol.* 64, 1019–1026.

Domart-Coulon, I. and Blanchoud, S. (2022). From Primary Cell and Tissue Cultures to Aquatic Invertebrate Cell Lines: An Updated Overview. In *Advances in Aquatic Invertebrate Stem Cell Research*, pp. 1–64. MDPI.

Dominy, J. E., Hwang, J. and Stipanuk, M. H. (2007). Overexpression of cysteine dioxygenase reduces intracellular cysteine and glutathione pools in HepG2/C3A cells. *Am. J. Physiol.-Endocrinol. Metab.* 293, E62–E69.

Downs, C. A., Fauth, J. E., Downs, V. D. and Ostrander, G. K. (2010). In vitro cell-toxicity screening as an alternative animal model for coral toxicology: effects of heat stress, sulfide, rotenone, cyanide, and cuprous oxide on cell viability and mitochondrial function. *Ecotoxicology* 19, 171–184.

Du, R., Huang, C., Chen, H., Liu, K., Xiang, P., Yao, N., Yang, L., Zhou, L., Wu, Q., Zheng, Y., et al. (2020). SDCBP/MDA-9/syntenin phosphorylation by AURKA promotes esophageal squamous cell carcinoma progression through the EGFR-PI3K-Akt signaling pathway. *Oncogene* 39, 5405–5419.

Eisler, R. and Hennekey, R. J. (1977). Acute toxicities of Cd2+, Cr+6, Hg2+, Ni2+ and Zn2+ to estuarine macrofauna. *Arch. Environ. Contam. Toxicol.* 6, 315–323.

Fan, W., Xu, Z. and Wang, W.-X. (2015). Contrasting metal detoxification in polychaetes, bivalves and fish from a contaminated bay. *Aquat. Toxicol.* 159, 62–68.

Fernandez, B., Passanisi, V. J., Ashraf, H. M. and Spencer, S. L. (2025). Single-cell RNA sequencing reveals a quiescence-senescence continuum and distinct senotypes following chemotherapy. *Nat. Commun.* 17, 169.

Florence, T. M., Stauber, J. L. and Ahsanullah, M. (1994). Toxicity of nickel ores to marine organisms. *Sci. Total Environ.* 148, 139–155.

Franchi, N., Ballin, F., Manni, L., Schiavon, F., Basso, G. and Ballarin, L. (2016). Recurrent phagocytosis-induced apoptosis in the cyclical generation change of the compound ascidian Botryllus schlosseri. *Dev. Comp. Immunol.* 62, 8–16.

Franchi, N., Ballin, F. and Ballarin, L. (2017). Protection from Oxidative Stress in Immunocytes of the Colonial Ascidian *Botryllus schlosseri* : Transcript Characterization and Expression Studies. *Biol. Bull.* 232, 45–57.

Fridlyanskaya, I., Alekseenko, L. and Nikolsky, N. (2015). Senescence as a general cellular response to stress: A mini-review. *Exp. Gerontol.* 72, 124–128.

Gallo, A., Boni, R., Buttino, I. and Tosti, E. (2016). Spermiotoxicity of nickel nanoparticles in the marine invertebrate *Ciona intestinalis* (ascidians). *Nanotoxicology* 10, 1096–1104.

Gao, Y., Chen, Y., Li, S., Huang, X., Hu, J., Bock, D. G., MacIsaac, H. J. and Zhan, A. (2022). Complementary genomic and epigenomic adaptation to environmental heterogeneity. *Mol. Ecol.* 31, 3598–3612.

Gardell, A. M., Qin, Q., Rice, R. H., Li, J. and Kültz, D. (2014). Derivation and Osmotolerance Characterization of Three Immortalized Tilapia (Oreochromis mossambicus) Cell Lines. *PLoS ONE* 9, e95919.

Gissi, F., Stauber, J. L., Binet, M. T., Trenfield, M. A., Van Dam, J. W. and Jolley, D. F. (2018). Assessing the chronic toxicity of nickel to a tropical marine gastropod and two crustaceans. *Ecotoxicol. Environ. Saf.* 159, 284–292.

Goldstein, O., Mandujano-Tinoco, E. A., Levy, T., Talice, S., Raveh, T., Gershoni-Yahalom, O., Voskoboynik, A. and Rosental, B. (2021). Botryllus schlosseri as a Unique Colonial Chordate Model for the Study and Modulation of Innate Immune Activity. *Mar. Drugs* 19, 454.

Granger Joly De Boissel, P., Fournier, M., Rodriguez-Lecompte, J. C., McKenna, P., Kibenge, F. and Siah, A. (2017). Functional and molecular responses of the blue mussel Mytilus edulis' hemocytes exposed to cadmium - An in vitro model and transcriptomic approach. *Fish Shellfish Immunol.* 67, 575–585.

Grasela, J. J., Pomponi, S. A., Rinkevich, B. and Grima, J. (2012). Efforts to develop a cultured sponge cell line: revisiting an intractable problem. *Vitro Cell. Dev. Biol. - Anim.* 48, 12–20.

Gregorin, C., Albarano, L., Somma, E., Costantini, M. and Zupo, V. (2021). Assessing the Ecotoxicity of Copper and Polycyclic Aromatic Hydrocarbons: Comparison of Effects on Paracentrotus lividus and Botryllus schlosseri, as Alternative Bioassay Methods. *Water* 13, 711.

Grochowski, C. M., Loomes, K. M. and Spinner, N. B. (2016). Jagged1 (JAG1): Structure, expression, and disease associations. *Gene* 576, 381–384.

Guillén Matus, D. G., Donaghy, C. M., Vijayan, N., Lane, Z. T., Howell, M., Glavin, G. G., Angeles-Boza, A. M., Nyholm, S. V. and Balunas, M. J. (2024). Multi-omics Analysis Reveals Important Role for Microbial-derived Metabolites from *Botryllus schlosseri* in Metal Interactions.

Guo, H., Liu, H., Wu, H., Cui, H., Fang, J., Zuo, Z., Deng, J., Li, Y., Wang, X. and Zhao, L. (2019). Nickel Carcinogenesis Mechanism: DNA Damage. *Int. J. Mol. Sci.* 20, 4690.

Hajimad, T. and Vedamanikam, J. (2013). Temperature effects on the toxicity of four trace metals to adult spotted Babylonia snails (*Babylonia areolata*). *Toxicol. Environ. Chem.* 95, 1380–1387.

Harrington, B. J. and Hageage, G. J. (2003). Calcofluor White: A Review of its Uses and Applications in Clinical Mycology and Parasitology. *Lab. Med.* 34, 361–367.

Helbert, W., Nishiyama, Y., Okano, T. and Sugiyama, J. (1998). Molecular Imaging of Halocynthia papillosa Cellulose. *J. Struct. Biol.* 124, 42–50.

Hendijani, F. (2017). Explant culture: An advantageous method for isolation of mesenchymal stem cells from human tissues. *Cell Prolif.* 50, e12334.

Hesp, K., Van Der Heijden, J. M. E., Munroe, S., Sipkema, D., Martens, D. E., Wijffels, R. H. and Pomponi, S. A. (2023). First continuous marine sponge cell line established. *Sci. Rep.* 13, 5766.

Hetrick, F. M., Stephens, E., Lomax, N. and Lutrell, K. (1981). *Attempts to Develop a Marine Molluscan Cell Line*. 1224 H. J. Patterson Hall College Park, MD 20742: Springer Nature Switzerland.

Hirose, E. (2009). Ascidian tunic cells: morphology and functional diversity of free cells outside the epidermis. *Invertebr. Biol.* 128, 83–96.

Hirose, E., Yasunori, S. and Watanabe, H. (1991). Tunic Cell Morphology and Classification in Botryllid Ascidians(Morphology). *Zoolog. Sci.* 8,.

Hiscock, K. (2008). *Star ascidian (Botryllus schlosseri): Marine Evidence–based Sensitivity Assessment (MarESA) Review*. Plymouth: Marine Biological Association of the United Kingdom.

Holland, L. Z. (2016). Tunicates. *Curr. Biol.* 26, R146–R152.

Huang, X., Zhuang, Z., Frenkel, K., Klein, C. B. and Costa, M. (1993). The role of nickel and nickel-mediated reactive oxygen species in the mechanism of nickel carcinogenesis. *Environ. Health Perspect.*

Jaśkiewicz, A., Pająk, B. and Orzechowski, A. (2018). The Many Faces of Rap1 GTPase. *Int. J. Mol. Sci.* 19, 2848.

Jeyapalan, J. C. and Sedivy, J. M. (2013). How to measure RNA expression in rare senescent cells expressing any specific protein such as $p16^{Ink4a}$. *Aging* 5, 120–129.

Johnson, E. L., Robinson, D. G. and Coller, H. A. (2017). Widespread changes in mRNA stability contribute to quiescence-specific gene expression patterns in a fibroblast model of quiescence. *BMC Genomics* 18, 123.

Johnson, C. J., Razy-Krajka, F. and Stolfi, A. (2020). Expression of smooth muscle-like effectors and core cardiomyocyte regulators in the contractile papillae of Ciona. *EvoDevo* 11, 15.

Kamer, I. and Rinkevich, B. (2002). In vitro application of the comet assay for aquatic genotoxicity: considering a primary culture versus a cell line. *Toxicol. In Vitro* 16, 177–184.

Kassmer, S. H., Nourizadeh, S. and De Tomaso, A. W. (2019). Cellular and molecular mechanisms of regeneration in colonial and solitary Ascidians. *Dev. Biol.* 448, 271–278.

Kawamura, K., Nishitsuji, K., Shoguchi, E., Fujiwara, S. and Satoh, N. (2021). Establishing Sustainable Cell Lines of a Coral, Acropora tenuis. *Mar. Biotechnol.* 23, 373–388.

Kenworthy, J. M., Rolland, G., Samadi, S. and Lejeusne, C. (2018). Local variation within marinas: Effects of pollutants and implications for invasive species. *Mar. Pollut. Bull.* 133, 96–106.

Kimura, S. and Itoh, T. (2007). Biogenesis and Function of Cellulose in the Tunicates. In *Cellulose: Molecular and Structural Biology* (ed. Brown, R. M.) and Saxena, I. M.), pp. 217–236. Dordrecht: Springer Netherlands.

Kültz, D., Gardell, A. M., DeTomaso, A., Stoney, G., Rinkevich, B., Qarri, A. and Hamar, J. (2025). Proteome-Wide 4-Hydroxy-2-Nonenal Signature of Oxidative Stress in the Marine Invasive Tunicate *Botryllus schlosseri*. *PROTEOMICS* 25, 12–25.

Kuroiwa, K., Mita-Yoshida, K., Hamada, M., Hozumi, A., Nishino, A. S. and Sasakura, Y. (2025). Tunicate-specific protein Epi-1 is essential for conferring hydrophilicity to the larval tunic in the ascidian Ciona. *Dev. Biol.* 520, 41–52.

Kwon, Y., Singh, S., Rodriguez, D., Chau, A. L., Pitenis, A. A., De Tomaso, A. W. and Valentine, M. T. (2023). Mechanical resilience of the sessile tunicate *Botryllus schlosseri*. *J. Exp. Biol.* 226, jeb245124.

Lanoizelet, M., Elkhoury Youhanna, C. and Darras, S. (2023). Molecular control of cellulosic fin morphogenesis in ascidians.

Lauzon, R. J., Kidder, S. J. and Long, P. (2007). Suppression of programmed cell death regulates the cyclical degeneration of organs in a colonial urochordate. *Dev. Biol.* 301, 92–105.

Law, C. W., Chen, Y., Shi, W. and Smyth, G. K. (2014). voom: precision weights unlock linear model analysis tools for RNA-seq read counts. *Genome Biol.* 15, R29.

Lee, H.-J., Jedrychowski, M. P., Vinayagam, A., Wu, N., Shyh-Chang, N., Hu, Y., Min-Wen, C., Moore, J. K., Asara, J. M., Lyssiotis, C. A., et al. (2017). Proteomic and Metabolomic Characterization of a Mammalian Cellular Transition from Quiescence to Proliferation. *Cell Rep.* 20, 721–736.

Leprêtre, M. and Kültz, D. (2025). Copper-induced stress and recovery impacts on organismal phenotypes and the underlying proteomic signatures in Botryllus schlosseri. *Sci. Total Environ.* 1004, 180803.

Leung, C. W. B., Wall, J. and Esashi, F. (2024). From rest to repair: Safeguarding genomic integrity in quiescent cells. *DNA Repair* 142, 103752.

Lévesque, M., Gatien, S., Finnson, K., Desmeules, S., Villiard, É., Pilote, M., Philip, A. and Roy, S. (2007). Transforming Growth Factor: β Signaling Is Essential for Limb Regeneration in Axolotls. *PLoS ONE* 2, e1227.

Liang, J., Wei, Y., Liu, H., Liang, S., Li, Y., Zhou, Z. and Guo, Y. (2025). Study on the physiological and molecular regulatory mechanisms of Sinonovacula rivularis in response to low-salinity stress. *Aquac. Rep.* 45, 103174.

Lin, J., Patel, S. R., Cheng, X., Cho, E. A., Levitan, I., Ullenbruch, M., Phan, S. H., Park, J. M. and Dressler, G. R. (2005). Kielin/chordin-like protein, a novel enhancer of BMP signaling, attenuates renal fibrotic disease. *Nat. Med.* 11, 387–393.

Liu, Z.-Y., Yu, Y. and Yu, X.-Z. (2026). Interplay Between Oxidative Stress and Inflammation in Aquatic Animals: Mechanisms, Consequences, and Implications for Aquaculture Health. *Antioxidants* 15, 208.

Luckenbach, T. and Epel, D. (2008). ABCB- and ABCC-type transporters confer multixenobiotic resistance and form an environment-tissue barrier in bivalve gills. *Am. J. Physiol.-Regul. Integr. Comp. Physiol.* 294, R1919–R1929.

Manni, L., Gasparini, F., Hotta, K., Ishizuka, K. J., Ricci, L., Tiozzo, S., Voskoboynik, A. and Dauga, D. (2014). Ontology for the Asexual Development and Anatomy of the Colonial Chordate Botryllus schlosseri. *PLOS ONE* 9, e96434.

Manni, L., Anselmi, C., Cima, F., Gasparini, F., Voskoboynik, A., Martini, M., Peronato, A., Burighel, P., Zaniolo, G. and Ballarin, L. (2019). Sixty years of experimental studies on the blastogenesis of the colonial tunicate Botryllus schlosseri. *Dev. Biol.* 448, 293–308.

Marescal, O. and Cheeseman, I. M. (2020). Cellular Mechanisms and Regulation of Quiescence. *Dev. Cell* 55, 259–271.

Martinez-Zamudio, R. and Ha, H. C. (2011). Environmental epigenetics in metal exposure. *Epigenetics* 6, 820–827.

Millward, G. E., Kadam, S. and Jha, A. N. (2012). Tissue-specific assimilation, depuration and toxicity of nickel in Mytilus edulis. *Environ. Pollut.* 162, 406–412.

Min, E. Y., Kim, J.-H., Lee, J. S. and Kang, J.-C. (2021). Nickel bioaccumulation and the antioxidant response in Pacific abalone Haliotis discus hannai, Ino 1953 exposed to waterborne nickel during thermal stress. *Aquac. Rep.* 20, 100726.

Mo, Y., Zhang, Y., Zhang, Y., Yuan, J., Mo, L. and Zhang, Q. (2021). Nickel nanoparticle-induced cell transformation: involvement of DNA damage and DNA repair defect through HIF-1α/miR-210/Rad52 pathway. *J. Nanobiotechnology* 19, 370.

Mojica, E. A. and Kültz, D. (2022). Physiological mechanisms of stress-induced evolution. *J. Exp. Biol.* 225, jeb243264.

Mukai, H. and Watanabe, H. (1976). Studies on the formation of germ cells in a compound ascidian *Botryllus, primigenus* oka. *J. Morphol.* 148, 337–361.

Naranjo, S. A., Carballo, J. L. and Garcia-Gomez, J. C. (1996). Effects of environmental stress on ascidian populations in Algeciras Bay (southern Spain). Possible marine bioindicators? *Mar. Ecol. Prog. Ser.* 144: 119–131, 1996,.

Niimi, H., Pardali, K., Vanlandewijck, M., Heldin, C.-H. and Moustakas, A. (2007). Notch signaling is necessary for epithelial growth arrest by TGF-β. *J. Cell Biol.* 176, 695–707.

Noren Hooten, N. and Evans, M. K. (2017). Techniques to Induce and Quantify Cellular Senescence. *J. Vis. Exp.* 55533.

Oren, M., Douek, J., Fishelson, Z. and Rinkevich, B. (2007). Identification of immune-relevant genes in histoincompatible rejecting colonies of the tunicate Botryllus schlosseri. *Dev. Comp. Immunol.* 31, 889–902.

Oren, M., Escande, M., Paz, G., Fishelson, Z. and Rinkevich, B. (2008). Urochordate Histoincompatible Interactions Activate Vertebrate-Like Coagulation System Components. *PLoS ONE* 3, e3123.

Osler, M. E., Smith, T. K. and Bader, D. M. (2006). *Bves* , a member of the *Popeye* domain-containing gene family. *Dev. Dyn.* 235, 586–593.

Outskouni, Z., Prapa, S., Goutas, A., Klagkou, E., Vatsellas, G., Kosta, A., Trachana, V. and Papathanasiou, I. (2025). Comparative analysis of transcriptomic profiles of mesenchymal stem cells at the onset of senescence and after exposure to acute exogenous oxidative stress. *Biochem. Biophys. Res. Commun.* 754, 151506.

Patro, R., Duggal, G., Love, M. I., Irizarry, R. A. and Kingsford, C. (2017). Salmon provides fast and bias-aware quantification of transcript expression. *Nat. Methods* 14, 417–419.

Payea, M. J., Dar, S. A., Anerillas, C., Martindale, J. L., Belair, C., Munk, R., Malla, S., Fan, J., Piao, Y., Yang, X., et al. (2024). Senescence suppresses the integrated stress response and activates a stress-remodeled secretory phenotype. *Mol. Cell* 84, 4454-4469.e7.

Peddibhotla, S., Gonzaga, M., Zhang, T., Goel, Y., Sun, J., Harrison, B. R., Promislow, D. E. L. and Ruohola-Baker, H. Natural Genetic Variation Impacts Stress-Induced Quiescence and Regeneration in Response to Rapamycin.

Permenter, M. G., Lewis, J. A. and Jackson, D. A. (2011). Exposure to Nickel, Chromium, or Cadmium Causes Distinct Changes in the Gene Expression Patterns of a Rat Liver Derived Cell Line. *PLoS ONE* 6, e27730.

Poole, L. B. (2015). The basics of thiols and cysteines in redox biology and chemistry. *Free Radic. Biol. Med.* 80, 148–157.

Qarri, A., Rosner, A., Rabinowitz, C. and Rinkevich, B. (2020). UV-B radiation bearings on ephemeral soma in the shallow water tunicate Botryllus schlosseri. *Ecotoxicol. Environ. Saf.* 196, 110489.

Qarri, A., Rinkevich, Y. and Rinkevich, B. (2022). Improving the Yields of Blood Cell Extractions from Botryllus schlosseri Vasculature. In *Advances in aquatic invertebrate stem cell research*, p. MDPI.

Qarri, A., Kültz, D., Gardell, A. M., Rinkevich, B. and Rinkevich, Y. (2023). Improved Media Formulations for Primary Cell Cultures Derived from a Colonial Urochordate. *Cells* 12, 1709.

Rabinowitz, C. and Rinkevich, B. (2003). Epithelial cell cultures from Botryllus schlosseri palleal buds: accomplishments and challenges. *Methods Cell Sci.* 25, 137–148.

Rabinowitz, C. and Rinkevich, B. (2004). *In vitro* delayed senescence of extirpated buds from zooids of the colonial tunicate *Botryllus schlosseri*. *J. Exp. Biol.* 207, 1523–1532.

Rabinowitz, C. and Rinkevich, B. (2011). De novo emerged stemness signatures in epithelial monolayers developed from extirpated palleal buds. *Vitro Cell. Dev. Biol. - Anim.* 47, 26–31.

Rabinowitz, C., Alfassi, G. and Rinkevich, B. (2009). Further portrayal of epithelial monolayers emergent de novo from extirpated ascidians palleal buds. *Vitro Cell. Dev. Biol. - Anim.* 45, 334–342.

Radford, J. L., Hutchinson, A. E., Burandt, M. and Raftos, D. A. (2000). Effects of Metal-Based Environmental Pollutants on Tunicate Hemocytes. *J. Invertebr. Pathol.* 76, 242–248.

Ranasinghe, N., Lee, S.-S., Gamage, L. and Lee, T.-H. (2025). 3D cell culture model – a substitution for future in vivo fish study? *Mol. Biol. Rep.* 52, 726.

Ricci, L., Chaurasia, A., Lapébie, P., Dru, P., Helm, R. R., Copley, R. R. and Tiozzo, S. (2016). Identification of differentially expressed genes from multipotent epithelia at the onset of an asexual development. *Sci. Rep.* 6, 27357.

Ricci, L., Salmon, B., Olivier, C., Andreoni-Pham, R., Chaurasia, A., Alié, A. and Tiozzo, S. (2022). The Onset of Whole-Body Regeneration in Botryllus schlosseri: Morphological and Molecular Characterization. *Front. Cell Dev. Biol.* 10, 843775.

Rinkevich, B. (2005). Marine Invertebrate Cell Cultures: New Millennium Trends. *Mar. Biotechnol.* 7, 429–439.

Rinkevich, B. (2011). Cell Cultures from Marine Invertebrates: New Insights for Capturing Endless Stemness. *Mar. Biotechnol.* 13, 345–354.

Rinkevich, B. and Pomponi, S. A. (2025). Advancing marine invertebrate cell line research: four key knowledge gaps. *Vitro Cell. Dev. Biol. - Anim.* 61, 493–505.

Rinkevich, B. and Rabinowitz, C. (1993). In vitro culture of blood cells from the colonial protochordate *Botryllus schlosseri*. *Vitro Cell. Dev. Biol. - Anim.* 29, 79–85.

Rinkevich, B. and Rabinowitz, C. (1994). Acquiring embryo-derived cell cultures and aseptic metamorphosis of larvae from the colonial protochordate *Botryllus schlosseri*. *Invertebr. Reprod. Dev.* 25, 59–72.

Rinkevich, B. and Rabinowitz, C. (1997). Initiation of epithelial cell cultures from palleal buds of Botryllus schlosseri, a colonial tunicate. *Vitro Cell. Dev. Biol. - Anim.* 33, 422–424.

Rinkevich, B. and Weissman, I. L. (1990). *Botryllus schlosseri* (tunicata) whole colony irradiation: Do senescent zooid resorption and immunological resorption involve similar recognition events? *J. Exp. Zool.* 253, 189–201.

Robinson, M. D. and Oshlack, A. (2010). A scaling normalization method for differential expression analysis of RNA-seq data. *Genome Biol.* 11, R25.

Rodriguez, D., Braden, B. P., Boyer, S. W., Taketa, D. A., Setar, L., Calhoun, C., Maio, A. D., Langenbacher, A., Valentine, M. T. and De Tomaso, A. W. (2017). In vivo manipulation of the extracellular matrix induces vascular regression in a basal chordate. *Mol. Biol. Cell* 28, 1883–1893.

Rodriguez, D., Taketa, D. A., Madhu, R., Kassmer, S., Loerke, D., Valentine, M. T. and Tomaso, A. W. D. (2021). Vascular Aging in the Invertebrate Chordate, Botryllus schlosseri. *Front. Mol. Biosci.* 8, 626827.

Rosner, A., Alfassi, G., Moiseeva, E., Paz, G., Rabinowitz, C., Lapidot, Z., Douek, J., Haim, A. and Rinkevich, B. (2014). The involvement of three signal transduction pathways in

botryllid ascidian astogeny, as revealed by expression patterns of representative genes. *Int. J. Dev. Biol.* 58, 677–692.

Rosner, A., Kravchenko, O. and Rinkevich, B. (2019). IAP genes partake weighty roles in the astogeny and whole body regeneration in the colonial urochordate Botryllus schlosseri. *Dev. Biol.* 448, 320–341.

Sabbadin, A. (1955). Osservazioni sullo sviluppo, l'accrescimento e la riproduzione di *Botryllus schlosseri* (Pallas), in condizioni di laboratorio. *Bolletino Zool.* 22, 243–263.

Schneider, C., Porter, N. A. and Brash, A. R. (2008). Routes to 4-Hydroxynonenal: Fundamental Issues in the Mechanisms of Lipid Peroxidation. *J. Biol. Chem.* 283, 15539–15543.

Shehadul Islam, M., Aryasomayajula, A. and Selvaganapathy, P. (2017). A Review on Macroscale and Microscale Cell Lysis Methods. *Micromachines* 8, 83.

Sheng, Y., Abreu, I. A., Cabelli, D. E., Maroney, M. J., Miller, A.-F., Teixeira, M. and Valentine, J. S. (2014). Superoxide Dismutases and Superoxide Reductases. *Chem. Rev.* 114, 3854–3918.

Shi, W., Liu, P., Yang, D., Zhuang, Y., Lin, B. and Dong, B. (2025). Transcriptome Analysis Reveals the Requirement of the TGFβ Pathway in Ascidian Tail Regression. *Cells* 14, 546.

Shipp, L. E. and Hamdoun, A. (2012). ATP-binding cassette (ABC) transporter expression and localization in sea urchin development. *Dev. Dyn.* 241, 1111–1124.

Shoeb, M., Ansari, N., Srivastava, S. and Ramana, K. (2013). 4-Hydroxynonenal in the Pathogenesis and Progression of Human Diseases. *Curr. Med. Chem.* 21, 230–237.

Slavov, N., Macinskas, J., Caudy, A. and Botstein, D. (2011). Metabolic cycling without cell division cycling in respiring yeast. *Proc. Natl. Acad. Sci.* 108, 19090–19095.

Soneson, C., Love, M. I. and Robinson, M. D. (2015). Differential analyses for RNA-seq: transcript-level estimates improve gene-level inferences. *F1000Research* 4, 1521.

Spina, E. J., Guzman, E., Zhou, H., Kosik, K. S. and Smith, W. C. (2017). A microRNA-mRNA expression network during oral siphon regeneration in *Ciona*. *Development* 144, 1787–1797.

Stohs, S. J. and Bagchi, D. (1994). Oxidative Mechanisms in the Toxicity of Metal Ions. *Free Radic. Biol. Med.* 19, 321–336.

Strappazzon, F., Torch, S., Chatellard-Causse, C., Petiot, A., Thibert, C., Blot, B., Verna, J.-M. and Sadoul, R. (2010). Alix is involved in caspase 9 activation during calcium-induced apoptosis. *Biochem. Biophys. Res. Commun.* 397, 64–69.

Svanfeldt, K., Lundqvist, L., Rabinowitz, C., Sköld, H. N. and Rinkevich, B. (2014). Repair of UV-induced DNA damage in shallow water colonial marine species. *J. Exp. Mar. Biol. Ecol.* 452, 40–46.

Swam-Jaramillo, L. M., Rider, M. M., Apeti, D. A. and Reed, L. A. (2025). NATIONAL STATUS AND TRENDS, MUSSEL WATCH PROGRAM: A 2019 Assessment of Trace Metals in the Pacific Northwest.

Tasselli, S., Ballin, F., Franchi, N., Fabbri, E. and Ballarin, L. (2017). Expression of genes involved in oxidative stress response in colonies of the ascidian Botryllus schlosseri exposed to various environmental conditions. *Estuar. Coast. Shelf Sci.* 187, 22–27.

Terzi, M. Y., Izmirli, M. and Gogebakan, B. (2016). The cell fate: senescence or quiescence. *Mol. Biol. Rep.* 43, 1213–1220.

Tobias, Z., Solow, A. and Tepolt, C. (2024). Geography and developmental plasticity shape post-larval thermal tolerance in the golden star tunicate, Botryllus schlosseri. *J. Therm. Biol.* 119, 103763.

Trott, D. A., Cuthbert, A. P., Overell, R. W., Russo, I. and Newbold, R. F. (1995). Mechanisms involved in the immortalization of mammalian cells by ionizing radiation and chemical carcinogens. *Carcinogenesis* 16, 193–204.

Tsuchiya, A., Okamura, Y., Kono, T., Hikima, J. and Sakai, M. (2023). Transcriptomic analysis of cultured kuruma shrimp primary lymphoid organ cells for identifying key cascades hindering sustainable culture. *Fish. Sci.*

Tveito, G., Hansteen, I.-L. and Dalen, H. (1989). Immortalization of Normal Human Kidney Epithelial Cells by Nickel(II).

Valcourt, J. R., Lemons, J. M. S., Haley, E. M., Kojima, M., Demuren, O. O. and Coller, H. A. (2012). Staying alive: Metabolic adaptations to quiescence. *Cell Cycle* 11, 1680–1696.

Valdez, J. M., Zhang, L., Su, Q., Dakhova, O., Zhang, Y., Shahi, P., Spencer, D. M., Creighton, C. J., Ittmann, M. M. and Xin, L. (2012). Notch and TGFβ Form a Reciprocal Positive Regulatory Loop that Suppresses Murine Prostate Basal Stem/Progenitor Cell Activity. *Cell Stem Cell* 11, 676–688.

Van Velthoven, C. T. J. and Rando, T. A. (2019). Stem Cell Quiescence: Dynamism, Restraint, and Cellular Idling. *Cell Stem Cell* 24, 213–225.

Voskoboynik, A., Reznick, A. Z. and Rinkevich, B. (2002). Rejuvenescence and extension of an urochordate life span following a single, acute administration of an anti-oxidant, butylated hydroxytoluene. *Mech. Ageing Dev.* 123, 1203–1210.

Voskoboynik, A., Rinkevich, B., Weiss, A., Moiseeva, E. and Reznick, A. Z. (2004). Macrophage involvement for successful degeneration of apoptotic organs in the colonial urochordate *Botryllus schlosseri*. *J. Exp. Biol.* 207, 2409–2416.

Voskoboynik, A., Neff, N. F., Sahoo, D., Newman, A. M., Pushkarev, D., Koh, W., Passarelli, B., Fan, H. C., Mantalas, G. L., Palmeri, K. J., et al. (2013). The genome sequence of the colonial chordate, Botryllus schlosseri. *eLife* 2, e00569.

Vyas, H., Schrankel, C. S., Espinoza, J. A., Mitchell, K. L., Nesbit, K. T., Jackson, E., Chang, N., Lee, Y., Warner, J., Reitzel, A., et al. (2022). Generation of a homozygous mutant drug transporter (ABCB1) knockout line in the sea urchin *Lytechinus pictus*. *Development* 149, dev200644.

Wagner, G. P., Erkenbrack, E. M. and Love, A. C. (2019). Stress-Induced Evolutionary Innovation: A Mechanism for the Origin of Cell Types. *BioEssays* 41, 1800188.

Wang, M. and Wang, G. (2009). Oxidative damage effects in the copepod Tigriopus japonicus Mori experimentally exposed to nickel. *Ecotoxicology* 19, 273–284.

Wang, F., Zieman, A. and Coulombe, P. A. (2016). Skin Keratins. In *Methods in Enzymology*, pp. 303–350. Elsevier.

Wolffe, A. P. and Tata, J. R. (1984). Primary culture, cellular stress and differentiated function. *FEBS Lett.* 176, 8–15.

Wu, M. Y. and Hill, C. S. (2009). TGF-β Superfamily Signaling in Embryonic Development and Homeostasis. *Dev. Cell* 16, 329–343.

Ya'la, Z., Dewi, T., Husni, A., Santoso, T., Ndobe, S., Rosyida, E., Maemunah, M., Mappatoba, M. and Nurdin, M. (2025). Assessment of Heavy Metal Contaminations in Coastal Sediments due to Nickel Mining Activities in Morowali Regency Central Sulawesi Indonesia. *J. Min. Environ.* 16,.

Yamaoka-Tojo, M., Ushio-Fukai, M., Hilenski, L., Dikalov, S. I., Chen, Y. E., Tojo, T., Fukai, T., Fujimoto, M., Patrushev, N. A., Wang, N., et al. (2004). IQGAP1, a Novel Vascular Endothelial Growth Factor Receptor Binding Protein, Is Involved in Reactive Oxygen Species—Dependent Endothelial Migration and Proliferation. *Circ. Res.* 95, 276–283.

Yao, G. (2024). Quiescence-Origin Senescence: A New Paradigm in Cellular Aging. *Biomedicines* 12, 1837.

Yihua, C., Min, D., Zhiguo, D., Yifeng, L. and Donghong, N. (2024). Function of taurine and its synthesis-related genes in hypertonic regulation of Sinonovacula constricta. *Comp. Biochem. Physiol. A. Mol. Integr. Physiol.* 287, 111536.

Zaniolo, G. (1981). Histology of the ascidian *Botryllus schlosseri* tunic: in particular, the test cells. *Bolletino Zool.* 48, 169–178.

Zavadil, J. and Cermak, L. (2004). Integration of TGF-b/Smad and Jagged1/Notch signalling in epithelial-to-mesenchymal transition.

Zerebecki, R. A. and Sorte, C. J. B. (2011). Temperature Tolerance and Stress Proteins as Mechanisms of Invasive Species Success. *PLOS ONE* 6, e14806.

Zhang, P. and Dressler, G. R. (2013). The Groucho protein Grg4 suppresses Smad7 to activate BMP signaling. *Biochem. Biophys. Res. Commun.* 440, 454–459.

Zhang, Y. F., Chen, S. Y., Qu, M. J., Adeleye, A. O. and Di, Y. N. (2017). Utilization of isolated marine mussel cells as an in vitro model to assess xenobiotics induced genotoxicity. *Toxicol. In Vitro* 44, 219–229.

Zhang, X., Jiang, T., Ye, L., Sun, J., Wang, L., Li, J., Wu, F., Ren, S. and Gao, G. (2025). WISP3 upregulates SDCBP expression to promote the progression of non-small cell lung cancer via the TGF-β signaling pathway. *Biochem. Pharmacol.* 240, 117082.

Zhao, Y. and Li, J. (2014). Excellent chemical and material cellulose from tunicates: diversity in cellulose production yield and chemical and morphological structures from different tunicate species. *Cellulose* 21, 3427–3441.

Zondag, L. E., Rutherford, K., Gemmell, N. J. and Wilson, M. J. (2016). Uncovering the pathways underlying whole body regeneration in a chordate model, Botrylloides leachi using de novo transcriptome analysis. *BMC Genomics* 17, 114.